The Sintering, Microstructural Analysis and Mechanical Properties of two β' MgSiAlON ceramics

by

Roger W. Bayliss, BSc (Liverpool University), MSc (Leeds University)

A Thesis for the Degree of

Doctor of Philosophy

of the

University of Warwick

Department of Physics

October 1986

CONTENTS

LIST OF FIGURES

19. Hot stage microscope results.
20. Phases produced by pressureless sintering of compositions on the 3:4 plane.
21. Analyses of the final glass compositions in as-sintered ceramics.
22. Grain size as a function of z level.
23. Effect of too high a sintering temperature on the high z ceramics.

CHAPTER FOUR

24. Microstructure of low z ceramic A in the as-sintered condition.
25. Microstructure of high z ceramic C in the as-sintered condition.
26. Partial crystallization of second phase is observed in some triple point regions of ceramic C.
27. Magnesium content of β' crystals vs substitution level.
28. Density vs annealing temperature.
29. Density vs annealing time.
30. Heat-treatment products of ceramic A.
31. Heat-treatment products of ceramic C.
32. Microstructure of ceramic B showing complete crystallization of grain boundary phase.
33. Microstructure of high z ceramic D: crystallised spinel in the grain boundaries is discontinuous indicating homogeneous nucleation.
34. Small areas of glass remaining in triple point regions of ceramic D.
35. Glass analysis for A, B, C and D and some other heat-treated samples.
36. Microstructure of a high z ceramic after sintering at 1800°C for 1 hour.
37. Thermal stability of A, B, C and D showing increase after heat-treatment.
38. Microstructure of the ceramic in the diffusion zone (a) low z ceramics (b) high z ceramic.

CHAPTER FIVE

LIST OF TABLES

Acknowledgements

I would like to acknowledge the help given to me by the following people during the course of this project and the submission of this thesis.

Firstly I would like to thank Dr. M.H. Lewis for his supervision and help with the thesis and to the Wolfson Trust for the finance enabling the work to be undertaken and this thesis to be presented.

In particular I would like to thank the following people which includes Mr. Andy Kemp for much advice, discussion and help throughout the project. Also thanks to Mr. Gerry Smith and Mr. Steve York for tuition, encouragement and help with all aspects of microscopy and also for technical help in constructing equipment necessary for this project. I am also grateful to Mr. Keith Briggs, Mr. Pat Beecraft and Mr. Dan Lee for encouragement and technical help. I would also like to thank my family - Sue and Gerry and my parents for help with the thesis. Also Dr. Phelim Daniels for comments after reading the final draft version of the thesis.

I am also indebted to my wife, Alison, who has shown considerable patience and understanding during the long period of writing, and for this I owe her my thanks.

Finally I would like to thank Mrs Sandra Beaufoy for her care and patience in the typing of this thesis.

Memorandum

This dissertation is submitted to the University of Warwick in support of my application for admission to the degree of Doctor of Philosophy. It contains an account of my work carried out in the Department of Physics of the University of Warwick during the period November 1981 to December 1985 under the general supervision of Dr. M.H. Lewis. No part of this dissertation has been used previously in a degree thesis submitted to this or any other university. The work described is the result of my own independent research except where specifically acknowledged in the text.

October 1986.

Roger W. Bayliss

SYNOPSIS

This work describes the preparation and the determination of some properties of two magnesium SiAlON ceramics, one with a low substitution level and one with a high substitution level β' phase. Each had a specific amount of spinel as second phase which would form on sintering or after a post-sintering heat-treatment.

The work was undertaken because (a) the improvement in the properties of pressureless-sintered yttrium SiAlON ceramics was not as high as anticipated and (b) by applying the knowledge gained with the widely researched yttrium system to the MgSiAlON ceramic system, the properties of the magnesium system may be further improved.

Under consideration in this thesis were the sintering of these ceramics and some sintering reactions are proposed. Also discussed, is the effect on the microstructure of heating the ceramic in both oxidising and inert atmospheres. Some mechanical properties were determined, including fracture toughness and hardness testing at ambient temperature, and creep testing at upto 1300°C.

It was expected that MgSiAlONs would be easier to sinter due to the lower ternary oxide eutectic temperature and from a sintering view-point the high z materials do offer an alternative system to the yttrium system by being easier to sinter, but the low z material was as difficult to sinter as the yttrium system.

Whilst the MgSiAlONs that were produced in this project were generally out-performed, encouraging results were obtained for the high z material in oxidation resistance. Low z material had the highest fracture toughness and hardness - both of which increased by heat-treatment. It is proposed that alterations to this heat-treatment would improve matters and would form a useful area for future work.

CHAPTER ONE

INTRODUCTION

1.1 Engineering Ceramics

The need for greater efficiency in gas turbine engines has required an increase in their working temperatures. It is now generally agreed that metals used for some of the critical parts of these turbines are reaching the limit of resistance to creep, creep rupture, oxidation and hot corrosion. Such components include turbine blades and inlet nozzles with typical inlet temperatures at present starting around 650°C for industrial and marine engines and rising to approximately 1300°C for high performance aeroengines. The use of ceramics in turbines should enable the operating temperature to be raised to 1350°C - 1370°C, and give better specific power. The components should also be more corrosion and creep resistant. Other advantages might include lower costs compared with nickel and cobalt alloys and the ability to use cheaper lower grade fuel oil than used with these alloys. The main reasons for the limited number of applications of ceramics in turbines to date are their brittleness, low thermal shock resistance and difficulty in fabrication.

Contenders for such applications are based on either silicon carbide or silicon nitride: some physical properties of these are listed in Table 1.

Property	Silicon Nitride		Silicon Carbide	
	Reaction bonded	Hot pressed	Self bonded	Hot pressed
Density (g cm^{-3})	2.4-2.6	3.1-3.2	3.1	3.2-3.3
Decomposition temperature (K)	2170	2170	3000	3000
Young's Modulus (GNm^{-2}) at 300 K	138-220	310	351-410	386-452
Rupture Modulus (MNm^{-2}) at 300 K	150-215	500-900	200-400	500-650

Table 1 - Physical properties of SiC and Si_3N_4.

(after Karunaratne - PhD Thesis, University of Warwick (1980))

These ceramics have high melting or decomposition temperatures and high hardness (greater than Mohs number 9) due to strong covalent bonding. At present ceramics based on silicon nitride are in favour due to their higher thermal shock resistance and superior fracture toughness.

The use of components made of nitride materials in gas turbines and internal combustion engines or the building of a totally ceramic engine has been the target for several years but there are other uses and these include:

(a) Metal cutting. New Syalon ceramic lathe cutting tools (based on mixtures of Al_2O_3 + Si_3N_4) can cut a range of materials from cast iron to super-tough alloys found in aircraft construction for longer working life than carbide or high-speed steel tools.

(b) Prosthetic devices. Replacement hip joints which have been made from alumina are now being made from silicon nitride for increased wear resistance.

(c) Welding. Components to be welded together in car production are held by hardened steel pins. Pins made of Syalon would last much longer.

Problems associated with producing dense articles in these ceramics are discussed in the next section.

1.2 Fabrication Problems

Inaccessibly high temperatures would be required for the production of dense pure silicon nitride ceramics due to the low diffusivities of reacting species (atoms) caused by strong covalent bonding.

A common fabrication method enabling lower temperatures to be used is liquid phase sintering (LPS) involving additives which form a second phase either with pressure (typically 20 MN m^{-2}) called hot die pressing or without by pressureless sintering. The driving force is the reduction in surface area of the very fine-grained starting material. With nitride ceramics there is an additional and dominant driving force due to the phase change $\alpha \rightarrow \beta$ silicon nitride. In LPS the production of a low viscosity liquid aids densification by particle rearrangement and allows rapid transport of atoms at sintering

temperatures which are in the region 1700-1800°C.

The advantage of hot pressing is that it can be used to achieve essentially 'monophase' material of similar or higher densities than that achieved with pressureless sintering. The main disadvantage of the uniaxial hot die pressed method is the inability to produce complex or large shapes. Also, the discontinuity of the process prevents an automatic production set-up, and the wear of dies usually made from graphite, alumina or silicon carbide makes the process expensive. An improvement on the uniaxial hot press is the hot isostatic pressing (HIP) technique involving sintering in an inert gas under very high pressures (typically 200 MN m^{-2}). This is under intensive development and will be much more common place in the future; at present it is a very expensive technique.

Pressureless sintering of nitride ceramics requires larger amounts of second phase as intercrystalline liquid. This produces a microstructure with a dominant nitride phase and often several grain boundary phases, see Figure 1.

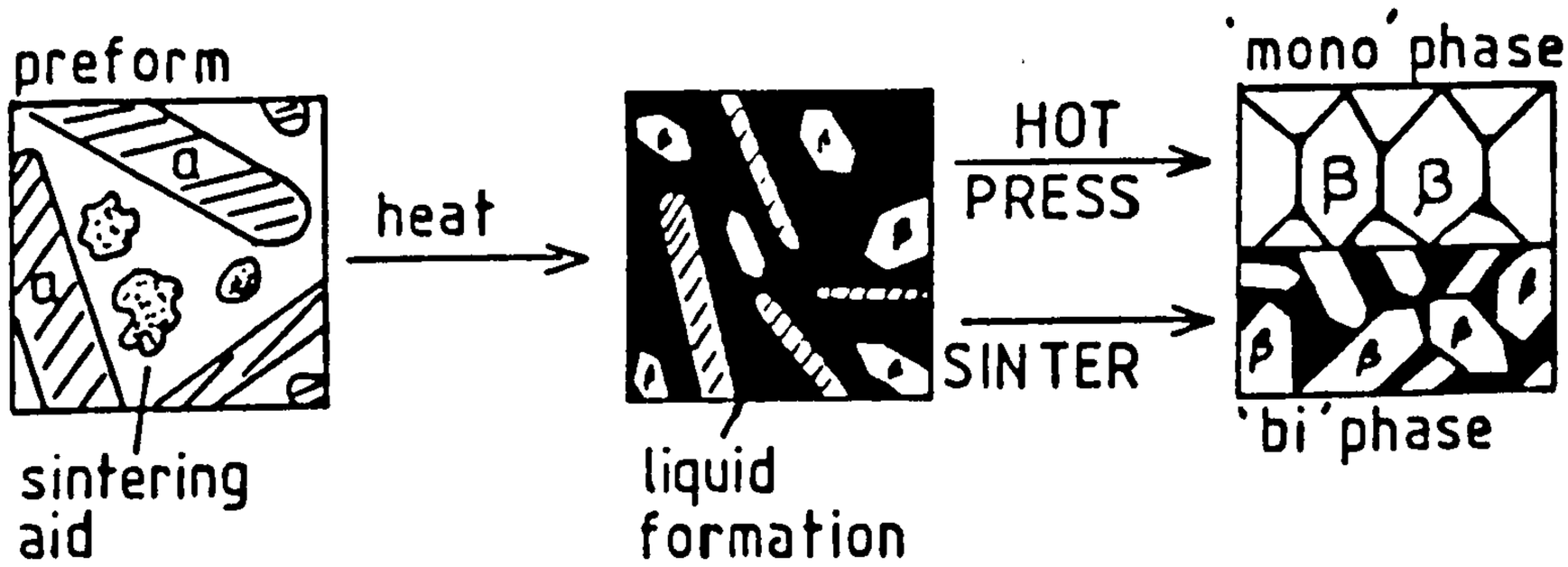

FIGURE 1: The liquid phase sintering process for nitride ceramics illustrating the difference in microstructure between hot pressing and pressureless sintering.

The advantages of pressureless sintering over hot pressing are that the equipment needed is less costly, more complex shapes can be sintered, and the method can be part of the production line.

1.3 Oxynitrides

The development of the oxynitride system was started by sintering mixtures of α silicon nitride and alumina[1]. This produced a range of new ceramics based on the β silicon nitride lattice called expanded β (or β' or generally SiAlONs) because β silicon nitride can accommodate the substitution of $^2/_3$ silicon by aluminium in solid solution.

The original sinters were not single phase β' material but contained other phases now recognised to be part of the general oxynitride system[2], namely some polytypoids and 'X' phase (see Chapter Two).

By balancing the excess silica thought to be on the surface of the α silicon nitride particles, with aluminium nitride (AlN) essentially single phase β' ceramics were produced. These 'balanced' ceramics have the general formula[3]:

$$Si_{6-z}\ Al_z\ \ O_z\ N_{8-z}$$

where z is the substitution level and $0 \leq z \leq 4$. For hot-pressed SiAlON as in early silicon nitride materials small amounts of magnesium oxide were added as sintering aid, but for pressureless sintering enough magnesium oxide must be added to produce 10-15 vol% liquid. This liquid is expected to have a composition near that of the ternary oxide eutectic, $MgO\text{-}SiO_2\text{-}Al_2O_3$, and to be very fluid

at the sintering temperature. SiAlONs have the advantage over silicon nitride in that alumina can be added which modifies the properties of the resulting glassy phase by reducing the liquidus temperature before partitioning into the β lattice. Hence there is greater flexibility possible in sintering these materials and more control over the final microstructure than with silicon nitride.

To date the main research has concentrated on the yttrium SiAlON system with z level $0 \leq z \leq 1$ (i.e. low z SiAlONs that have been produced using yttrium oxide (Y_2O_3) as sintering aid). The range of ceramics produced shows good high temperature performance due to the refractory properties of the grain boundary phase(s).

The work presented here is based on the properties of the SiAlON system when using magnesium oxide as sintering aid with z level $0 \leq z \leq 4$, to compare the properties of both low and high z material with each other and to those of the yttrium system. The advantages of the magnesium SiAlON system include the possibility of (a) easy sintering due to the low ternary oxide eutectic temperature giving low viscosities of the liquid phase between 1600-1800°C and (b) crystallizing the interpenetrating glass to more refractory crystalline phases e.g. spinel. This is attractive since spinel is hard and has a high decomposition temperature and was once regarded as a structural ceramic in its own right.

1.4 Objectives of the Project

The main objectives of the work described in this thesis have been:

1. To analyse the sinterability of the SiAlONs produced using magnesium oxide as sintering aid. This has been achieved by pressureless sintering of a series of compositions across the range of z level .05 $\leq$ z $\leq$ 4 with specific amounts of second phase and is discussed in Chapter Three.

2. To optimise both the sintering and the post sintering heating schedules with respect to the resulting microstructure; also its influence on thermal stability in an oxidising environment and on mechanical properties. This is discussed in Chapters Four and Five.

3. To compare the sintering reactions and response to post sintering heat treatment of this system with the more widely researched yttrium SiAlON system and to make a comparison of mechanical behaviour. This is discussed in Chapter Six with conclusions from the work.

CHAPTER TWO

REVIEW OF NITRIDE CERAMICS

The review is presented in four parts. The first will discuss phase relationships of nitride ceramics; the second part will describe mechanisms suggested to occur during liquid phase sintering; the third part will discuss oxidation problems found in nitride ceramics and the fourth part will describe the methods of determining the mechanical properties of these ceramics with an emphasis on fracture toughness and creep testing.

2.1 Phase Relationships of Nitride Ceramics

2.1.1. Phases

Silicon nitride exists in two crystalline forms, α and β, both built up of covalently bonded Si and N in the form of SiN_4 tetrahedra. The β' phase consists of the β lattice expanded to accommodate alumina by solid substitution. The increase in lattice parameters of β' as a function of increasing z level is shown in Figure 2.

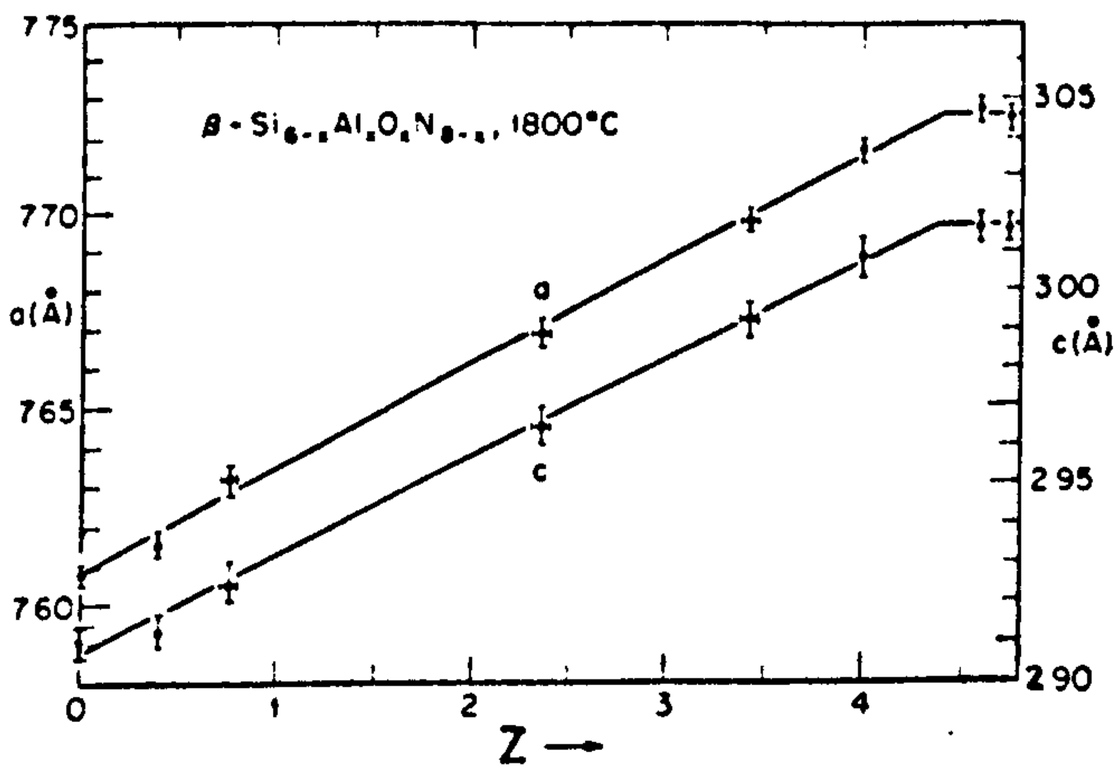

Figure 2: Cell dimensions of β' for $0 \leq z \leq 4$ (after Hohnke and Tien[5]).

There has been much debate[5] as to whether α is an oxynitride with the formula $Si_{12}N_{15}O_{.5}$, the appropriate number of silicon sites remaining vacant to preserve charge neutrality. Other hypotheses are that either α is the low temperature polymorph[6] or it is generally less stable than β under all conditions[7]. Since there has not been a detailed account of a β→α transformation, the latter suggestion is more appealing. It has been shown[8] that although α might accommodate oxygen it may not be essential to its stability, and the wide range of values observed for the lattice parameter indicate structural variations. This oxygen content can vary with the manufacturing process but a typical value is ≈ 1.5 At%. It is generally considered[3] to be in the form of a silica surface layer on the α silicon nitride particles, and is believed to be important to the sintering of β and β' ceramics. The α→β transformation has been described by Messier et al[6].

Another oxynitride phase often produced when sintering SiAlON ceramics is 'X' phase. The composition of this is close to $Si_3Al_6O_{12}N_2$ ($3SiO_2:2Al_2O_3:2AlN$) although it does have a small range of silica solubility[9]. The structure is believed to be triclinic but variations in lattice parameters and crystal symmetry were reported (10, 11, 12). As the silica level increases low 'X' phase which is highly crystalline is replaced by a high 'X' phase, which forms as fine needles and gives more diffuse X-ray patterns due to frequent faulting.

2.1.2 The SiAlON System

Various methods have been used to describe the oxynitride system. Initially it was represented by using ternary phase diagrams,

either SiO_2-Si_3N_4-Al_2O_3 [10] or AlN-Si_3N_4-Al_2O_3 [13] or a combination of them both[14]. An alternative approach, first used by Gauckler et al[2] and shown in Figure 3 is now universally adopted. It is described as a reciprocal salt system. The figure shows results from hot pressings at 1750°C and it is an idealized representation rather than an equilibrium diagram. What can be seen is a number of phases which have a constant metal atom:nonmetal atom (M:X) ratio stretching across regions of the diagram e.g. β' phase (3:4) and the polytypoid phases 15R (5:6) and 21R (7:8) where silicon and nitrogen are being mutually exchanged for aluminium and oxygen.

Most ceramics are formed via LPS and therefore contain a sintering aid (usually magnesium oxide or yttrium oxide): these multicomponent systems are represented by a Jänecke prism, with the diagram shown in Figure 3 as the base of the prism. For the MgSiAlON system this representation is shown in Figure 4. Of particular interest to the present work is the 3:4 plane of the Mg SiAlON system since within this is contained the β' range of solid solution phases. It is bounded by three phases: silicon nitride, forsterite (Mg_2SiO_4),and spinel ($MgAl_2O_4$), as well as an aluminium oxynitride (Al_3O_3N). This important 3:4 plane has already been studied by Jack[15] and by Tien et al[16], shown in Figure 5 (a) and (b) respectively. These contrasting summaries show differing reaction products: (a) shows both 21R and 15R as additional phases whereas (b) shows only the 15R polytypoid as second phase. That 15R and 21R occur at all indicates that deviations from the 3:4 plane have taken place.

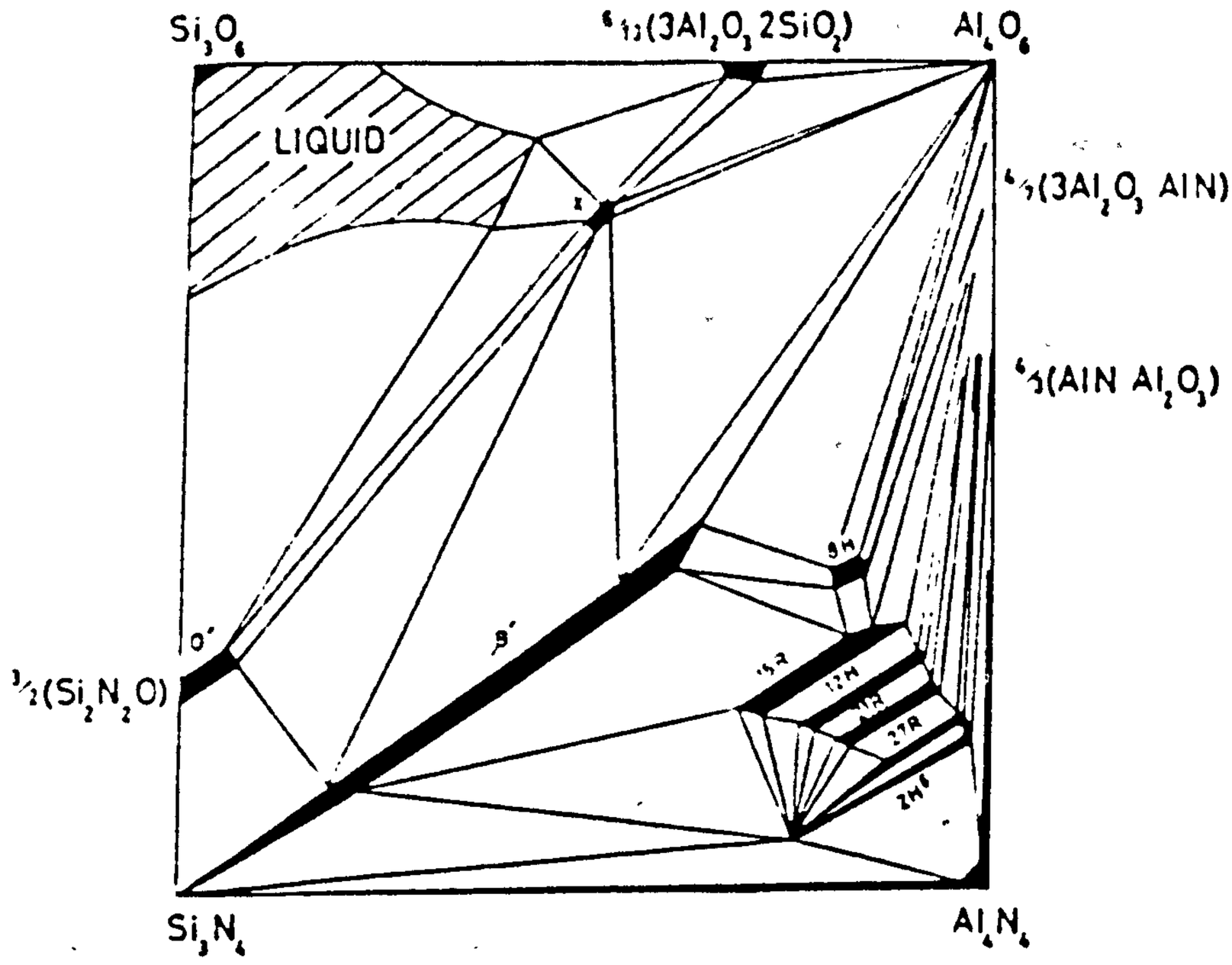

Figure 3: The oxynitride system (after Gauckler et al.[2])

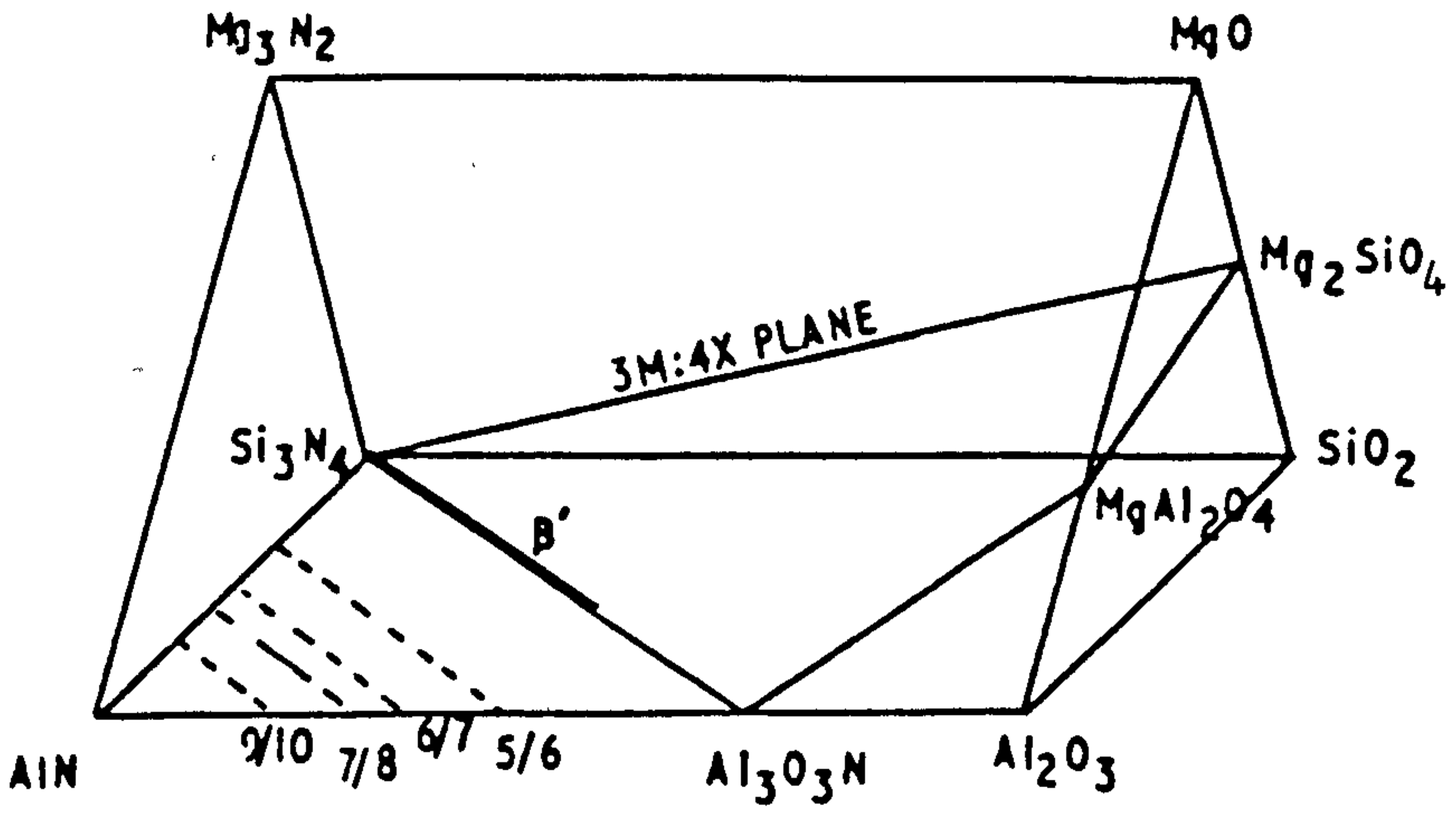

Figure 4: Prism representation of the Mg-SiAlON system.

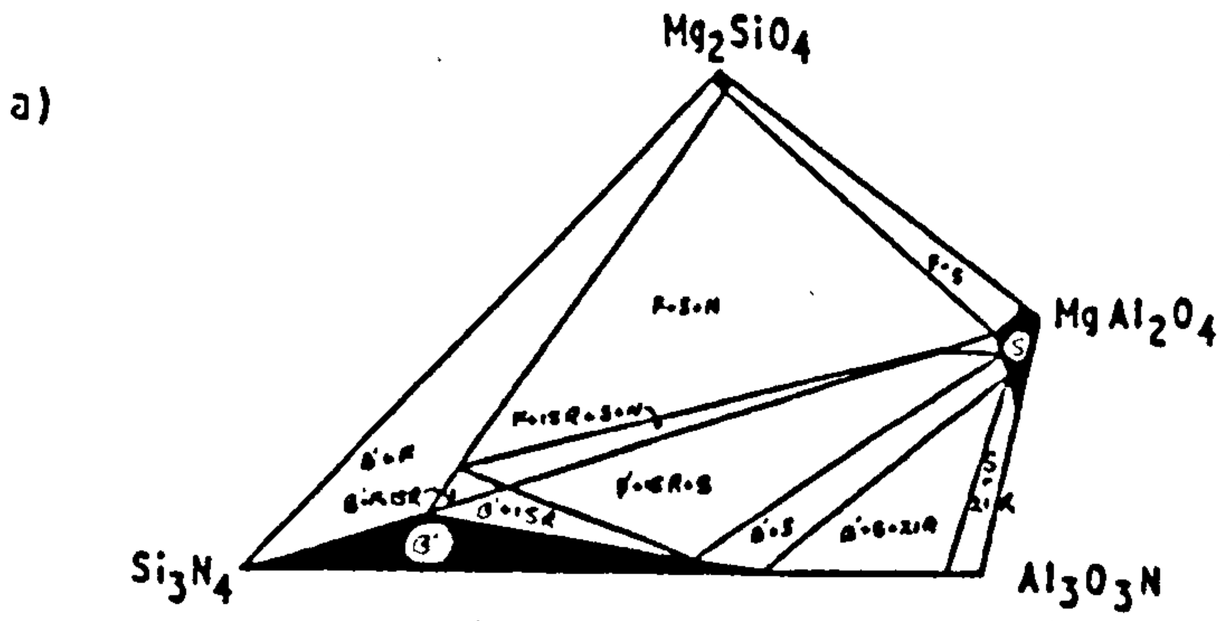

Figure 5: The 3:4 plane of the MgSiAlON system ((a) after Jack[15] and (b) after Tien et al[16]).

Other phases observed included forsterite and spinel, but these are expected. A glass forming region was also observed which is an extension of the ternary oxide eutectic at the edge of the prism. Both these diagrams were produced from results of hot pressing at about 1750°C.

Another discrepancy to arise was the deduction from Tien et al[16] that no magnesium enters the β' lattice. There is conflicting evidence about this. Jack[17] found that up to six weight percent magnesium could be dissolved whereas Hofmann and Gauckler[18] suggested no magnesium could be dissolved. 'Very

little' solubility was also reported[19] and Lewis et al[20] found only a 'small' magnesium solubility when pressureless sintered β' was produced with spinel as the major grain boundary phase. Polytypoid 15R was also found in small amounts as might be expected from the 3:4 plane according to Jack[15]. The experimentally determined z level of z=1 deviated from the predicted z level of z=2 but no explanation was offered[20]. Also the grain size of the β' crystals was much smaller than expected and was stated as being smaller than hot-pressed materials. The densities achieved were quoted as 3.04 to 3.10 g cm^{-3} and compared well with theoretical densities of 3.13 and 3.15 g cm^{-3}.

The beneficial use of yttrium oxide (Y_2O_3) as a sintering aid for the pressureless sintering of nitride ceramics was started by Gazza[21]. He added up to 20 wt% Y_2O_3 to silicon nitride and sintered for short times at 1650°C. Good high temperature modulus of rupture and a density of better than 80% theoretical led him to the conclusion that the use of silicon nitride in gas turbines "was not far away" (1975!). Sintering of SiAlON ceramics with Y_2O_3 by Lewis et al.[22] confirmed the presence of an yttrium alumino silicate liquid phase above 1600°C. A typical sintering schedule was a one hour rise to 1800°C with a one hour "soak" and a 'furnace cool'. The resulting β' had no yttrium within the lattice and the resulting glass matrix was partially crystallized after a prolonged heat-treatment. The main advantage of the yttrium SiAlON's over their magnesium counterparts is due to the higher viscosity of the glassy phase and the ability to crystallize this to more refractory crystalline phases, a topic discussed in the next section.

2.1.3. Glassy Residual Phases and Their Crystallization

The properties of the transient liquid and the residual glassy phases affects both the sinterability and high temperature performance of the ceramic. For good sintering properties low viscosities are required but for good performance the glassy phase must have a high viscosity. The properties of the residual glass form the subject of this section.

The viscosity of the glassy liquids found in various oxynitride systems for a fixed nitrogen content has been found to vary in the order[23]:

$$Mg < Ca < Nd < Y$$

and the transformation temperature (T_g) of these glasses is expected to rise in the same order with a typical value of T_g for the yttrium system of around 920-980°C. Viscosity is also dependent upon (a) the Al_2O_3 content[24], Al_2O_3 rich liquids having the higher viscosities, and (b) the nitrogen content. In 1970 Harding and Ryder[25] noted that T_g of a silicate glass increased with silicon nitride additions. Later Shillito et al[26] found that hardness also increased with nitrogen additions. Loehmann[27] concluded that the glass with the higher nitrogen level could be expected to have a higher T_g and hardness and lower thermal conductivity. The limit of nitrogen solubility has been determined to be between 20 and 25 equivalent percent[28,29].

The dependence of grain boundary phase viscosity as a function of impurity or modifier content has been determined with both low and high temperature strength decreasing with increasing modifier content(30).

The glass forming region for the MgSiAlON system is shown on the ternary oxide diagram and in the prism in Figures 6(a) and (b) respectively. The eutectic for the 3:4 plane is shown in Figure 7.

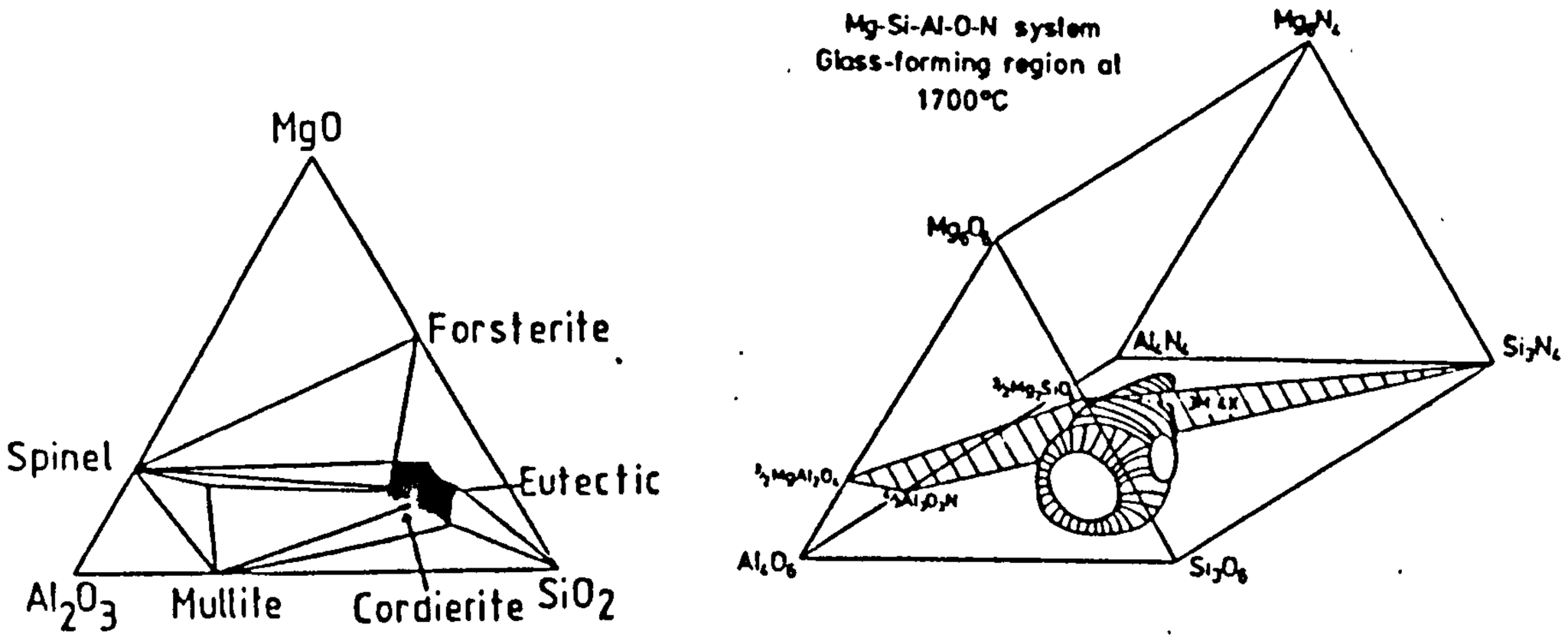

Figure 6: (a) Ternary oxide phase diagram for the $MgO-SiO_2-Al_2O_3$ system(31) and (b) the Mg SiAlON prism showing glass forming region (after Drew et al(23)).

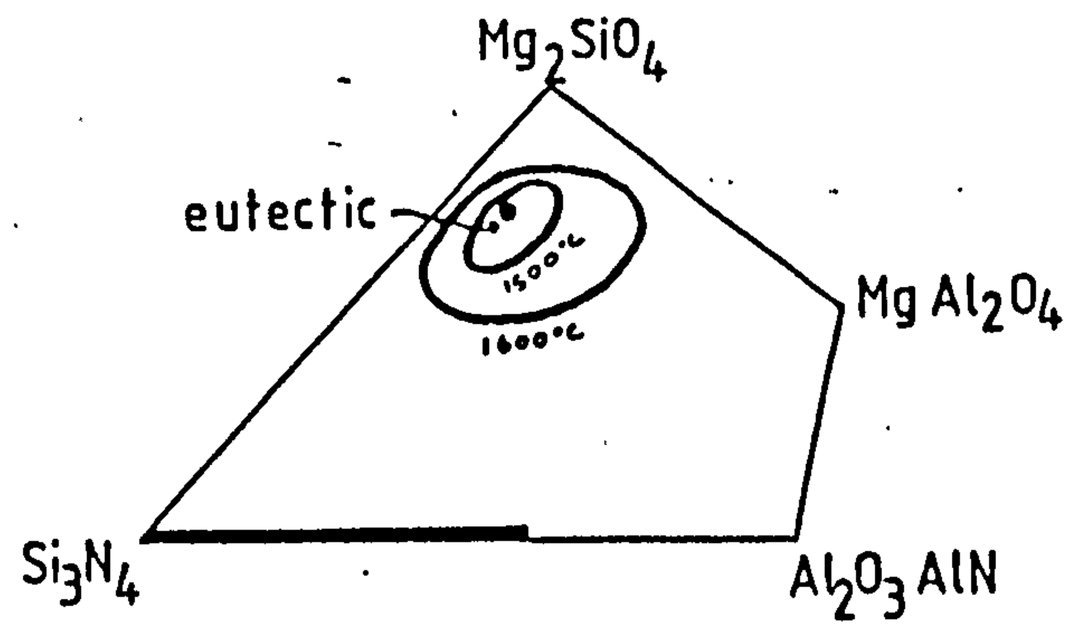

Figure 7: The 3:4 plane showing the glass forming region (after Leng-Ward et al(38)).

The ability to crystallize these glasses has been known for some time[20] The advantage in this has been expressed by Nathan-Katz[32] who deduced that as an estimate the high temperature strength could be doubled if the grain boundary glass was totally crystallized. Raj[33], however, has suggested that this glass may be thermodynamically quite stable in the grain boundary triple point regions. Clarke et al.[34] crystallized a eutectic composition glass (Mg system) to silicon oxynitride and forsterite. The production of the former indicated the presence of nitrogen in the glass (5 At%) but there was no record of a phase increasing in aluminium content. The crystallization of this glass was by standard glass ceramic techniques, namely a nucleation treatment followed by a crystal growth treatment.

It has been found that increasing the aluminium and magnesium concentration of a silicate glass increases the enthalpy of vitrification[35] i.e. it is easier to crystallize. In the MgSiON system the glasses produced required nitrogen to prevent crystallization in the as-sintered condition[36]. It has also been shown[37] that some MgSiAlON glasses could be rapidly quenched to give a dispersion of β and β' crystals. If they were subsequently annealed the resulting crystallization on the β' nuclei produced another phase called β" magnesium SiAlON . It was impossible to crystallize the glass totally and it was suggested that this was due to the presence of impurities, typically calcium[39], being segregated into the glass. There were also deviations of the glass composition with respect to the crystallising β" front. The β" composition forming region lies between the glass forming region on the 3:4 plane and the β' solid solution line. The density of the glasses produced was 2.5-2.7 g cm^{-3}

and a crystallization temperature of between 900°C and 1000°C(37). Both hardness and toughness of silicate glasses increased with increasing nitrogen content, thought to be due to the substitution of divalent oxygen by trivalent nitrogen causing a high cross-linking effect(39).

In the yttrium SiAlONs a suitable heat-treatment can produce refractory phases such as YAG. The reaction, suggested by Lewis et al(20), occurs with a decrease in z level of the β' crystals; this has since been summarized by the equation(23):

$$\underset{(z=1)}{Si_5AlON_7} + YSiAlON = Si_{5+x}Al_{1-x}O_{1-x}N_{7+x} + \underset{(YAG)}{Y_3Al_5O_{12}}$$

The phase relationship is shown in Figure 8, and shows the decreasing z level due to heat-treatment. The glass was assumed to have a near ternary eutectic composition with some additional nitrogen. A typical crystallization temperature was 1400°C. More grain boundary phases are now being produced in this yttrium system, for example N-melilite, N-apatite and N-wollastonite. The advantage that these crystalline phases have is that they can accommodate quite large amounts of calcium and other impurities found in the silicon nitride starting material. These may act as modifiers in the residual glass but major problems can occur with the out diffusion of yttrium in some circumstances.

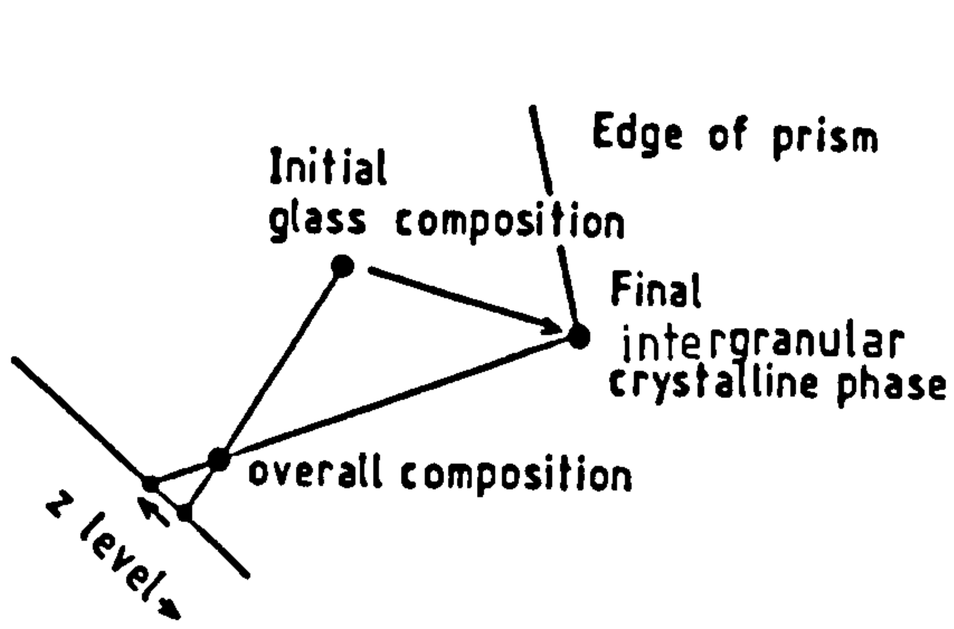

Figure 8: Effect of heat-treatment on z level.

Similar relationships are expected in the magnesium SiAlON system but at a much lower temperature. Phases expected to crystallise include spinel, which would be desirable as it has high hardness and high melting point[40]. Fine grained hot pressed spinel retained its strength to over 1200°C but above this temperature purity played a crucial role. Forsterite has also already been produced by heat-treatment although with its substantially lower hardness it might be less desirable.

To conclude: the high temperature strength of the ceramic requires a sufficiently refractory grain boundary phase which does not impair the beneficial properties of the β' crystal. The use of pressureless sintering to produce commercially viable ceramics may be attained despite having a residual glassy phase on sintering if the glass (a) has a high glass transition temperature or (b) can be crystallised by a post-sintering heat-treatment to produce a more refractory interpenetrating glass ceramic[41,42]. The mechanism by which these materials are sintered is now discussed.

2.2 Liquid Phase Sintering

The interest in nitride ceramics was started after early work by Deeley et al[43]. They achieved high densities after hot pressing with magnesium oxide as sintering aid. Reactions suggested later involved the production of a magnesium silicate type liquid via MgO and surface silica[20][44], through which the α→β transformation had occurred. This transformation is described as a solution-reprecipitation process. It is a special case of the liquid phase

sintering (LPS) mechanism because of phase transformation. LPS is a common route by which many ceramics are thought to densify. Current theories postulate that this occurs in three stages:

Stage I: Immediately after the formation of the liquid phase, primary particle rearrangement occurs. This is an effective densification mechanism and depends upon the amount and viscosity of the liquid[45], particle size, shape distribution and surface roughness as well as the number of particle-particle contacts. The rate of densification decreases once the initial movement has occurred[46]. The mechanism is via liquid bridge formation between the particles. These cluster and migrate together, held by surface tension of the liquid phase. This produces high density areas surrounded by adjacent porosity[47]. The driving force available is too small to close these pores completely[46] since the force required to do so becomes larger as the pores become smaller.

Once the major part of primary rearrangement has been completed Stage II occurs. For this secondary rearrangement to occur the solid particles need to be at least slightly soluble in the liquid phase. At the contact points the solubility is higher than that for other areas and material is transported away from the contact points allowing centre to centre distances to decrease. This process was designated as 'contact flattening' by Kingery[46] and forms the basis for the current theories on sintering mechanisms. Other processes are expected to occur. One of these is shape-accommodated Ostwald ripening[48] shown in Figure 9. Here smaller particles are dissolved and are reprecipitated onto the larger ones. The driving force is due to the decrease in free surface area and densification by a shape-accommodation process.

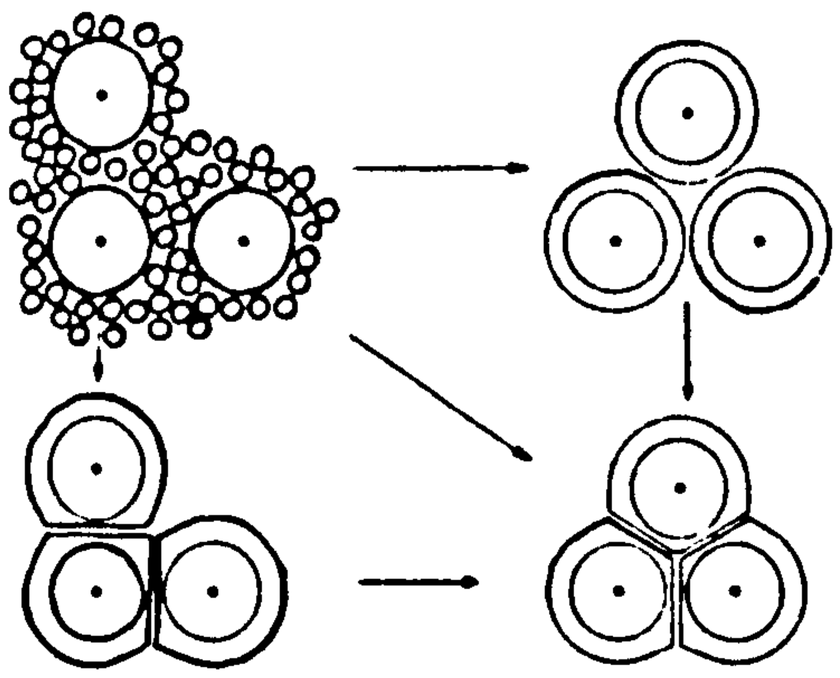

Figure 9: Shrinkage provided by rearrangement due to a shape-accommodated grain growth process.

Although this process has not yet been observed in a ceramic system it has been observed in some metallic systems.

With the nitride system the $\alpha \rightarrow \beta$ phase transformation occurs and appears necessary for high densification[6]. As α is dissolved and reprecipitated as β the processes that occur are more probably an extension of Stage I rather than the idealised contact flattening of Stage II. Once small particles have formed then Ostwald ripening seems an appropriate mechanism to explain grain growth.

The final stage of the sintering process, Stage III, often called coalescence or closed pore elimination, operates by other diffusion mechanisms but is not observed in pressureless sintering.

For complete $\alpha \rightarrow \beta$ transformation and closed pore elimination, hot pressing[49] is required for an optimum time[50] .

The mechanisms above apply to both pressureless sintering and hot pressing, but in hot pressing stage I is over too fast to be observed. Rapid densification was found to occur between 1500°C and 1600°C[51].

In pressureless sintering high viscosities at low temperatures can cause these mechanisms to proceed slowly. The activation energy for sintering could be expected to decrease with increasing temperature if it was dependent upon the liquid viscosity (Kingery model). The fact that the activation energy remains reasonably constant[52] at about 600 $kJmol^{-1}$ and a very rapid grain growth, reported by Lewis et al[20], indicates the presence of a process with a large driving force. This might be the phase transformation $\alpha \rightarrow \beta$[51] (or β').

The sintering of β' ceramics using either magnesium oxide or yttrium oxide as sintering aid to provide a liquid phase, has been studied by Hampshire and Jack[53]. With magnesium oxide the initial liquid formation occurred at 1390°C, which corresponds well to the ternary oxide eutectic of 1355°C, and sintering occurred at 1600°C. This produced a "fully" dense but only partially transformed β ceramic. With Y_2O_3 total $\alpha \rightarrow \beta$ transformation occurred but only partial densification. The results were described as solution control for the magnesium system (i.e. the rate determining step was solution into and dissolution out of the transient liquids) and diffusion control for the yttrium system (i.e. the rate determining step was diffusion through the liquid phase). Both systems were said to agree with the Kingery model. Messier et al[6] found contradicting results i.e. very little $\alpha \rightarrow \beta$ transformation occured when using Y_2O_3 at 1600°C, and

magnesium oxide was needed for complete transformation at these temperatures.

Thus the $\alpha \rightarrow \beta$ transformation is very important in achieving dense β or β' ceramic although it has not yet been fully explained.

2.3 Oxidation Problems in Nitride Ceramics

2.3.1 Reactions

Nitride ceramics are in general inherently unstable in oxidising environments. Passive oxidation of silicon nitride occurs between 1000° and 1400°C by the following reaction[54]:-

$$Si_3N_4 + 3O_2 \rightarrow 3SiO_2(s) + 2N_{2(g)}$$

This occurs with a thin intermediate film of silicon oxynitride (Si_2N_2O) which also forms along the grain boundaries and forms a rapid diffusion path for oxygen[55]. To help stop such a reaction which also occurs during sintering, nitride ceramics are usually sintered under a nitrogen atmosphere[56,57], which allows higher temperatures to be used and hence higher densities achieved. Another reaction found during sintering is[58]:-

$$Si_3N_4 \xrightarrow{1700^oC} 3Si(l) + 2N_2(g)$$

To help stop this reaction Raj and Baik[59] suggested "adding a few extra weight % Si" and high densities were achieved using such methods.

The reactions of silicon nitride are summarised below:-

$$2Si_3N_4 + 3Al_2O_3 \xrightarrow{1750^\circ C} 3Al_2O_{(g)} + 6SiO_{(g)} + 4N_{2(g)}$$

(after Kuwabara et al (58)).

$$Si_3N_4 + 1.5O_2 \xrightarrow{1750^\circ C} 3\ SiO_{(g)} + 2N_{2(g)}$$

$$Si_3N_4 + 3SiO_2 \xrightarrow{1850^\circ C} 6\ SiO_{(g)} + 2N_{2(g)}$$

(after Lange (60)).

$$Si_3N_4 \xrightarrow{MgSiON} Si_2N_2O$$

1300-1400°C

(after Tsai and Raj (61))

Multiphase oxidation scales occur in both hot pressed silicon nitride and pressureless sintered SiAlONs. The oxidation resistance is highly dependent upon the nature and quantity of the sintering aid and follows the sequence yttria > ceria > magnesia, due to the viscosity and degree of crystallinity of the grain boundary phase[62,63].

Lewis and Barnard[64] suggested that the advantage of hot pressed SiAlON over silicon nitride was the higher viscosity due to the higher alumina levels, as well as production of mullite on the surface. A reaction was suggested as:

$$4\ Si_5AlON_7 + 21O_2 \rightarrow \underline{20SiO_2 + 2Al_2O_3} + 14N_2(g)$$

as a protective mullite layer

Using magnesium oxide as a sintering aid to silicon nitride, one reaction product was forsterite as a grain boundary phase. This did

not oxidise further itself but reacted with SiO_2 to form enstatite ($MgSiO_3$)[65]. The formation of intermediate compounds which then react with the β', has been suggested as a major problem as these can occur below the oxide layer[66].

2.3.2 Reaction Mechanisms

Current theories for the rate controlling process include the inward diffusion of oxygen and the outward diffusion of metallic cations (Mg^{2+} or Y^{3+}) found in the grain boundary phases in the sub-surface material[64]. Oxidation of some pressureless sintered SiAlONs that have YAG as an intergranular phase can produce a porous yttrium silicate layer with no "stabilized" zone. This is due to the large amounts of yttrium available to diffuse outwards, and thus there is little defence against oxidation.

The activation energy for oxidation of MgO additive materials is reasonably constant between 380 kJ mol^{-1} and 430 kJ mol^{-1} whereas for the yttria materials there is a much wider range, between 260 kJ mol^{-1} and 623 kJ mol^{-1}[67].

Generally the reactions rely on the fact that the metal cation Mg^{2+} or Y^{3+} is the rate determining species due to its migration through the grain boundaries or through the surface to produce an oxide layer. Over-saturation of these species in the grain boundary phase is therefore to be avoided[68]. Clarke and Lange[65] suggested a reaction couple between SiO_2 forming on the surface and the interior glassy or partially crystallised grain boundary phases. The inward diffusion of oxygen ions as the rate determining species was excluded on the grounds that oxidation was independent of oxygen

partial pressure[54,58]. Shaeffer[69] suggested that this might not be the case. The diffusion rates of oxygen ions or molecules in a MgO containing glass was not dependent upon pO_2 but the activation energy measured for this process was thought to be high enough to be rate controlling.

Parabolic reaction kinetics have usually been observed and hence oxidation resistance improves as the reaction proceeds. Desmaison et al[70] have suggested an intermediate rate (between parabolic and linear) for single phase SiAlON with the reaction occurring as:

$$Si_{(6-z)}Al_zO_zN_{(8-z)} + (6-\tfrac{1}{2}z)O_2 \rightarrow 6-zSiO_2 + z/2\ Al_2O_3 + \frac{8-z}{2}\ N_{2(g)}$$

The nitrogen evolved caused the oxide layer to be porous and therefore not totally protective. Typical reaction temperatures were between 1400 and 1600°C. The rate controlling species in these cases was the diffusion of oxygen through the alumino silicate glass film[66]. The reactions took place at the SiAlON-silicate interface rather than the silicate-air interface. They concluded that the oxidation rate was a function of the nature and composition of the surface oxide layer (governed by z level of β') rather than the amount and composition of the grain boundary phase.

Knowing that magnesium oxide additive materials are easier to sinter and yttrium oxide additive materials produce higher oxidation resistance materials, Babini and Vincinzini[71] hot-pressed material with both MgO + Y_2O_3. This produced a sinterable material with high oxidation resistance to 1150°C. Up to this temperature the

material's oxidation resistance approached that of the Y_2O_3 additive material. Above this temperature the oxidation rates were similar to MgO HPSN (hot-pressed silicon nitride). This material appears to be the best compromise available.

To summarise: most authors agree that the rate determining process is the diffusion of the additive or impurity through the grain boundary or surface oxide scale, and that parabolic kinetics are observed for most systems containing a sintering aid.

Increasing the magnesia level decreases the oxidation resistance because of the production of more low viscosity silicate phases. With yttrium additive systems several crystalline phases can be produced which minimise cation diffusion. Hence increases in yttria, which would be necessary for easier sintering, are not as critical.

2.4 Mechanical Properties

2.4.1 Fracture toughness

As stated in Chapter One, ceramic materials have only rarely been used in engineering applications although they are now being used in more general applications. The main drawback is due to the fact that these materials are brittle and this is aggravated by the presence of flaws. Because of the nature of the flaws' size distribution ceramics exhibit a wide variation in strength. The approach taken in the present work, to give a better understanding of the mechanism of fracture, involves the determination of the fracture toughness of the material via fracture mechanics.

Fracture mechanics arose to try to explain the increasing number of fractures of engineering components which had been designed using the concept of critical applied stress i.e. to ensure the component did not fail one had to keep the applied stress below the limit

determined for that material. Early in this century Inglis[72] had shown that in a notched plate which was stressed, the stresses around the tip of the notch rose to several times the applied stress and he developed formulae to describe this. Griffiths[73] used these formulae and derived a criterion for the extension of a crack under an applied load in terms of a reversible thermodynamic process. This work which led to the entire field of fracture mechanics is summarized below:

For a static crack:

$$\Delta U = (-W_L + U_E) + U_S$$

1 2

ΔU = Free energy of the system

W_L = Work done by applied load

U_S = Stored strain energy

U_E = Surface energy of new crack surfaces

Thermodynamic equilibrium is attained by balancing the mechanical and surface energy (terms (1) + (2)) over a crack extension: term (1) favours crack extension, term (2) opposes it. This is the 'Griffiths energy balance concept' and at equilibrium $\Delta U = 0$. For the case of a narrow crack under plane tensile stress conditions:

$$\sigma_c = \sqrt{\frac{2\gamma E}{\pi c}}$$

where γ = surface energy

E = Young's modulus

c = crack length

σ_c = critical stress

As this is a maximum at equilibrium the crack is unstable and if the applied stress > critical stress the crack is free to propagate spontaneously without limit. The critical applied stress is thus

dependent upon crack length. Griffiths then proved the existence of small cracks or flaws in glass and their nucleation on ageing. Work in the 1950's by Irwin[74] further developed the study of fracture and defined two parameters:

(i) in terms of energy G_C, the critical energy release rate and

(ii) in terms of intensification of stress ahead of the crack tip, defined as the stress intensity factor (K) where;

$$K = \sigma y\sqrt{c}$$

and σ is the remotely applied load

y is a constant dependent upon loading and crack configuration.

The maximum stress intensification occurs around the dominant or critical flaw. The value of K a material can withstand before catastrophic failure occurs is called the critical stress intensity factor, K_C or fracture toughness.

To remove doubt about the size of the dominant pre-existing flaw a new dominant flaw of known dimensions is introduced to the specimen. At present two methods are in use:

(a) cutting of a sharp deep notch in the edge of a rectangular cross section bar by a diamond edged saw, called a single edged notch beam (SENB) test or

(b) the indenting of the material with a diamond indentor (often a Vickers diamond as used for hardness testing)

In the SENB test there are constraints on the dimension of the specimen and the notch. This follows from early work on fracture toughness testing by Brown and Srawley[75], and, despite the fact that the formulae were derived from tests involving large steel or aluminium alloy test pieces, the use of these formulae on small

ceramic bars is permissible since there is a very small plastic stress field around the large and dominant flaw. The limiting size of specimen width has been represented as (75):-

$$B > 2.5 \left(\frac{K_C}{\sigma_y}\right)^2$$

where B is the specimen thickness, σ_y the yield stress and K_C the fracture toughness. Standard specimen dimensions were used and these are shown in Chapter Five. The equation used to calculate fracture toughness is that used by Smith and Piper[76] and is also quoted in Chapter Five. This formula is more flexible in specimen and crack dimensions, producing a narrower range of K_C values[77] than some other formulae[75, 78, 79].

In the indentation method there are two procedures to calculate K_C:

(a) The first method[80] involves measurement of the crack dimensions after indentation under a known load. The hardness and fracture toughness are functions of the load and the dimensions of the plastic region (a and c) shown in Figure 10. This method gives large numbers of results per sample but the drawback is the difficulty of measuring the radial cracks accurately. A good 'optical finish' is required with final polishing using at least a 1 μm diamond paste.

(b) The second method uses the radial crack system (shown in Figure 10) as a dominant flaw[81]. The bar is then broken as in the SENB test (the formulae for this method[82,83] are given in Chapter Five). The dimensions of the bar for this method are similar to those used for the SENB test.

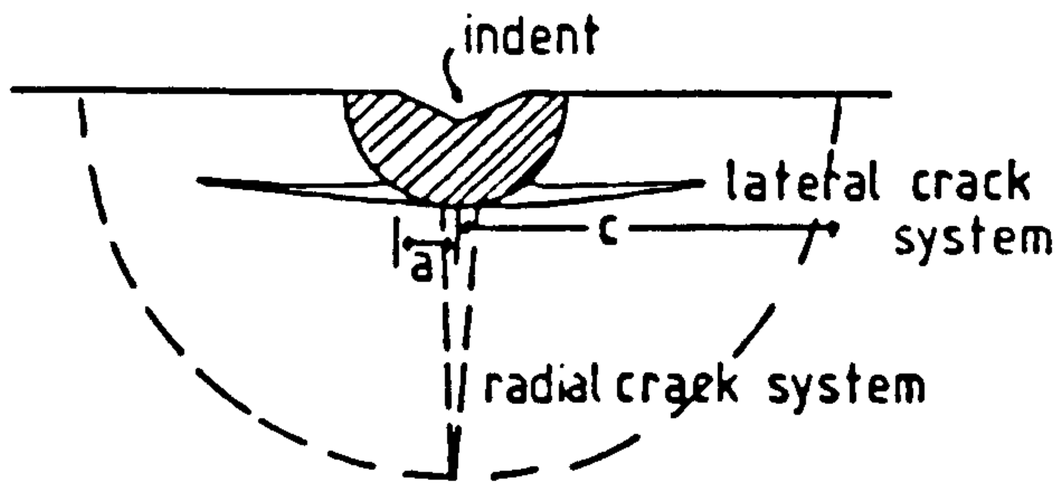

Figure 10: The crack system initiated by indenting the material.

This test has the same disadvantage as the SENB method; that only one result per bar is usually obtained. Indenting the material before or after polishing can affect the fracture toughness. Kc can appear to increase if the indent was prior to polishing(84) or to decrease if it was afterwards(85). The results were interpreted in terms of residual compressive stresses in the outer layers of the test bars due to machining damage caused by coarse polishing. The degree of polishing required to remove such a layer is of the order of 100μm. If tests are conducted after this treatment similar results are achieved although the indentation method still gives values of Kc lower by a factor of 1.4 then those obtained by the SENB method(86).

Typical values of Kc are greater than 30 $MPam^{-\frac{1}{2}}$(87) for steels and between 7-9 $MPam^{-\frac{1}{2}}$ for pressureless sintered multiphase SiAlONs with YAG and silicon oxynitride as grain boundary phases(85). Single phase hot pressed SiAlONs have a Kc around 3-4 $MPam^{-\frac{1}{2}}$ whilst Mg SiAlONs

have K_C between 3-3.5 $MPam^{-\frac{1}{2}}$(89). Hot-pressed silicon nitride has a K_C of 4-5 $MPam^{-\frac{1}{2}}$(90,91). Polycrystalline spinel has a K_C of between 1.1 and 1.9 $MPam^{-\frac{1}{2}}$(92). Glasses have a K_C typically less than 1 $MPam^{-\frac{1}{2}}$ although this increases to 2.5 $MPam^{-\frac{1}{2}}$ for glass ceramics(93). Values of K_C for Mg SiAlON glasses (with nitrogen) have been put at between 1.1 to 1.5 $MPam^{-\frac{1}{2}}$(49).

2.4.2 Factors Effecting K_C

One parameter that could affect K_C is the grain size of the material. There have been reports of K_C increasing, decreasing, or being independent of grain size(94). The test technique is another important parameter(95) as is the need for a precise bending rig, suggested by Hoagland et al(96). Porosity can also increase or decrease K_C, the important parameter here is the size of pores when compared to the grain diameter(97). Large pores reduce K_C, as expected, but very small pores can act as crack stoppers and increase K_C slightly. A high aspect ratio (length/width) of the β' grains can produce a fine grained interlocking morphology resulting in a high K_C(98). Bowen and Carruthers(99) suggest that as the β' crystals are elongated some must lie perpendicular to the stressing axis as shown in Figure 11.

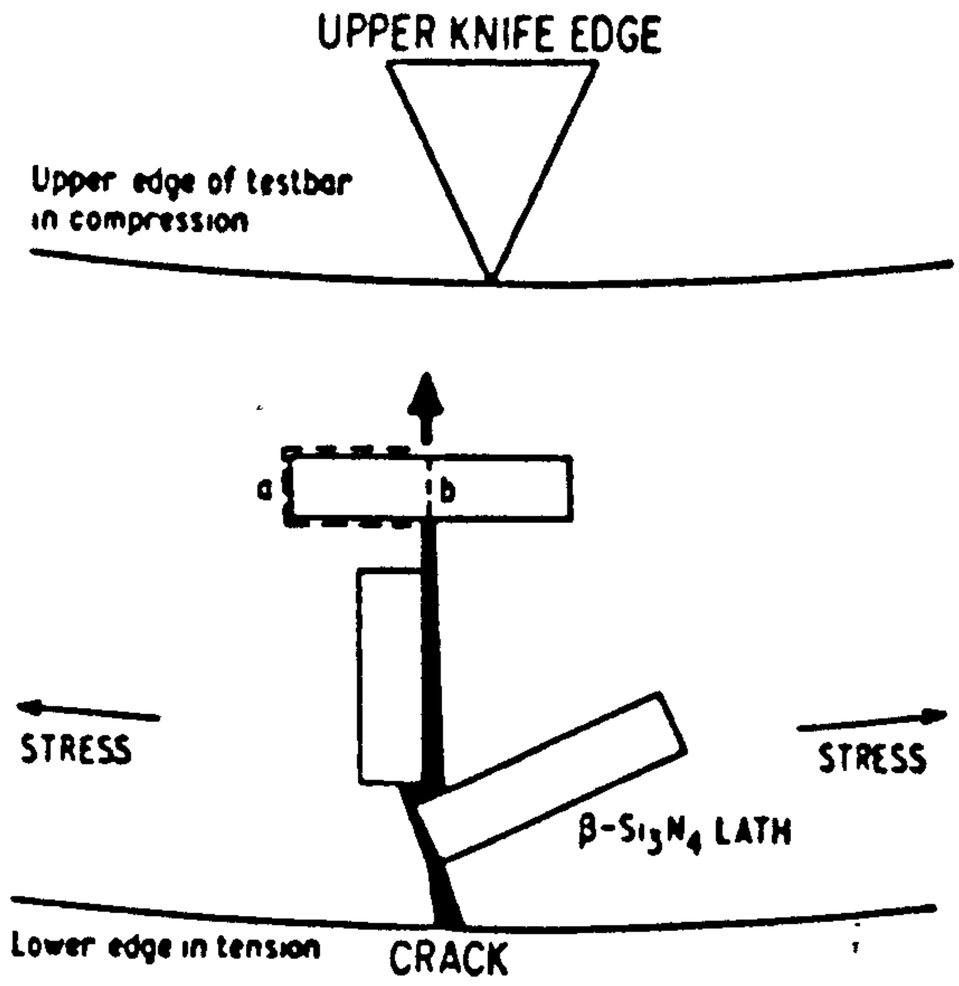

Figure 11: Effect of interlocking grains on crack propagation.

(after Bowen and Carruthers[99])

The crack propagates either (a) parallel to the applied stress, which is unfavourable energetically or (b) through the grain. Both routes increase K_C. Kirchner et al[100] concludes that a high K_C material requires a large percentage of intergranular fracture. This is because initially cracks extend from flaws by transgranular fracture but as the crack grows there is insufficient time for transgranular fracture so the crack is forced to find another path. Pure intergranular fracture is prevented, probably due to the above reasons, so what usually happens is that a fracture surface of hummocks and depressions is formed as the crack avoids resistant agglomerates.

To achieve high strength ceramics the production of lath-like β' crystals is required and this is achieved by using a high α% silicon nitride starting powder. If a high β% silicon nitride is used, equiaxed grains result with a corresponding lower fracture strength[101]. The amount of glassy phase is important although Caval et al.[102] suggest that a thin residue would not diminish the strength and this strength could remain up to high temperatures[103]. A thin glass residual film would be the best compromise of sinterability and good high temperature fracture toughness.

2.4.3. Creep

The time-dependent plastic deformation produced by the action of a constant load or stress, which is often considerably less than the yield stress, is called "creep". This occurs in ceramics mainly at high temperatures i.e. $>.5T_{melting}$, and usually follows the normal form which has been accepted for metals.

Upon the application of a suitable load an instantaneous strain results leading to a three stage process. The primary stage exhibits a decreasing creep rate, due to viscoelastic effects. The secondary stage follows this and is characterised by a constant creep rate and is often called steady state creep; this then leads to the final stage. Here the creep rate accelerates until the material fails, this stage is called ternary creep. There are various forms of creep curves[104] and some may have one stage missing completely or very much reduced. This is usually the case for primary creep which can be small compared to steady state creep which sometimes extends for long times before failure. It is in this steady state region of the creep curve that better understanding of the creep mechanisms is required.

The relationship used to describe steady state creep[104] is given in its simplified form below[105]:

$$\dot{\varepsilon} = A(1/d)^{p}\sigma^{n}\exp(^{-Q}/_{RT})$$

where $\dot{\varepsilon}$ = creep (strain) rate

d = grain size

R = gas constant

T = temperature

Q = activation energy

A = a constant

σ = stress

n and p are exponents by which the mechanism of creep is identified

2.4.4. Creep Mechanisms

Creep mechanisms can be identified using microscopy together with the value of exponent n determined via creep rate experimentation. For nitride ceramics containing a glassy phase the high temperature performance is dominated by the properties of this viscous layer separating the silicon nitride grains. If this layer is thick then Newtonian or viscous flow could be observed, and for this mechanism n=1. If the viscous layer is thin then irregularities present on the nitride grains can interfere; this leads to mechanisms which are identified by a value of $n > 1$[105]. These grain boundary phases are very important in nitride ceramics produced via LPS due to the production of partially crystallised grain boundary phases. If deformation of the major crystalline nitride phase occurs on creep

then the process is termed Lifshitz sliding[106], but if not the process is termed Rachlinger sliding[107]. Lifshitz sliding can include the process where diffusion of material is through the crystal lattice by vacancy movement, called Nabarro-Herring creep[108] or if the movement of material is along grain boundaries the process is called Coble creep[109]. Rachlinger sliding[107] can occur with a continuous glassy second phase in which cavity formation occurs and the process is dependent upon the viscosity of this grain boundary phase, see Figure 12. Also Rachlinger sliding can occur with dislocation movement along or adjacent to the grain boundaries. This can cause opening of cavities and is important with the smaller grain ceramics since $\varepsilon \alpha \sigma^2$ i.e. n=2[110].

Other processes in glass containing materials include the role of solution- reprecipitation. Tsai and Raj[111] have suggested that as the activation energies are similar for creep and sintering, similar processes are likely in both cases. They concluded that material movement along grain boundaries might occur, lengthening and narrowing the β' crystal in the direction of the tensile stresses.

The increase in creep resistance after a suitable annealing treatment is shown for both hot-pressed and pressureless sintered ceramics in Figure 13. The hot-pressed SiAlON has been annealed for 950 hrs at 1400^{o}C which has allowed glassy phase impurities to diffuse to the surface or into the β' crystals[112]. The creep rate is two orders of magnitude less after this treatment and n changes from n=1.6 (cavitating) to n=1 (diffusional Coble creep). There is also a change in activation energy Q from 430 kJ mol^{-1} to 840 kJ mol^{-1}. Pressureless sintering biphase yttrium SiAlONs can produce crystalline grain boundary phases of yttrium disilicate, if the glass has a low nitrogen content, or yttrium aluminium garnet (YAG) if the

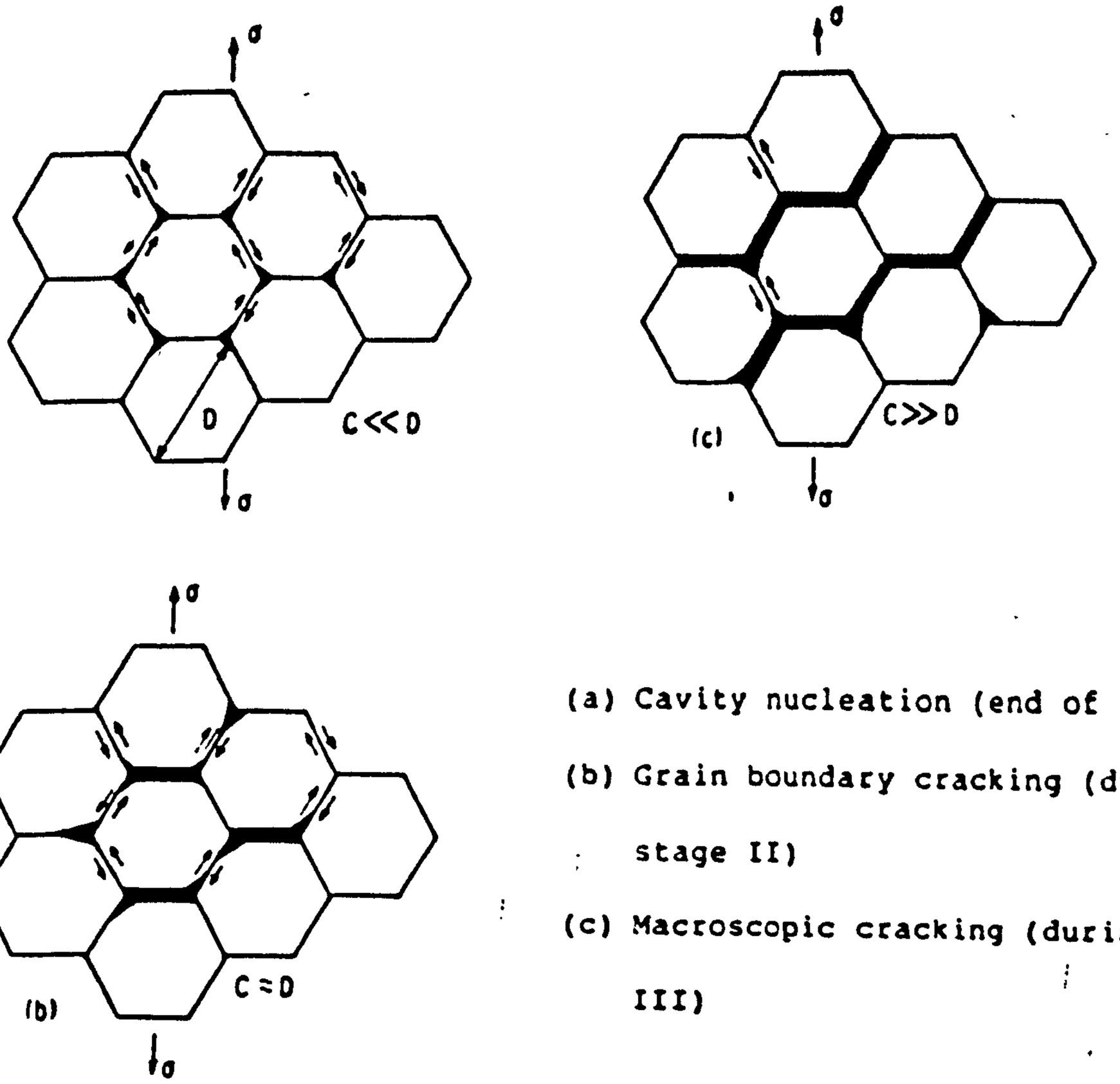

(a) Cavity nucleation (end of stage I)

(b) Grain boundary cracking (during stage II)

(c) Macroscopic cracking (during stage III)

Figure 12: The progression of cavity growth caused by non-accommodating deformation with grain boundary sliding. (after Kossowsky et al[107])

glass has a high nitrogen content[88]. The creep rate of both these ceramics is also shown in Figure 13 along with that achieved after a prolonged heat-treatment of the YAG containing ceramics.

The effect of the heat treatment on the YAG containing ceramics is two fold: (a) in the bulk of the material there is a decrease in z level of the β' phase, grain growth occurs and the YAG becomes isolated in the grain boundary triple point and (b) at the surface YAG remelts and yttrium diffuses outwards enabling silicon oxynitride (Si_2N_2O) to crystallise along the grain boundaries. This increases oxidation and creep resistance. Q for such materials is of the order 800-900 kJ mol^{-1} i.e. the same order as that for hot pressed SiAlON which was found earlier. The upper temperature limit for these biphase SiAlONs is of the order of 1300°C, with the limit for lower nitrogen containing ceramics below this.

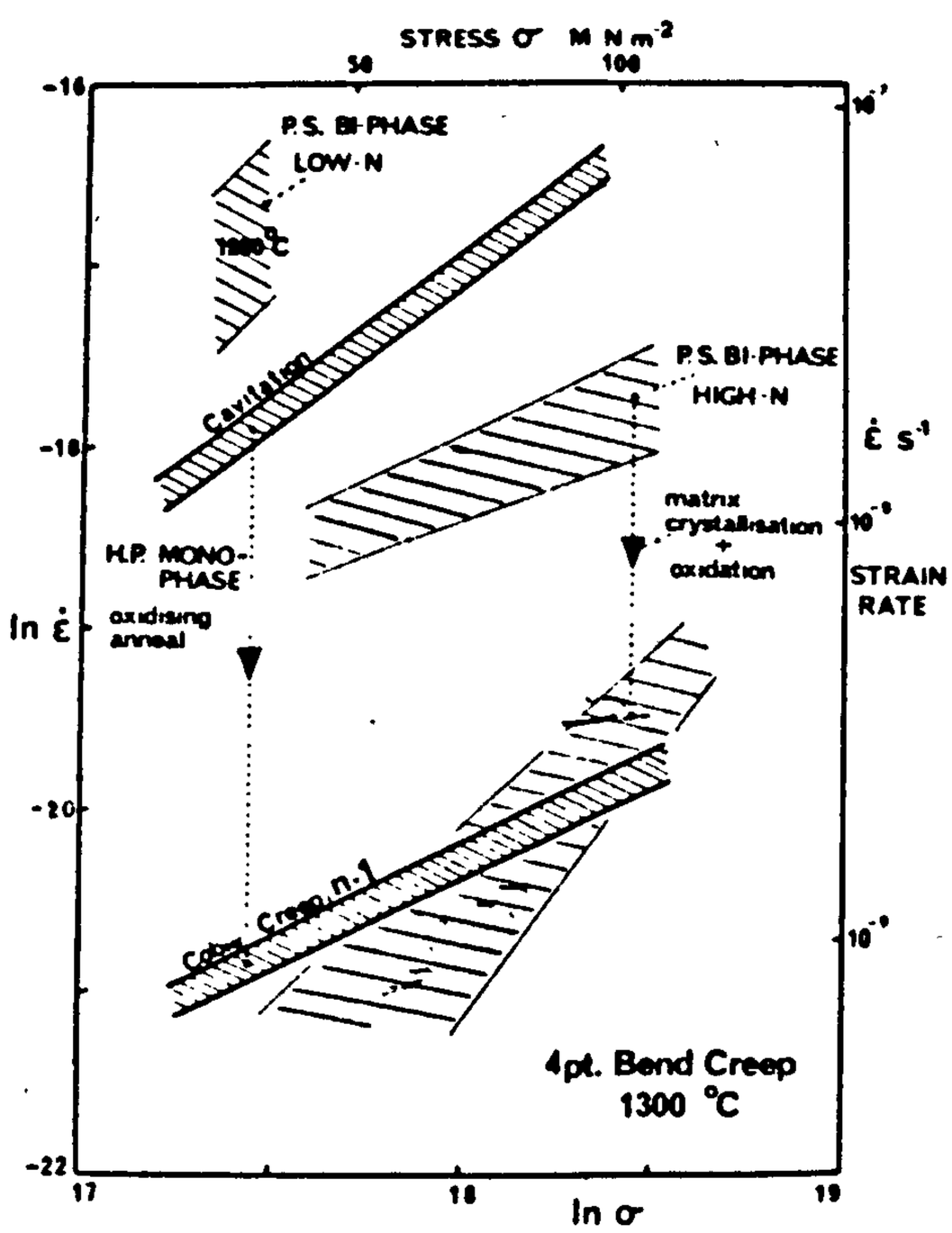

Figure 13: Creep data for both hot-pressed SiAlON (after Karunaratne and Lewis[112]) and pressureless sintered biphase SiAlON (after Lewis et al[88]) showing the effect of heat treatment on creep rates.

The creep mechanisms and data for ceramics described as being in the as-sintered condition should be taken as less reliable than those for heat treated ceramics since the annealing process will be present during creep testing. The grain boundary glassy phases may be crystallizing and this may result in a continuously changing mechanism, and hence creep rate. Indeed no mechanism for the low nitrogen containing SiAlON was suggested since the creep rate was high at a temperature as low as 1260°C. For the high nitrogen content ceramics the mechanism for the as sintered ceramic was viscous flow and after a prolonged heat treatment a Coble creep mechanism was considered to be due to the high value of Q determined (no value of n was reported).

Values of Q found by Kossowsky et al[107] are of the order of 500 kJ mol^{-1} for hot-pressed silicon nitride and as this agreed with the value of Q for viscous flow in silicate glasses, it led them to the conclusion that this glassy phase determined the creep properties.

To summarise:

(a) The $\alpha \rightarrow \beta$ transformation is important in producing dense β or β' material although it is not fully understood.

(b) In the MgSiAlON ceramic system early workers found different reaction products on the 3:4 plane, including phases not expected to be found on the plane.

(c) In pressureless sintered material, the initial liquid is expected to have the composition of the ternary oxide. For the MgSiAlON system this is expected to lead to easier (lower temperature) sintering although it is also envisaged that they have a lower working temperature.

(d) Heat-treatment of SiAlON ceramics has led to a distinct improvement in creep and oxidation resistance. This is due to grain boundary glass crystallisation, a consequence of this is a slight change of substitution level of the β' phase.

The aim of this work is to produce Mg SiAlON ceramics with z in the range $0 < z < 4$ which after suitable heat treatment would be subjected to creep testing. The MgSiAlONs would form an alternative system to the more widely used yttrium SiAlONs and might have the advantage of easier sintering and therefore be cheaper to produce. The sintering of these ceramics is the subject of the next chapter.

CHAPTER THREE

SINTERING TECHNIQUES AND MECHANISMS

This chapter describes the formation of β' ceramics by pressureless sintering using magnesium oxide as a sintering aid. Reactions that may occur during sintering are suggested and parameters that affect the resulting density are discussed including the α-β transformation.

3.1 Powder Preparation and the Sintering Procedure

The starting materials used are listed in Table 2. They were mixed in appropriate amounts to produce a range of ceramics of known composition on sintering. Each ceramic is composed of a primary phase of β' crystals with predicted substitution (z) level and a specific amount (15 wt%) of spinel as the final matrix or grain boundary phase assuming total crystallization had occurred. The compositions (see Appendix 1) formed a series on the 3:4 plane of the MgSiAlON system and this is shown in Figure 14.

STARTING POWDER	MANUFACTURER	PARTICLE SIZE	PURITY
αSi_3N_4	H.C. Starck, Berlin	3μm	.4% O .04% Fe .006% Al .03% Cu .1% Free Si
AlN	Koch Light Labs	4μm	.05% C (No other details available)
αAl_2O_3	B.D.H.	10μm	.005% Fe, Cl, SO
MgO	B.D.H.	6μm	.5% CO .03% Fe, Cl, NO .2% Na
$SiAl_6N_6O_2$ 2IR Polytypoid	Lucas Cookson Syalon	6μm	some Al O , AlN, and Si N present

Table 2 - Details of starting powders

To achieve submicron particle size the mixture was milled in isopropyl alcohol using high purity alumina balls (i.e. wet ball milling) for six hours. This had previously been found to be sufficient to produce a thoroughly mixed submicron grain size powder. Particle sizes were determined by scanning electron microscopy of a dispersion of the milled powder on a carbon support film using amyl acetate as a transfer medium.

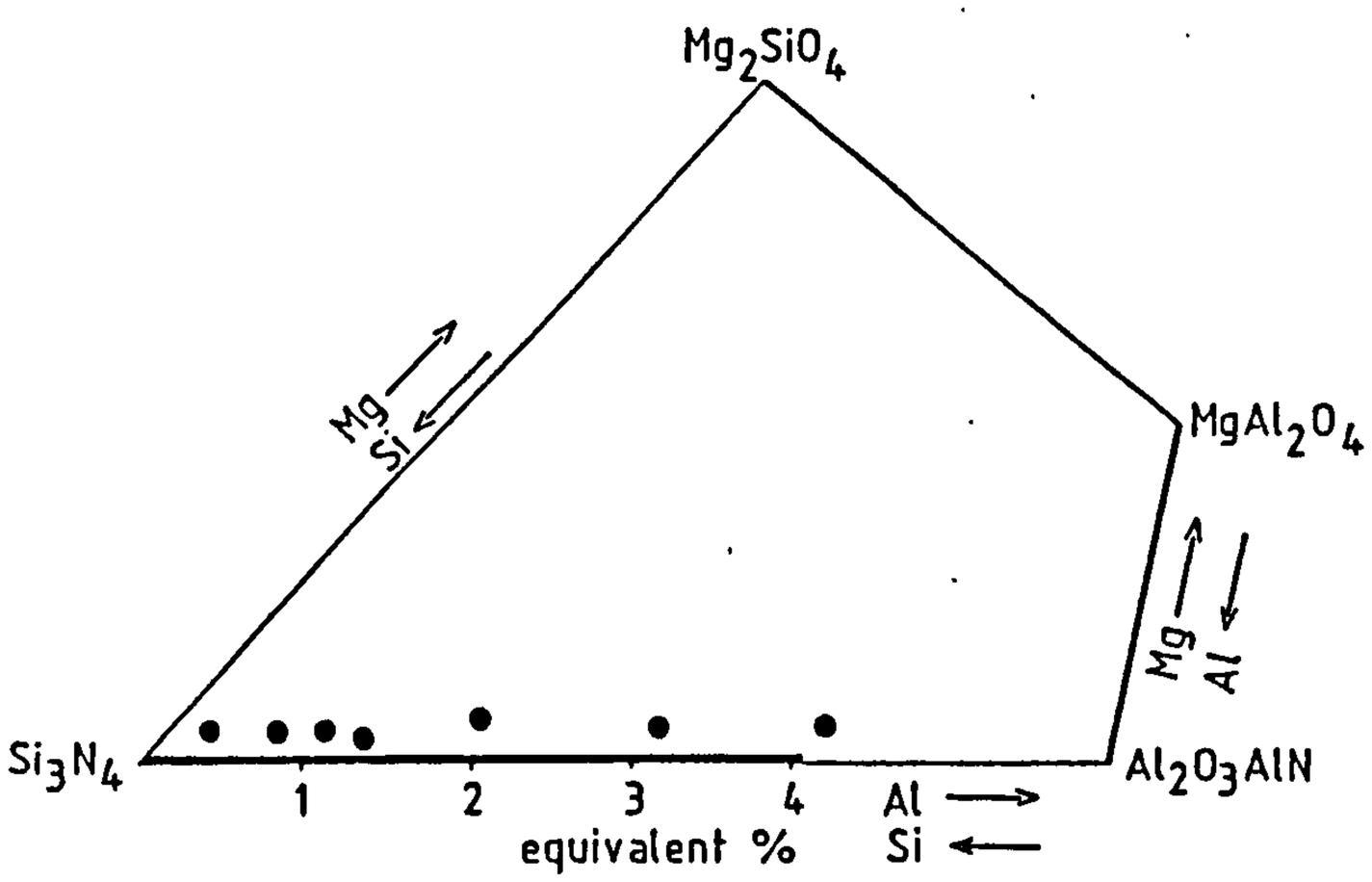

Figure 14: Initial ceramics compositions projected onto the 3:4 MgSiAlON plane.

The grinding medium for a 100 g charge was approximately 2 kg of 6.25 mm diameter alumina (Al_2O_3) balls. During the milling operation some wear of the medium took place. This was monitored by weighing before and after milling and an appropriate amount was subtracted from the quantity of alumina in the compositions to account for the contamination.

The milled powder was sieved to remove the larger debris, i.e. broken alumina balls which were included in the above monitoring, and then tray-dried. The large quantity of alcohol used in the milling operation was evaporated and collected for re-use. The dried powder 'cake' was then broken up and resieved using a 35 μm aperture sieve, ready for pressing.

Powder pressing was initially carried out on a single acting die. This could produce rectangular billets of approximately 55% relative density (where relative density = $\frac{\text{experimental density}}{\text{theoretical density}} \times 100$)

which was comparable to that produced by isostatic pressing. Large amounts of material were wasted due to pressing cracks which sometimes appeared only after sintering. Also approximately one hour was needed to press a billet so use of the die was limited. Isostatic pressing to produce rods (at Lucas Cookson-Syalon), was preferred.

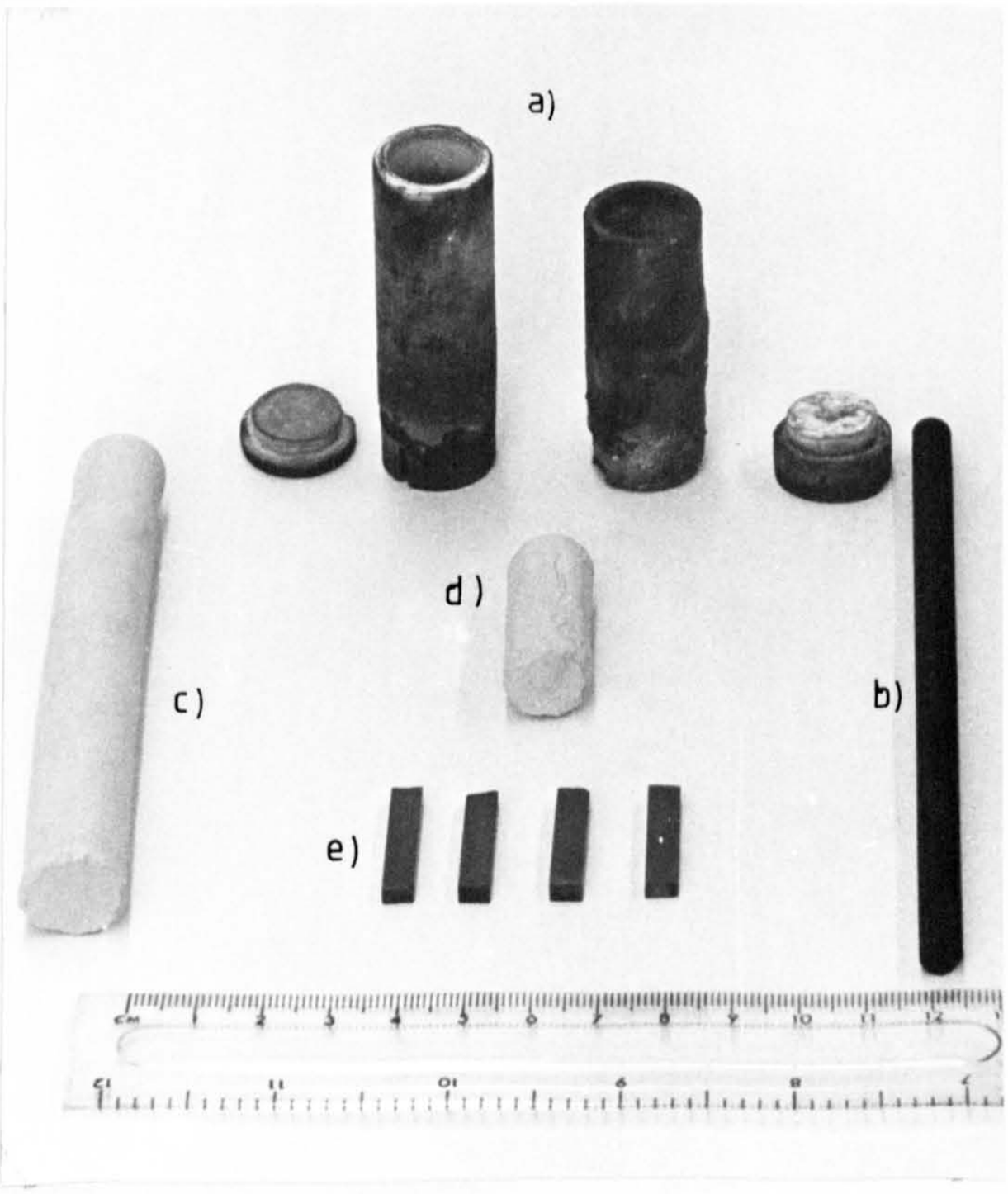

(a) crucible

(b) support rod

(c) pressed rod

(d) sintered billet

(e) machined as-sintered ceramic

Figure 15: Sintering components and products

The pressed rods were cut to form several billets and after sintering each of these was cut to form several bars of size 5 x 3 x 25 mm or 3 x 3 x 25 mm (see Figure 15). The billets were sintered in a boron nitride-filled carbon crucible heated by an RF induction furnace of construction shown in Figure 16.

Although the furnace was capable of temperatures up to 2000°C, sintering was usually carried out between 1750°C and 1850°C using heating schedules that would optimise the final density (see Figure 18). The furnace was inexpensive to construct and consisted of an alumina work tube in which the crucible rested on a graphite support rod. Water-cooled end pieces sealed the ends of the work tube enabling sintering to be carried out in a controlled atmosphere of oxygen-free nitrogen. The work tube was surrounded by a graphite susceptor 153 mm long x 76 mm diameter which was 'coupled' to a Radyne generator capable of 40 kW at 450 kHz. The lifetime of the susceptor, surrounded by calcined alumina powder, was doubled to 40 hrs at 1750°C by feeding in argon at the base of the furnace and allowing the gas to diffuse upwards to provide an inert atmosphere. Temperature control was achieved by a West Instruments power controller via a saturable core reactor using the output from a W/W26Re thermocouple. The thermocouple was in its own sealed argon atmosphere. The constant temperature hot-zone was determined to be approximately 5 cm long at 1600°C. A typical sintering schedule would be a heating at a rate of 15-20°C min^{-1} to 1850°C and then holding at that temperature for 1 hour. A 'furnace cool' was achieved when the RF power was turned off. The cooling rate fell from 25°C min^{-1} at 1600°C to 10°C min^{-1} at 900°C. The sintered billets were then sliced into bars using a diamond-edged saw.

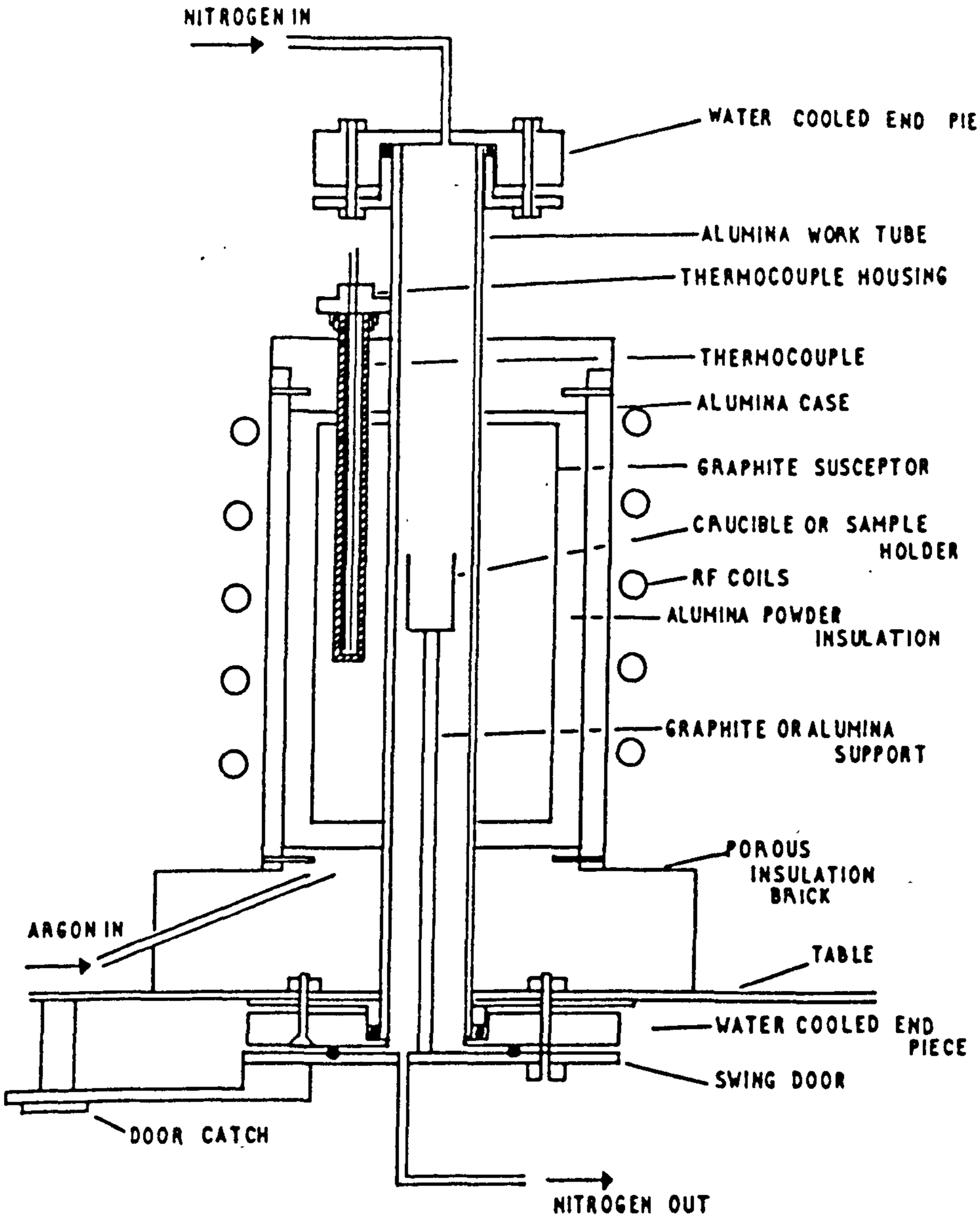

Figure 16: Components of the sintering furnace.

3.2 Density Measurements

The densities of the ceramic in the as-pressed condition and at various stages through the sintering process were measured using an immersion into mercury technique. The density of the sample ρ can be found from:-

$$\rho = \frac{W_A}{W_m - W_s} \times \rho_{Hg}$$

where W_A is the weight of the sample in air

W_m is the upthrust when immersed in mercury

W_s is the upthrust on the sample holder only

ρ_{Hg} is the density of mercury at ambient temperature.

The densities are recorded in Figures 17 and 18. The increase in density above that of the as-pressed condition when the temperature was increased to 1600°C indicated that above 1200°C stage I, primary particle rearrangement, had occurred. Temperatures above 1700°C were required for the main densification through stage II of the sintering process. The maximum density achieved was for a ceramic with a β' substitution level z = 1.0, using a schedule of 1850°C for 1 hour followed by 1 hour at 1750°C. The theoretical density of β' decreased with z level from $\rho = 3.15$ g cm^{-3} at z = 1.0 to $\rho = 2.95$ g cm^{-3} at z=4. The value of the relative density measured for the higher substitution ceramics approached that achieved for the low z material for z = 1.0 ρ_{rel} is 98%, for z = 3.0 ρ_{rel} is 97%.

Lower temperatures are in general required for densification of high z ceramics. Indeed sintering high z materials at 1800°C only

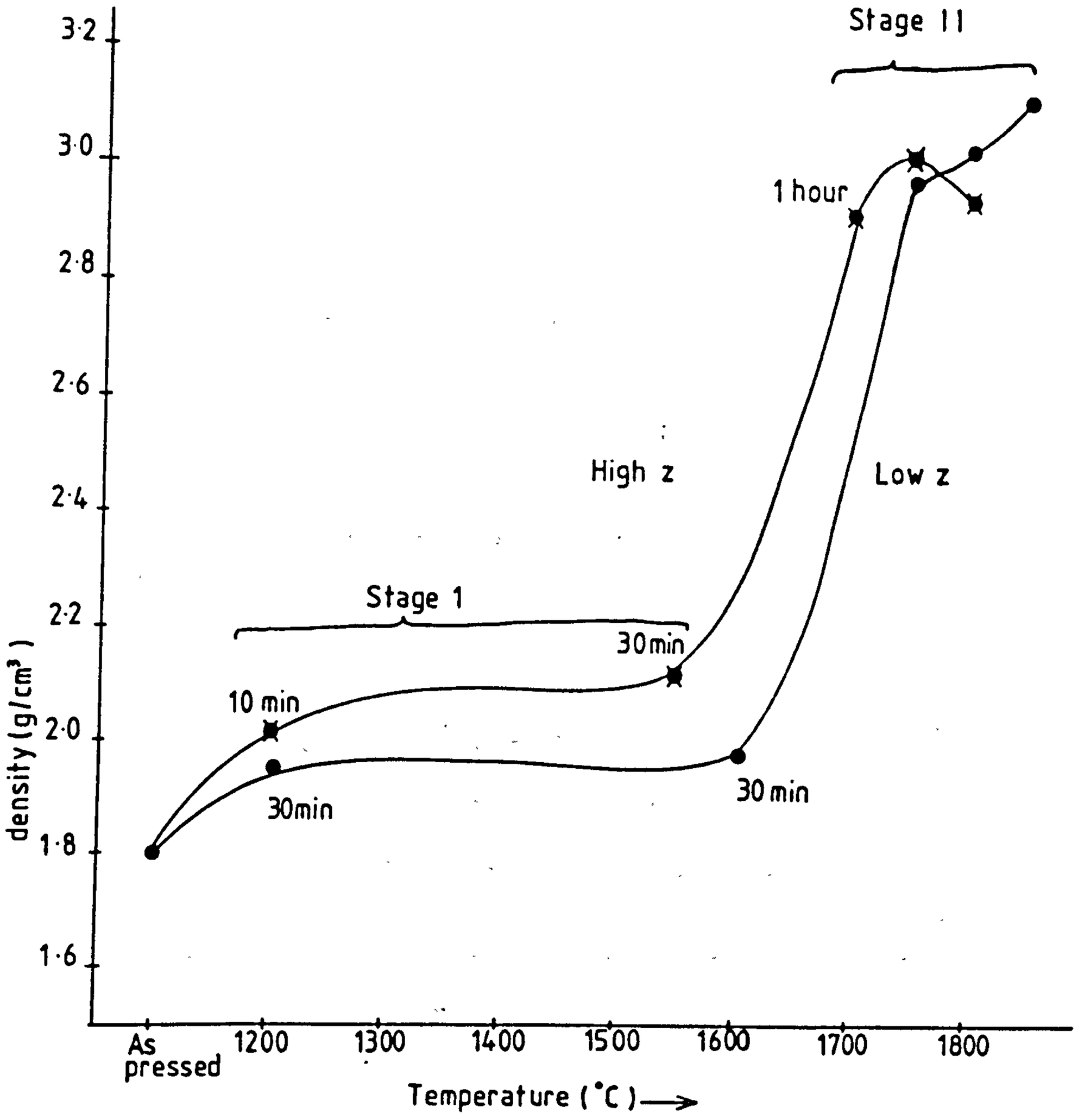

Figure 17: Density vs sintering temperature for low and high z ceramics

50°C above that for optimum sintering schedule, caused severe bloating to occur (see Figure 23).

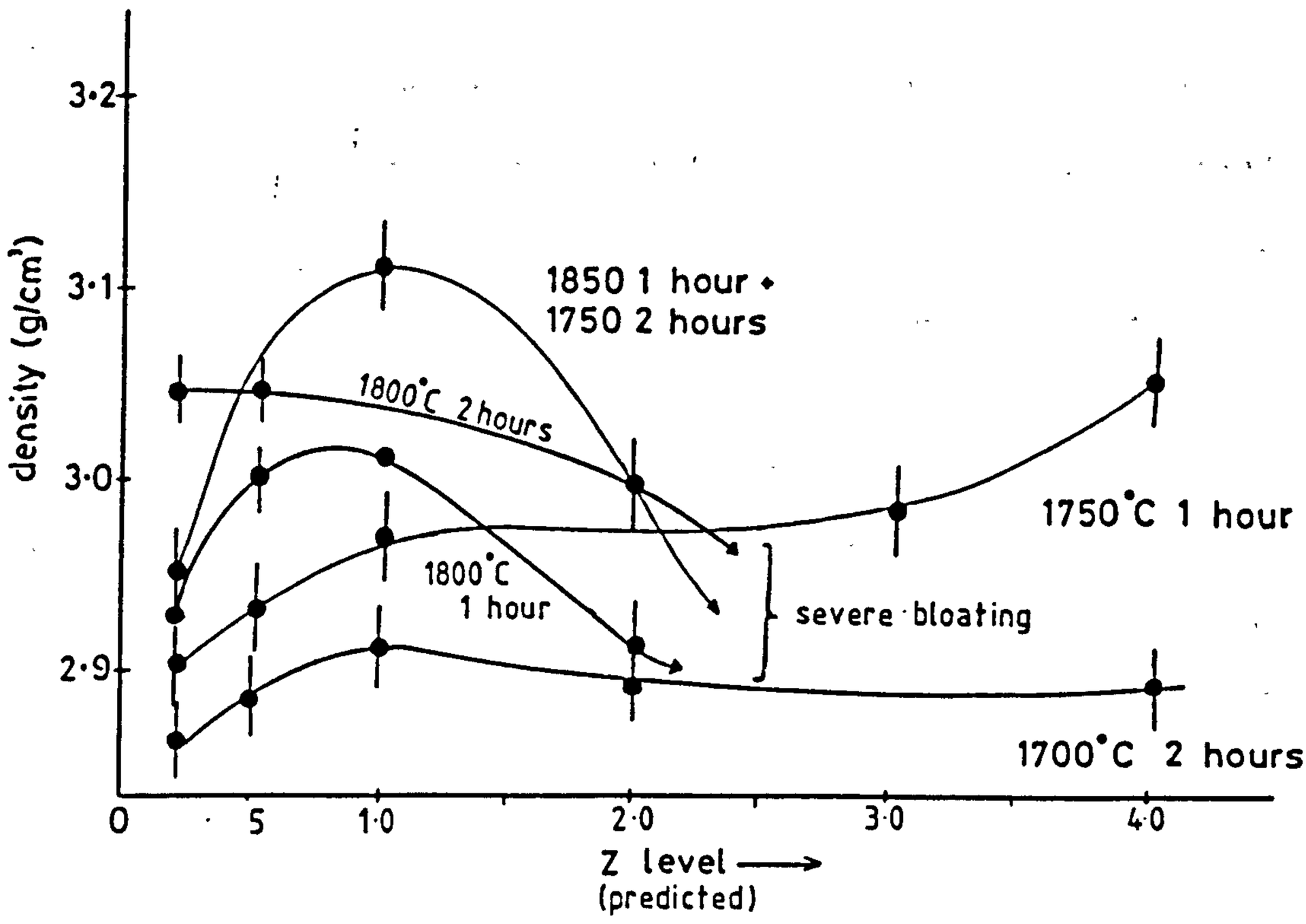

Figure 18: Density vs substitution level for various sintering schedules.

3.3 Hot Stage Microscopy

In an attempt to clarify the sintering mechanism, measurements were made of the temperature of (a) the melting point of the initial liquid phase and (b) the onset of the secondary particle rearrangement i.e. stage II of the sintering process which was taken as the temperature at which the particles began to be pulled together.

These were measured for the range of ceramics using a Griffin and George hot stage microscope and the results are shown in Figure 19. For the higher temperatures up to 1850°C the platinum 6% rhodium/platinum 26% rhodium thermocouple-heater could not be used and was replaced by a fine tungsten wire heating element. Temperature measurement was made using a disappearing filament pyrometer.

The melting point of the liquid phase was in the region of 1100-1200°C for the whole range of ceramics (for z = 0.1 to 4.0). The decrease in temperature of the onset of stage II is observed from over 1850°C for very low z material to 1600°C for z = 4.0 material confirming the increased ease of sintering as the z level increases.

3.4 X-ray Diffraction

As a means of identifying sintering reactions X-ray diffraction (XRD) was used to identify crystalline phases that formed during and at the end of the sintering process. XRD is a well established technique and discussion of the theory and applications is given elsewhere[113]. Analyses were carried out on a standard Philips diffractometer operating at 30 mA at 40 kV using CuKα radiation. The scanning speed was 0.5° min^{-1}. Samples were cut and surface ground and mounted using 'Blutac' adhesive. Data were collected using either an interfaced Commodore PET microcomputer or a single pen chart recorder.

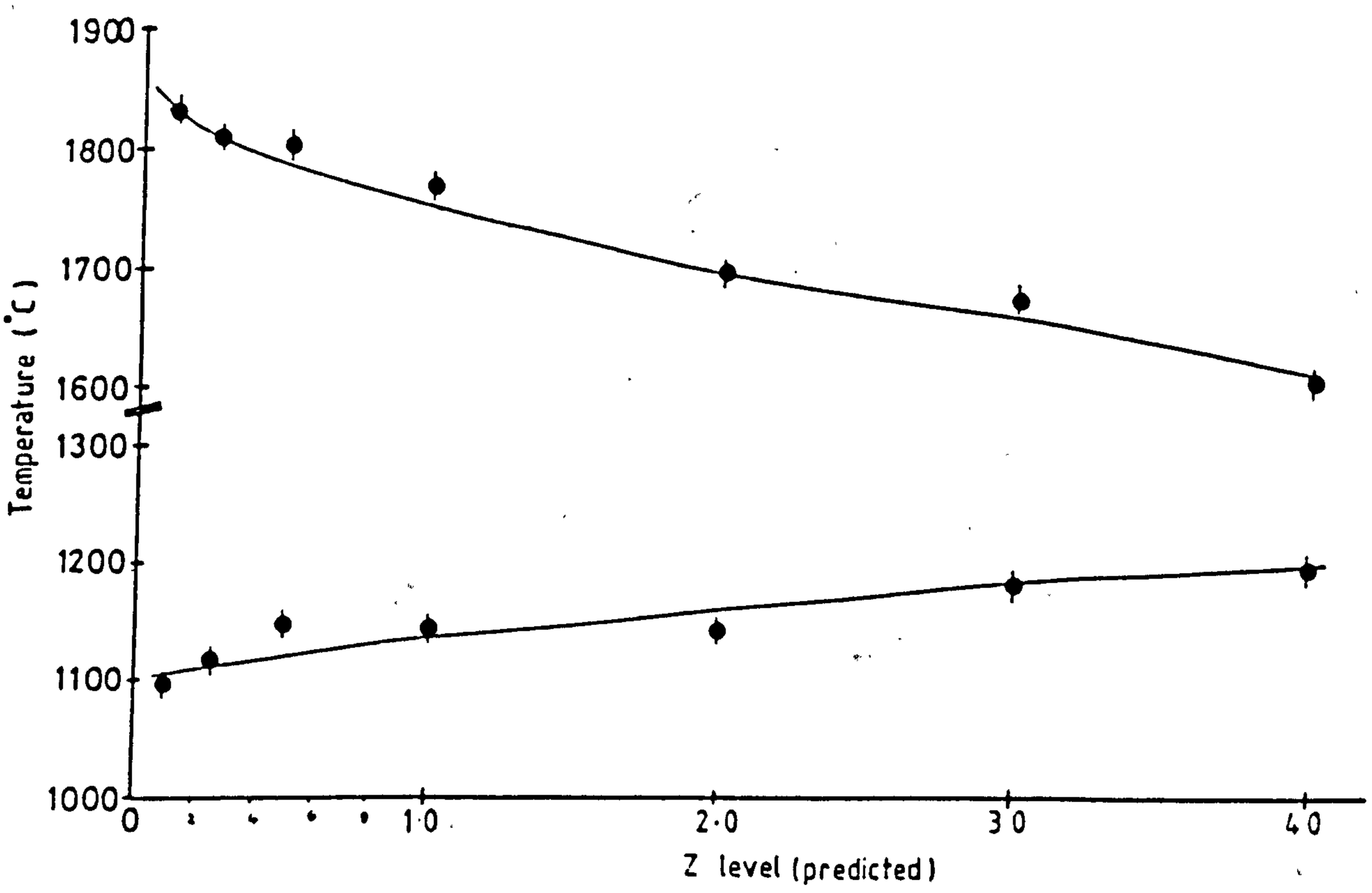

Figure 19: Hot-stage microscope results. The lower plot indicates initial liquid formation. The upper plot indicates the onset of stage II densification.

Identification of the crystalline phases was made with reference to the ASTM powder file. The as sintered products were found to differ from those found by either Jack[15] or Tien et al[16] shown in Figure 5 so samples were prepared to determine the phases found within the 3:4 plane. These samples would sinter to form β' with specific amounts of either forsterite or spinel. The newly determined 3:4 plane is shown in Figure 20.

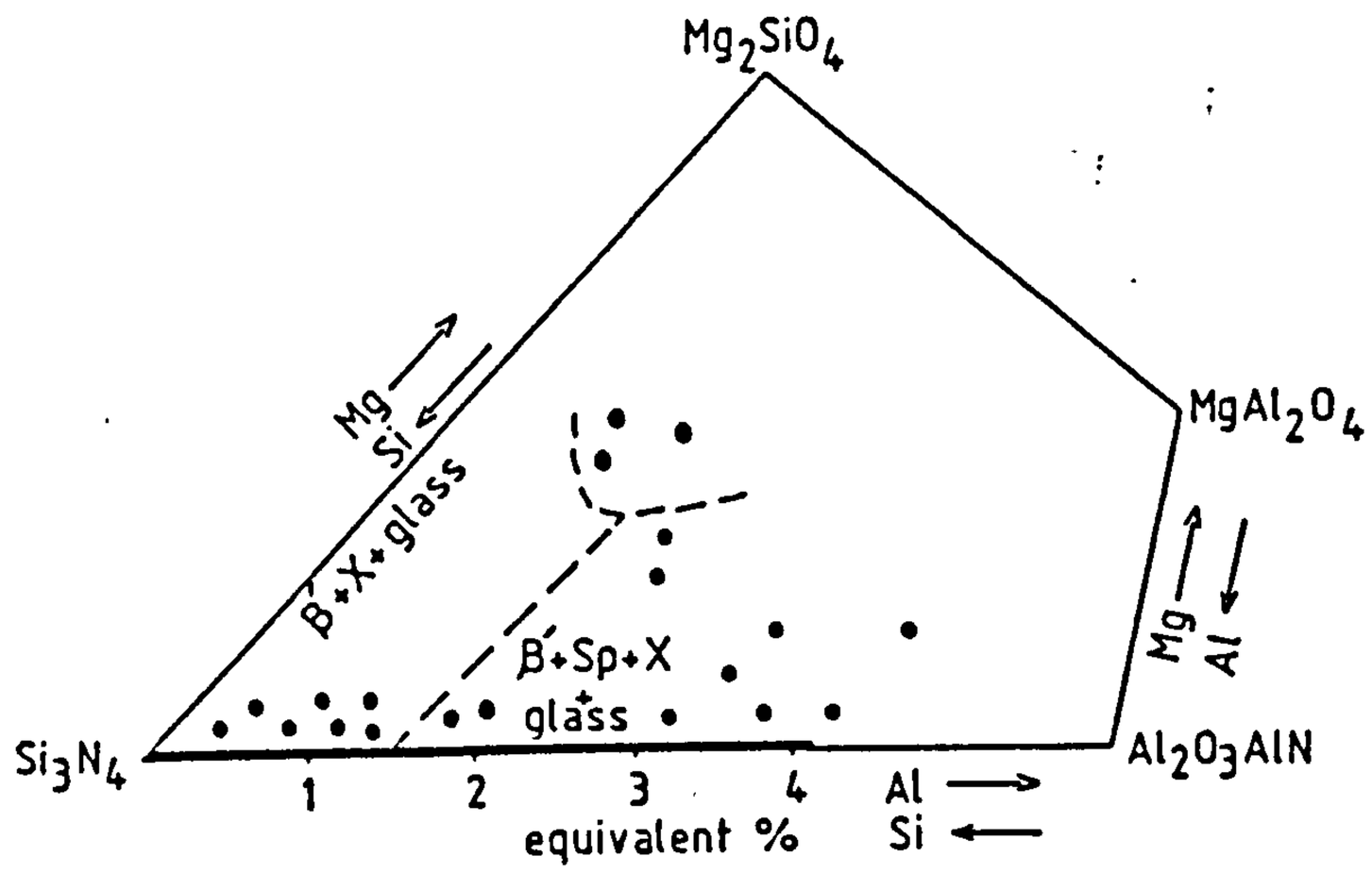

Figure 20: Phases produced by pressureless sintering of compositions on the 3:4 plane.

The sintering products showed generally β' and glass for low z ceramics O ($z \leq 1.5$) and β' and spinel with some residual glassy phase for $z > 1.5$. All ceramics contained a little 'X' phase.

Since there are two distinct regions on this diagram, a low z ceramic with z=.75 and a high z ceramic with z=3.0 were chosen and the reactions during sintering were studied in greater detail. Both had enough second phase to produce 15 wt% spinel if totally crystallised.

Samples were examined using XRD during the sintering process. The results shown in Tables 3 and 4 are of quenched samples, for data see Appendices 2 and 3.

Above 1200°C and up to 1600°C reactions took place to produce magnesium 21R polytypoid and 'X' phase. This occurred for both high and low z ceramics. In addition spinel was formed in the high z ceramic. At 1600°C unreacted α silicon nitride and alumina were still observed. Above this temperature is the onset of stage II of the sintering process. Pyrope and then protoenstatite were formed on cooling for the low z ceramics and sapphirine and subsequently sillimanite for high z ceramics. The reactions that are suggested to occur are described in the next section.

3.5 Discussion

Compositions were determined to produce a range of ceramics on sintering. Each ceramic in the range was designed to have a β' major phase of specific z level and a grain boundary phase which if totally crystallized could produce spinel. This grain boundary phase was added as magnesium oxide and aluminium oxide rather than preformed and crushed spinel. Mashai and Kamugaito[114] had produced "fully" dense silicon nitride using spinel rather than stoichiometric amounts of MgO and Al_2O_3. The production of spinel on sintering the high z level ceramics and the high relative densities achieved (97-98% theoretical) was taken as sufficient justification for using MgO + Al_2O_3 rather than preformed spinel.

The compositional diagram of the 3:4 plane shows that β' and glass are produced on sintering. Small amounts of 'X' phase were also observed in all cases where β' existed. The high z ceramics also contained spinel as predicted by the starting composition. This

Treatment	Phases identified by XRD on quenched samples
Starting Powder	α Silicon nitride, magnesia, alumina and 21R polytypoid ($SiAl_6N_6O_2$)
1200°C ↓ 1600°C	α Silicon nitride, alumina, magnesium, 21R polytypoid ($Mg_7Si_7Al_{14}O_{12}N_{20}$) and 'X' phase ($Si_3Al_6O_{12}N_2$)
1700°C	β, Residual α, pyrope and 'X' phase ($Mg_3Al_2(SiO_4)_3$)
1750°C	β, Trace α, β', protoenstatite, 'X' phase and glass ($Mg(SiO_4)_3$)
1850°C 1 hour + 1750°C 1 hour (slow cooled)	β', 'X' phase and glass

Table 3: Products found for low z ceramics (1200-1850°C)

Treatment	Phases identified by XRD on quenched samples
Starting Powder	α Silicon nitride, magnesia, alumina and 21R polytypoid
1200°C ↓ 1600°C	α Silicon nitride, alumina, magnesium, 21R polytypoid ($Mg_7Si_7Al_{14}O_{12}N_{20}$) Spinel and 'X' phase ($MgAl_2O_4$) ($Si_3Al_6O_{12}N_2$)
1700°C	β', Sapphirine, spinel and 'X' phase ($Mg_7Al_{10}Si_2O_{16}$)
1750°C	β', Sillimanite, trace spinel, trace 'X' phase ($Al_2O_3SiO_2$) and glass
1750°C 1 hour (slow cooled)	β', Spinel, 'X' phase, glass

Table 4: Products found for high z ceramics (1200-1750°C)

differs from work by Jack[15] and Tien et al[16] who found several polytypoid phases. Jack finds a region comprising β' and spinel but only between z=4 and spinel, but elsewhere polytypoid 15R or 21R are present. These phases were not observed in the present work.

3.5.1 Sintering Mechanisms

The evidence for a low temperature liquid phase has been shown using hot stage microscopy in Figure 19. This phase occurred with the onset of stage I as indicated by the small increase in density at about 1200°C, shown in Figure 17. The liquid formed at 1200°C which is 150°C lower than the ternary oxide eutectic temperature[31] is therefore not of this composition: a likely candidate is suggested in the next section. The density remained constant with increasing temperature until 1600°C which marked the onset of stage II of the sintering process and also the start of the α→β transformation. XRD and density data shows a clear correspondence between the α→β transformation and stage II densification. This differs from the Kingery model[46] where densification is due to a slight increase in solubility at the contact points. Here in contrast the phase change is believed to enable further densification by collapse of the α framework and formation of a new β one, probably via mechanisms similar to those in stage I. The density levels which determined the temperatures of the optimum sintering schedules correspond very well to the temperatures at which XRD data indicated total α→β transformation and to the hot stage microscope results, i.e. > 1800°C for low z ceramics and slightly lower than this for high z ceramics. The reactions that are believed to occur during the sintering process will now be discussed.

3.5.2 Sintering Reactions

Hot stage microscopy and XRD data, shown in Figure 19 and Tables 3 and 4, indicate that by 1200°C reactions have occurred to produce a liquid phase. When the samples were quenched, new products included a magnesium 21R polytypoid and 'X' phase; the liquid is believed to be composed of one or both of these phases. The reaction, which applies to both low and high z ceramics is believed to be:-

$$40\ SiAl_5N_5O_2 + 4\ Al_2O_3 + 98\ MgO + 21\ Si_3N_4 + SiO_2$$

21R Polytypoid — Surface silica

$$\xrightarrow{-1200^{\circ}C}\quad 14\ Mg_7Si_7O_{12}N_2O + 2\ Si_3Al_6O_{12}N_2$$

Magnesium 21R Polytypoid — 'X' Phase

With the high z ceramics spinel is also produced. No other reactions take place until the onset of stage II at above 1700°C. As the low and high z ceramics produce different sintering products and different transient liquids phases they will be discussed separately.

For the low z ceramics the α→β transformation begins above 1700°C. XRD of quenched samples indicate the transient liquid could be magnesium alumino silicate, i.e. pyrope ($Mg_3Al_2(SiO_4)_3$), with 'X' phase, see Table 3. There is some α silicon nitride still present. Above 1750°C the α→β transformation is nearly complete with only residual α. The liquid phase on cooling produces a magnesium

silicate, protoenstatite ($MgSiO_3$), see Table 3 (and Appendix 2), as well as a residual glassy phase and 'X' phase. For total $\alpha \rightarrow \beta$ conversion higher temperatures are needed and the optimum sintering schedule which included 1 hour at 1850°C is in agreement with this. The as sintered products are β', 'X' phase and a glassy phase. The transient liquid is a reactive medium through which the $\alpha \rightarrow \beta$ transformation takes place. It is continually changing in composition, alumina is removed and the precipitated β changes to β'.

For the high z ceramics a modified reaction sequence was determined. The main difference is due to the much larger alumina content, and the continual production of spinel on rapid cooling throughout the process probably reduces the amount of available reactive liquid phase. At 1700°C the $\alpha \rightarrow \beta$ transformation is completed. The XRD data of rapidly cooled samples indicates the transient liquid phase could be composed of a magnesium alumino silicate sapphirine ($Mg_7Al_{10}Si_2O_{26}$) as well as spinel and 'X' phase, see Table 4. As with the low z ceramics, the transient liquid is continually changing in composition. As the temperature is increased removal of magnesium and aluminium from this liquid phase is deduced due to the production of sillimanite ($Al_2O_3SiO_2$) and a glassy phase. The spinel and 'X' phase peak heights are much reduced indicating, possibly, that they are partially dissolved in the glass, see Table 4 and Appendix 3. On prolonged heating and slow cooling, the as sintered products are β' spinel and 'X' phase with a small residual glassy phase.

This suggests that for both cases β' forms first with very low z level and then the z level increases as aluminium is removed from the transient liquid. That β' forms first with a low substitution level is in complete contrast to earlier work[115] where 'X' phase was suggested as the transient liquid phase and β' formed with a high z level which then gradually reduces.

The surface silica on the α silicon nitride particles was also stated in Chapter Two to be extremely important with regard to stage II of the sintering reaction mechanism. The reactions suggested here do include silica but at stage I only, indeed the reactions cannot be balanced without it. There is a slight discrepancy since the higher z ceramics were found to be the more easily sintered despite the fact that they contain lower amounts of silica. The increased sinterability could be due to the lower viscosity of the final glassy phase of the high z ceramics, a topic now discussed.

3.5.3 Glassy Phases

The final glass compositions determined by EDAX (see next Chapter) are shown in Figure 21 as pure oxide glasses on the ternary oxide system $MgO-SiO_2-Al_2O_3$, which forms the edge of the MgSiAlON prism. The nitrogen content of the glass was not determined.

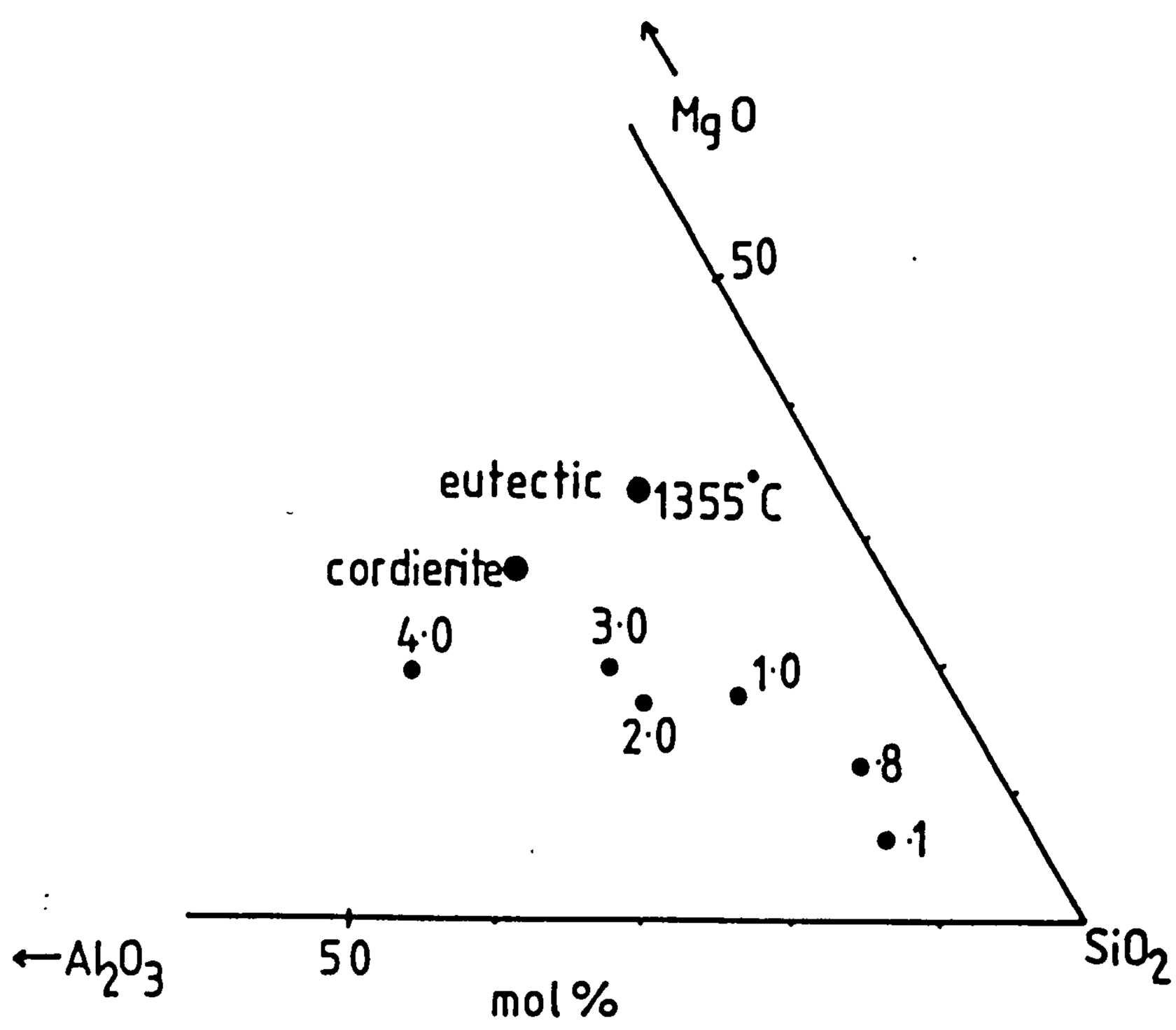

Figure 21: Analyses of the final glass compositions in as-sintered ceramics (number indicates z level).

The high silica content ($MgOAl_2O_36SiO_2$) of the glass found in the low z ceramics, with a resulting high viscosity, could be one reason why only small grain growth was observed for these ceramics. The grain size of the high z ceramics is much larger (Figure 22) due to the resulting glass ($2MgOAl_2O_36SiO_2$) which is near to the eutectic composition ($3MgOAl_2O_36SiO_2$) and therefore more fluid at the sintering temperatures. The continual production of spinel from the glass indicated that the microstructure might be less homogeneous. This was indeed found and is discussed in Chapter Four.

Grain size determinations were made from etched polished surfaces using scanning electron micrographs. The etchant used was 10% HF acid, and etching times were 10s-30s. The results are shown in

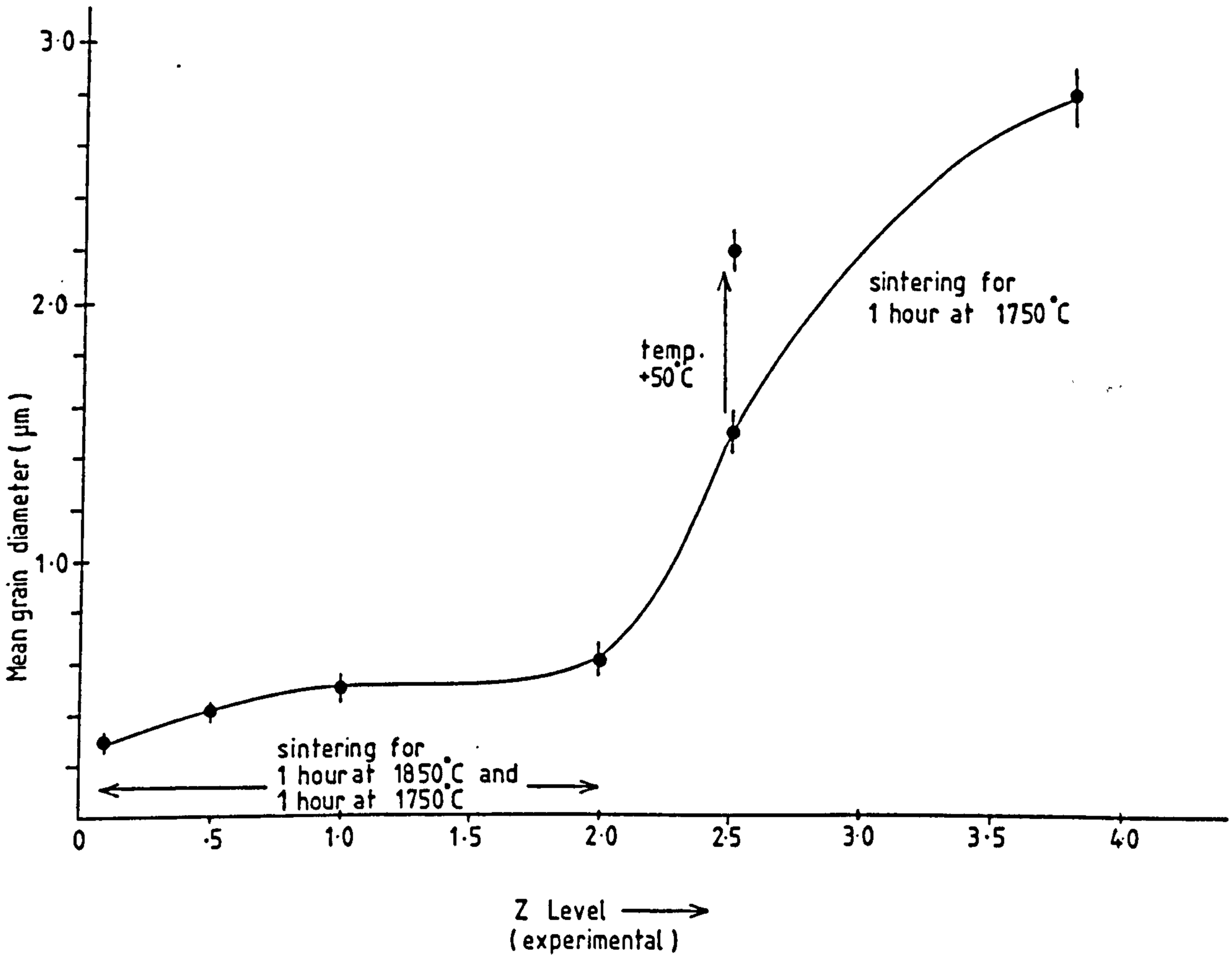

Figure 22 : Grain size as a function of alumina level.

Figure 22. The high z ceramics have a mean grain diameter of > 1.5 μm whereas the low z ceramics have a grain diameter of < 1 μm despite the differing sintering schedules, which should favour grain growth in the low z ceramics.

The critical effect of excessive temperature on the high z ceramics was also noted and is shown in Figure 23. Severe bloating occurred at only 50°C above the optimum sintering schedule i.e. at 1800°C for 1 hr. The grain size increased to over 2 μm (Figure 22). XRD indicated only spinel and 'X' phase as grain boundary phases indicating either SiO losses or the evolution of nitrogen from the glass. This deleterious effect puts an upper limit of < 1800°C on the sintering temperature with at least 1600-1700°C required for total $\alpha \rightarrow \beta$ transformation. The optimum sintering temperature for maximum densification was found to be 1 hour at 1750°C.

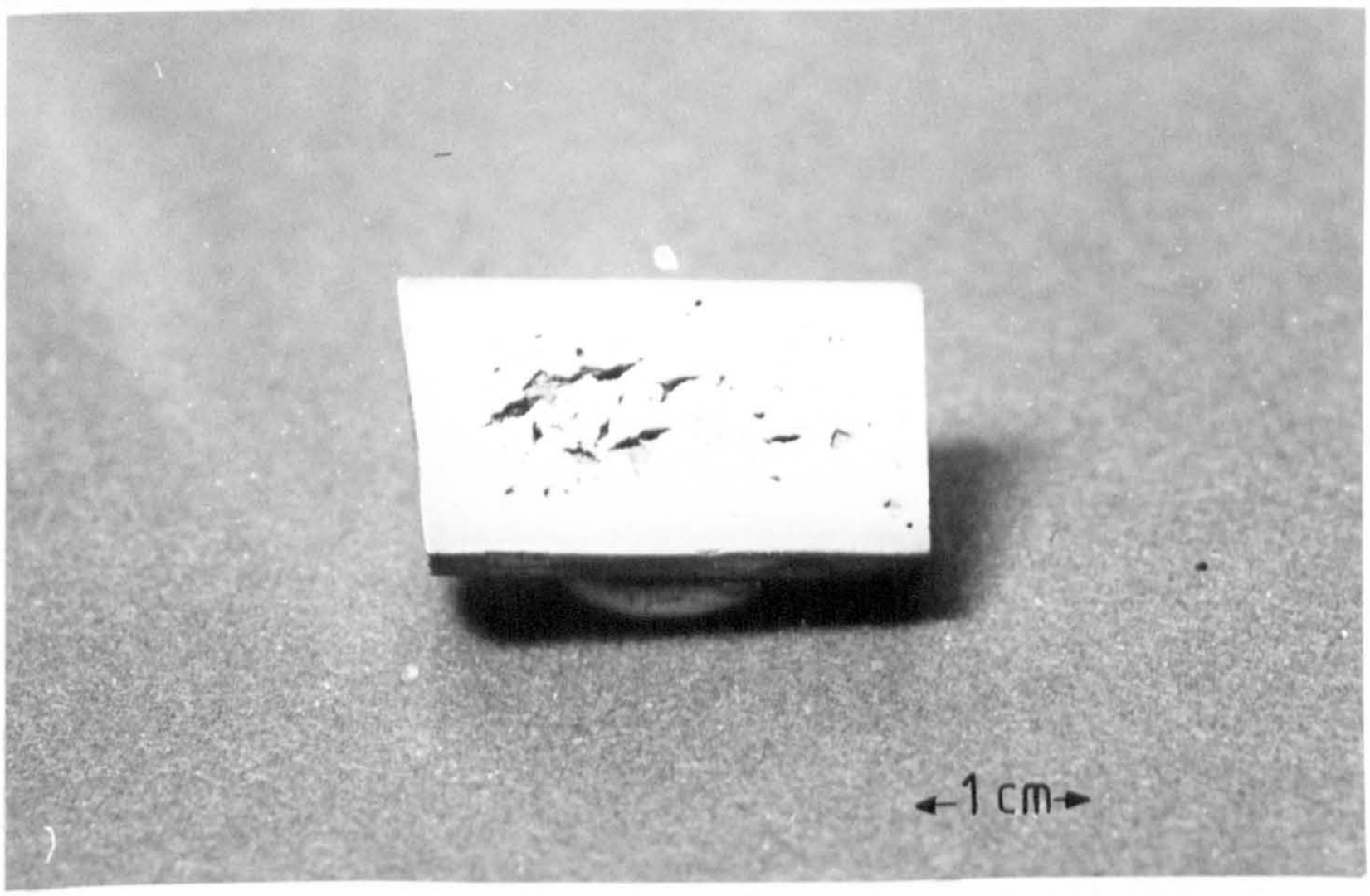

Figure 23: Effect of too high a sintering temperature on the high z ceramics.

To summarise: high relative density ceramics consisting of β' as the primary phase with a partially crystallized grain boundary phase have been produced through the pressureless sintering of a range of ceramics $0 < z < 4$ by a liquid phase sintering mechanism using a magnesium oxide additive. Very high temperatures are required for the production of lower z compositions, due to the low reactivities and high viscosities of the transient liquid phase needed to provide the driving force for the α→β transformation believed to be necessary for high densification. This high temperature requirement is a severe limitation to one of the anticipated advantages of using low z magnesium SiAlONs i.e. the prospect of easy sintering. Lower temperatures and shorter times are required for the higher z ceramics, due to the formation of a lower viscosity liquid.

In both cases the initial molten phase probably consists of a magnesium 21R polytypoid which aids stage I of the densification process. During stage II the transient liquids produced constantly changing composition as aluminium and magnesium in the higher z ceramics are removed. In both cases a residual glassy phase is left in the grain boundaries.

The microstructure of a low z (z=.75) and a high z (z=3.0) ceramic will be compared in greater detail in the next chapter. Additionally there will be discussed the effect on the microstructure of a post sintering heat treatment, and of heating it in an oxidising environment.

CHAPTER FOUR

THE MICROSTRUCTURE OF Mg-Si-Al-O-N CERAMICS

This chapter describes the microstructure of the as-sintered ceramic and the effect of heat-treatment upon it. The stability of these microstructures in high-temperature oxidising environments is also examined, to explore the possibilities of using these materials in engineering applications, and is important in relation to high temperature strength.

4.1 Experimental Procedure

Transmission electron microscopy (TEM) and scanning electron microscopy (SEM) were used throughout the present work. Both are now well established techniques and accounts of them can be found elsewhere: for example see Bowen and Hall[116]. Experimental methods are discussed only briefly here.

4.1.1 TEM

Observations and analyses of the microstructures were made and recorded from thin sections of ceramics, using a JEOL 100C microscope operating at 100 keV. The sections had been prepared by the following method. Samples were sliced to approximately 100 μm thickness and mounted on a glass slide using a low melting point resin (Lakeside 70). They were then ground and polished to between 30-50 μm thickness and finally polished using $^1/_4$ μm diamond paste. After mounting on 3 mm diameter brass rings they were further thinned by ion beam erosion. This technique involves the removal of material from a rotating specimen by bombardment with argon ions which have been accelerated by voltages of the order of 5 kV. This produces a hole in the disc and an adjacent area which is electron transparent. The samples were then carbon coated

to prevent build up of charge from the electron beam.

An energy dispersive analysis of X-rays (EDAX) detector was fitted to the microscope. This was coupled to an EDAX 9100 microcomputer which allowed rapid collection and analysis of data. The resulting spectra were converted to atomic percentages for β' or other crystalline phases and to molecular oxide percentages for any glass present.

4.1.2 SEM

SEM was used primarily to determine the mean grain size which has already been discussed in Chapter Three and to analyse the z level and magnesium content of the β' grains. This was conducted on a Cambridge Stereoscan 250 microscope fitted with an EDAX detector and a Link Analysis system microcomputer.

Specimens for analysis were ground flat and polished using 1 μm diamond paste and if necessary etched in HF acid to remove the glassy phase. Fracture surfaces of bars which had undergone Kc testing were also examined. All samples were gold or carbon coated to prevent charging. The fine scale of the grain boundary phase coupled with the very low atomic number contrast imposed severe limitations on the use of SEM in both secondary and back scattered modes.

4.1.3 Optical Microscopy

Low magnification photographs of cross sections of bars that had undergone thermal stability tests were recorded on a Zeiss Ultraphot optical microscope. The very high reflectivity of the samples meant that the normal incidence lighting arrangement could not be used to record the contrast which was easily observed with the naked eye.

Oblique illumination of the sample was used and the contrast was enhanced by under exposure of the negative and over development of the prints.

The sizes of the indents from hardness testing were also measured on the Ultraphot. A Vickers micro-hardness instrument (M21A) was used for indenting the samples.

In Chapter Three it was stated that a low and a high z ceramic would be under investigation. The notation used to describe the various samples is summarised in Table 5 below.

Sample	As sintered	Heat-treated	Predicted z level
low z	A	B	.75
high z	C	D	3.0

Table 5: Notation used for samples.

4.2 Results and Discussion

4.2.1 The Microstructure of the As-sintered Ceramic

The microstructure of A, typical of that found for low z ceramics, is shown in Figure 24. This shows prismatic β' grains indicating growth was in a liquid phase, which cooled to produce a glass as the dominant grain boundary phase. XRD indicated that a little 'X' phase was present. Glass was recognized by its mottled appearance caused by electron irradiation damage and by its lack of diffraction contrast on tilting. The predicted z level was .75 but the experimentally determined z level was 1.2 because of production of a silica rich liquid rather than spinel. The z level was consequently far higher than expected.

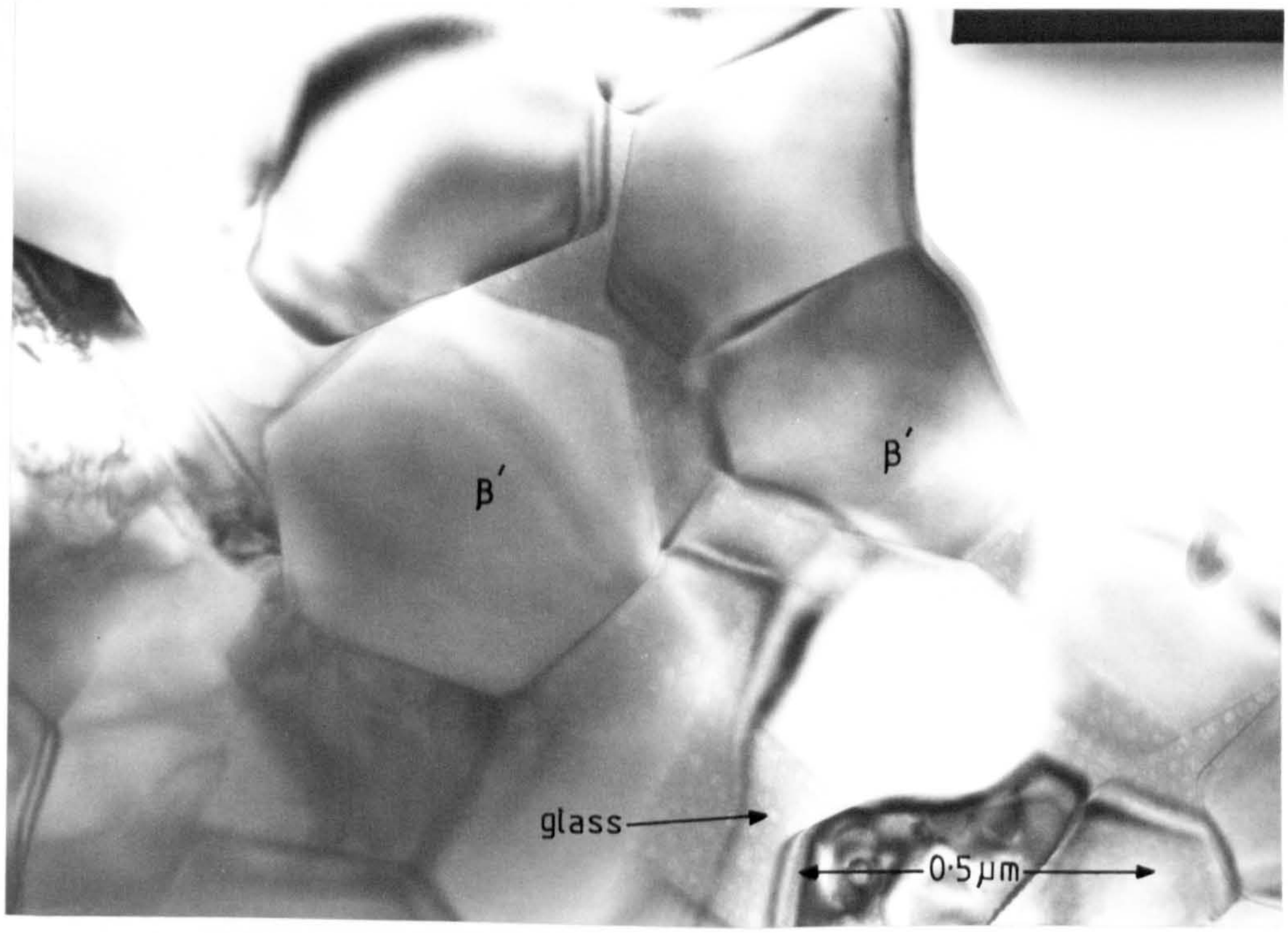

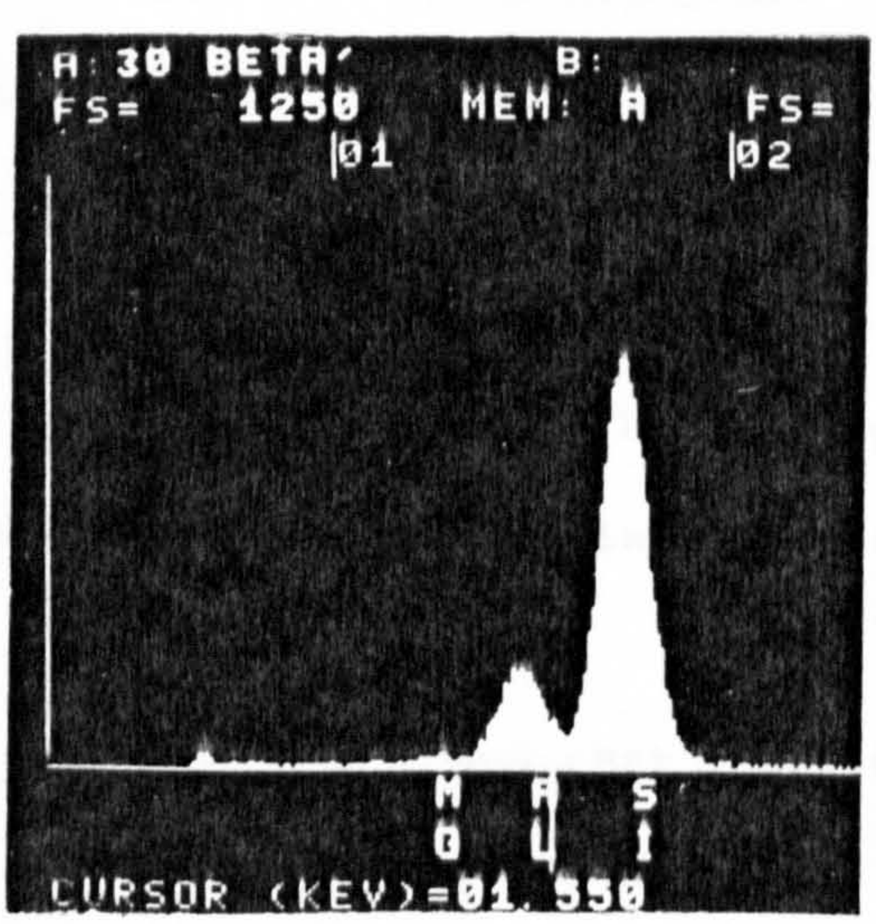

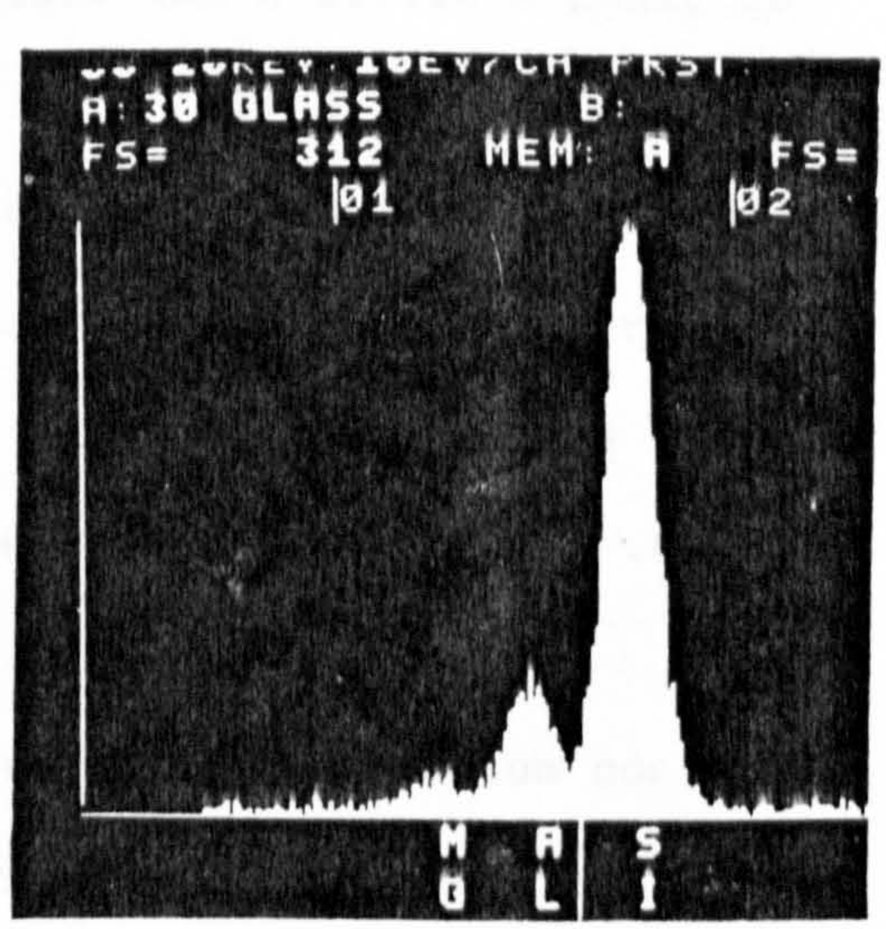

Figure 24: Microstructure of low z ceramic A in the as-sintered condition

Predicted z = .75 with 10 wt% spinel

Experimental z = 1.2 with glass and a little 'X' phase.

The microstructure of the high z ceramic C is shown in Figures 25 and 26. Comparing these to that for A (Figure 24), it is seen that there are areas where there are low amounts of glass or other grain boundary phases and the mean grain diameter is larger (see Chapter Three). In regions where glass is present it is often partially crystallised. The figures show that the main problem with the higher substitution level ceramics is inhomogeneity, which was also observed by Pickering[117]. As the particle size of the starting powder was submicron it is suggested that the inhomogeneity is not due to the much reduced ball milling times used in the present work compared to industrial practice (6 hrs as opposed to 24 hrs) but to the continued production of spinel in the sintering process. This could reduce the amount of liquid available at stage II of the sintering process. Spinel is the major grain boundary phase although glass and a little 'X' phase is present. The predicted and experimentally determined z level for ceramic C was found to be 3.0 and 2.5 respectively.

The magnesium content of the β' crystals was determined for each of the ceramics in the z level range $0 < z < 4$. The results are given in Figure 27 and show an increase in Mg content from 0 At% at $z = .01$ to 4.6 At% at $z = 4$.

It was also found that there was no variation of magnesium content of β' with increasing second phase levels. The data presented in Figure 27 is in contrast to earlier work whose authors found only "small" and constant magnesium solubility with varying z levels. Jack[15] had reported a maximum in this solubility at $z = 2$ but gave no explanation for the decrease above this z level. As a consequence of this increased solubility extra magnesia powder was included in the starting compositions for the high z ceramics.

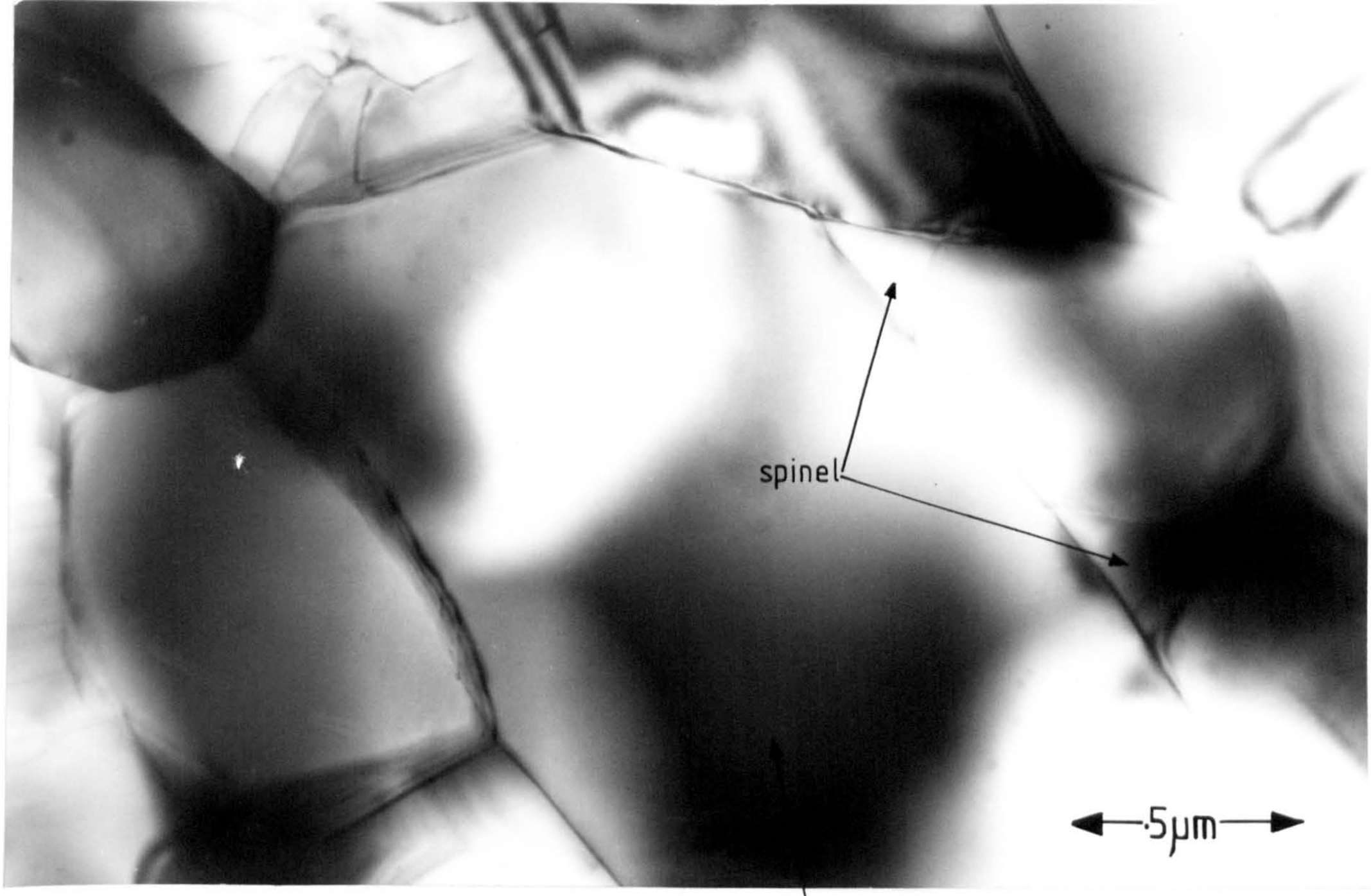

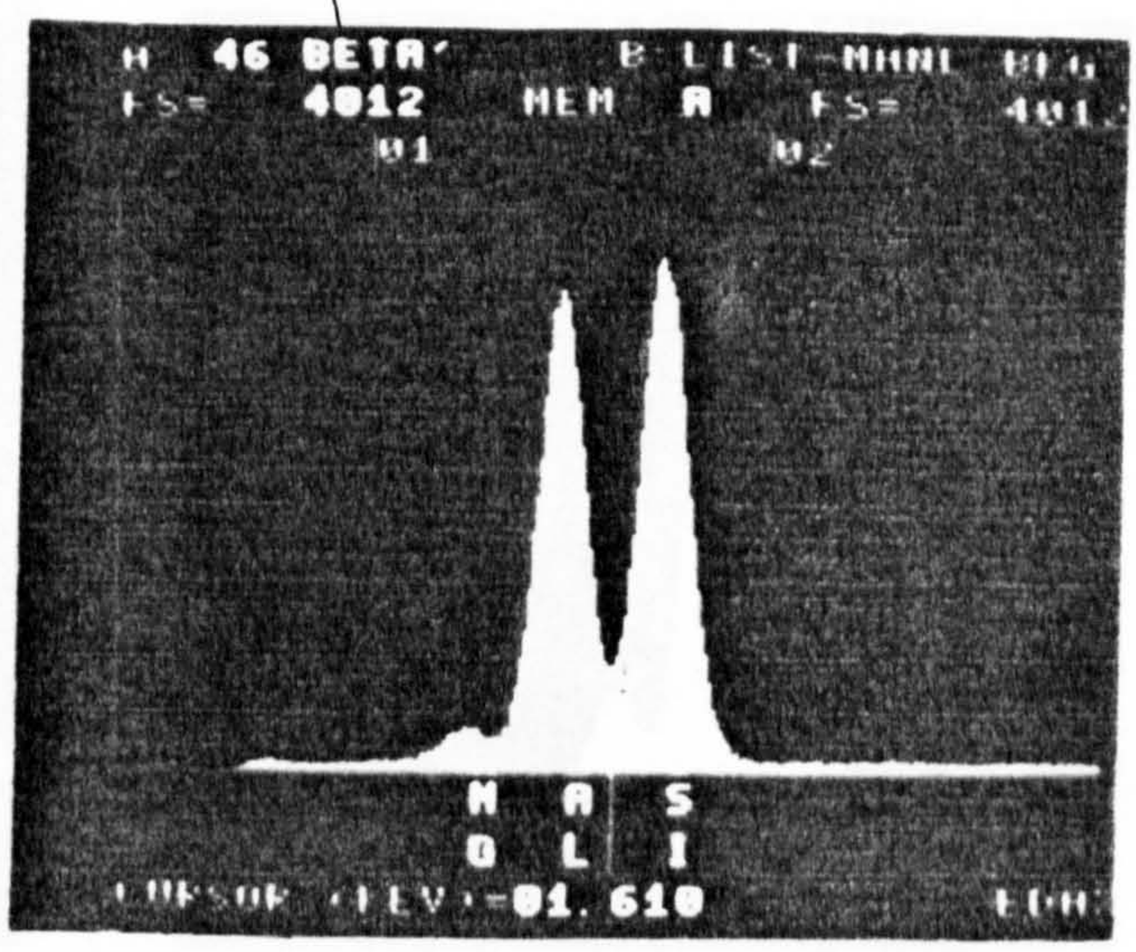

Figure 25: Microstructure of high z ceramic C in the as sintered condition.

Predicted z level = 3.0 10 wt% spinel as second phase

Experimental z level = 2.50 spinel with a little glass and 'X' phase.

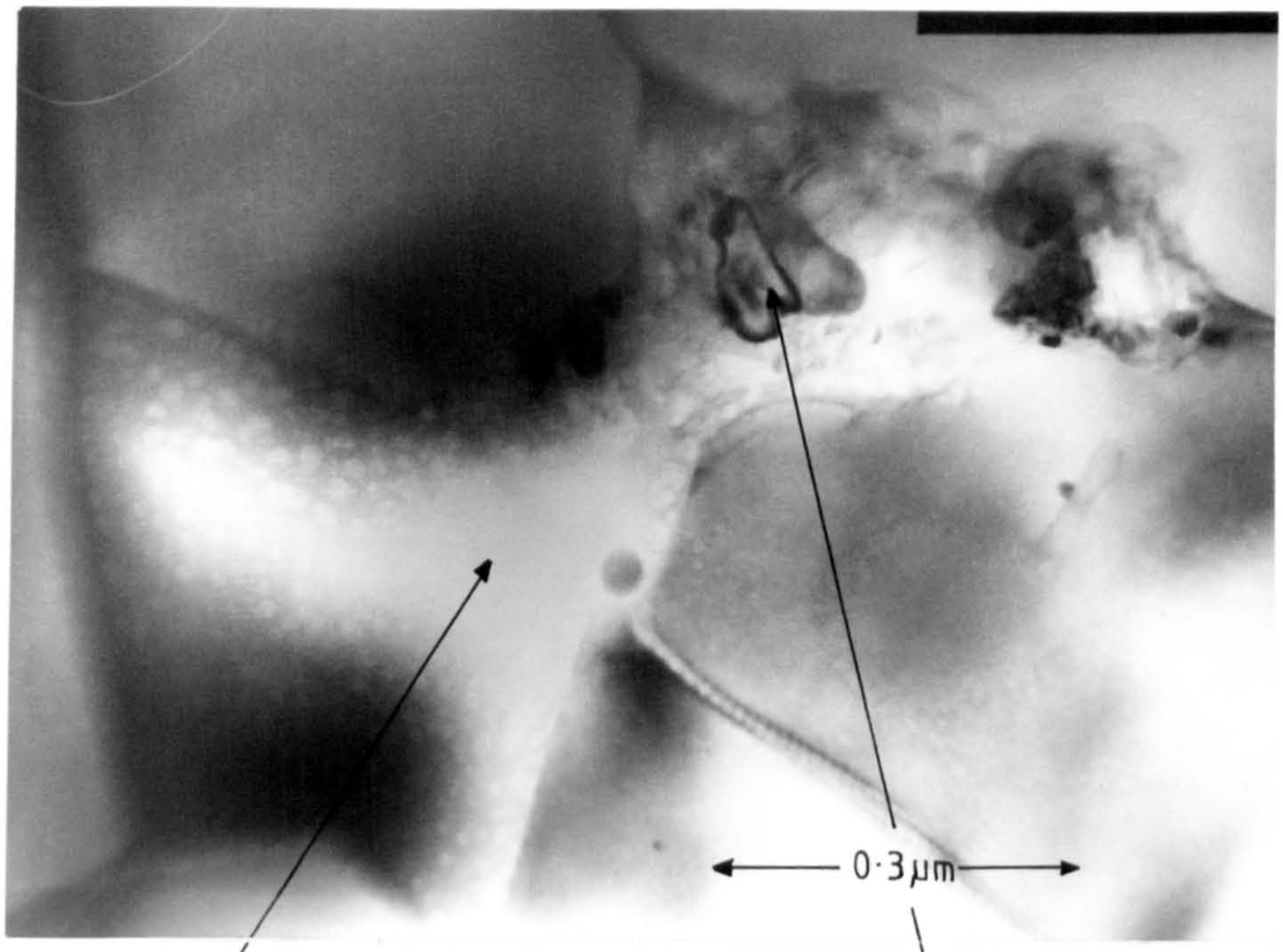

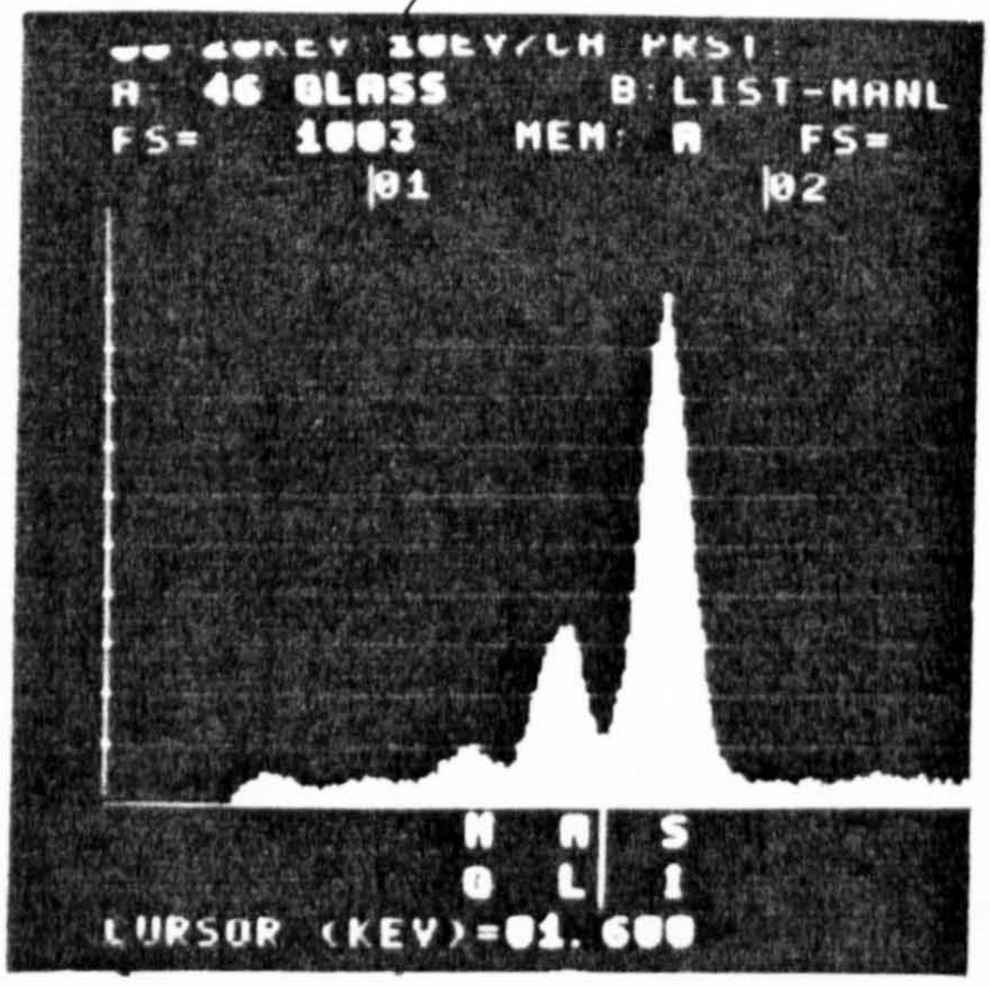

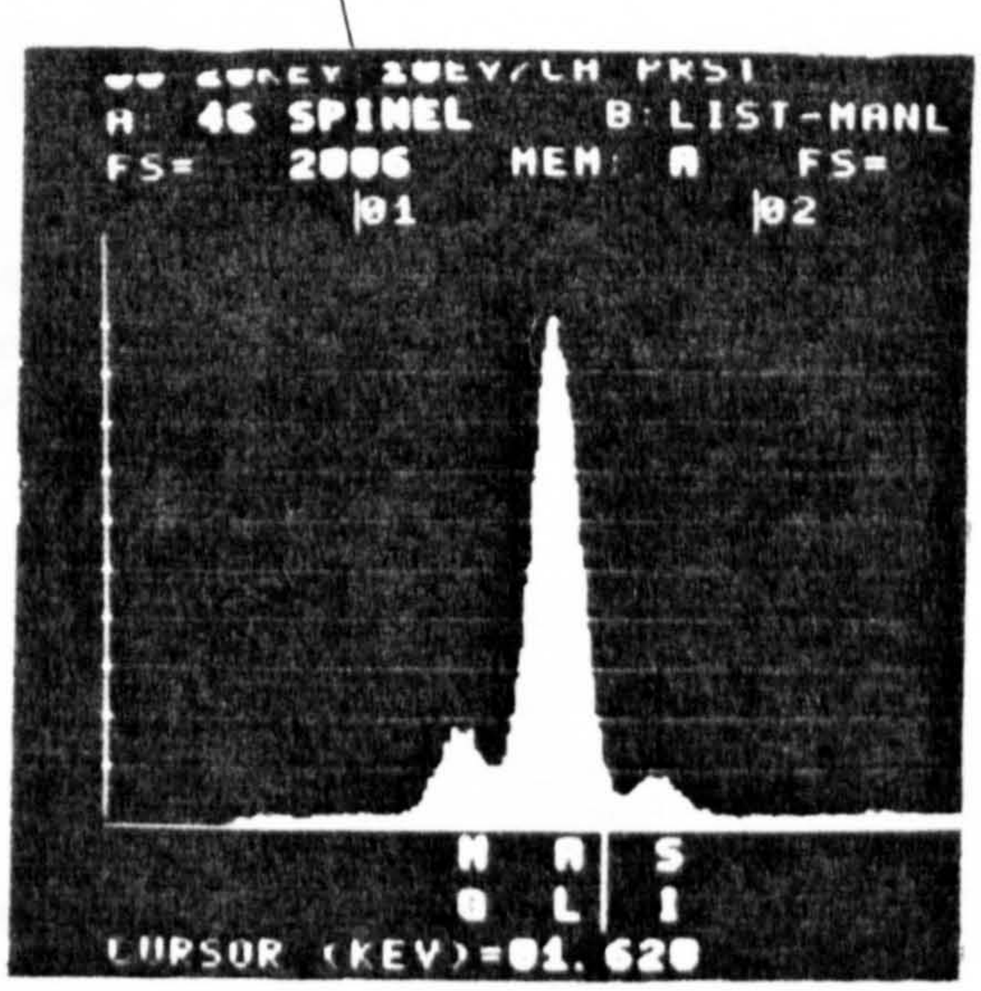

Figure 26: Partial crystallization of second phase is observed in some triple point regions of ceramic C.

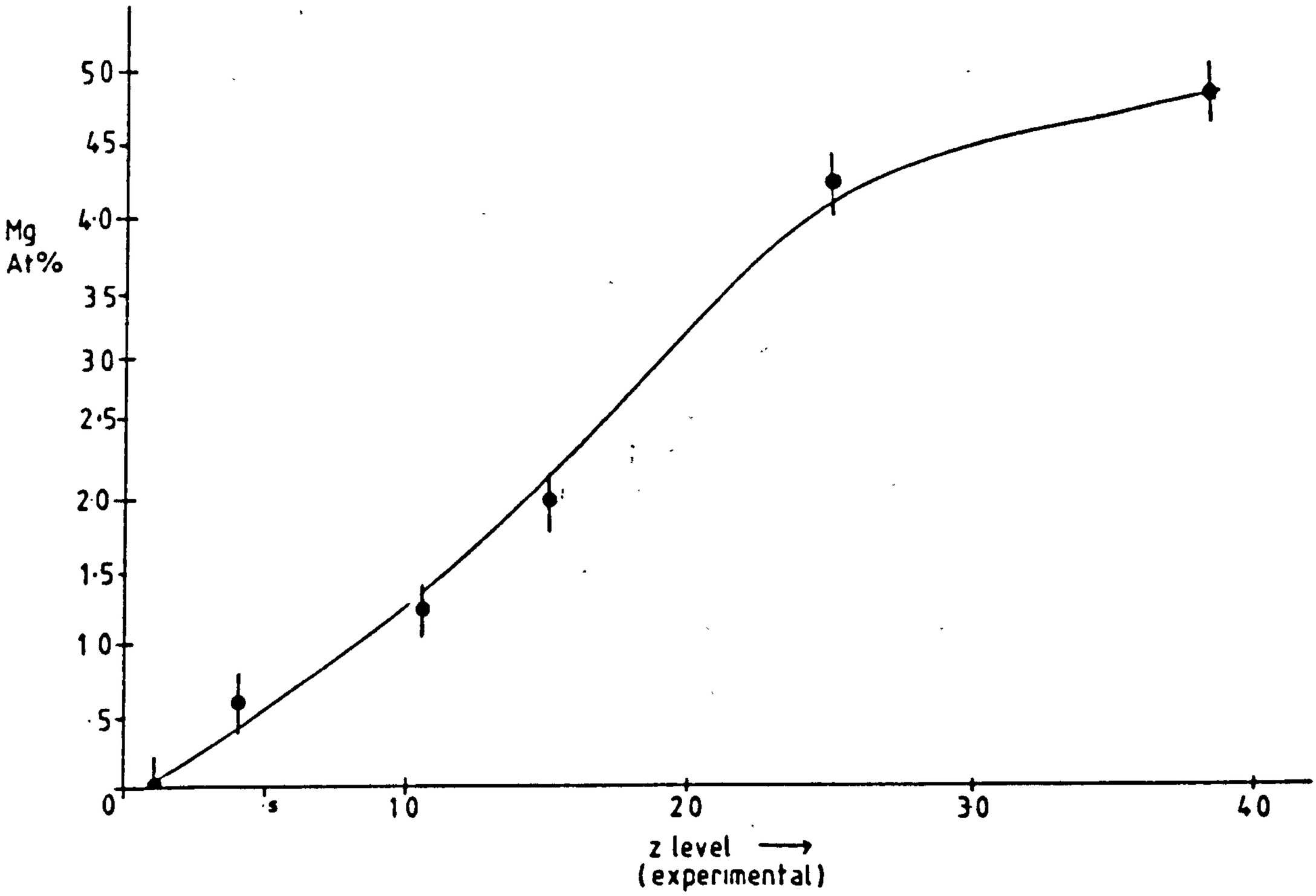

Figure 27: Magnesium content of β' crystals vs substitution level.

4.2.2 Effect of Heat-treatment on the Microstructure

A post-sintering heat-treatment was carried out in a nitrogen atmosphere in order to crystallize the glassy grain boundary phase to a more refractory glass ceramic. If this crystallization occurred through homogeneous nucleation i.e. nucleation throughout the glass and not initiated at the surface then it would be expected that there would be an increase in density of the ceramic. This increase is bound to be quite small as at most only 15 wt% is expected to be glass. If the density changes from 2.70 gcm^{-3} for glass to 3.60 gcm^{-3} for spinel then the overall density increase is of the order of 0.15 gcm^{-3}. The observed increase in density was only of the order 0.05 gcm^{-3} because during the conversion of A to B cordierite was produced as a grain boundary crystallization product. The density of this phase is the same as that for the original glass so a smaller overall increase in density was observed, spinel was produced but in smaller amounts than predicted. For the conversion of ceramic C to D the grain boundary phase is partially crystallized on sintering and total crystallization did not occur on heat-treatment hence the overall density change in this case was also lower than expected. The optimum heat-treatment was taken to be that for maximum increase in density, and this was determined from graphs of density vs annealing temperature or time. These are presented in Figures 28 and 29 and the optimum heat-treatment schedule was determined to be 24 hrs at 950°C. The reaction products formed are shown in Figures 30 and 31. Heat-treatment was performed in a nitrogen atmosphere to prevent the formation of cordierite on the surface.

The rather rapid fall off in density of samples heat-treated above 950°C for A and 1000°C for C is believed to be caused either by

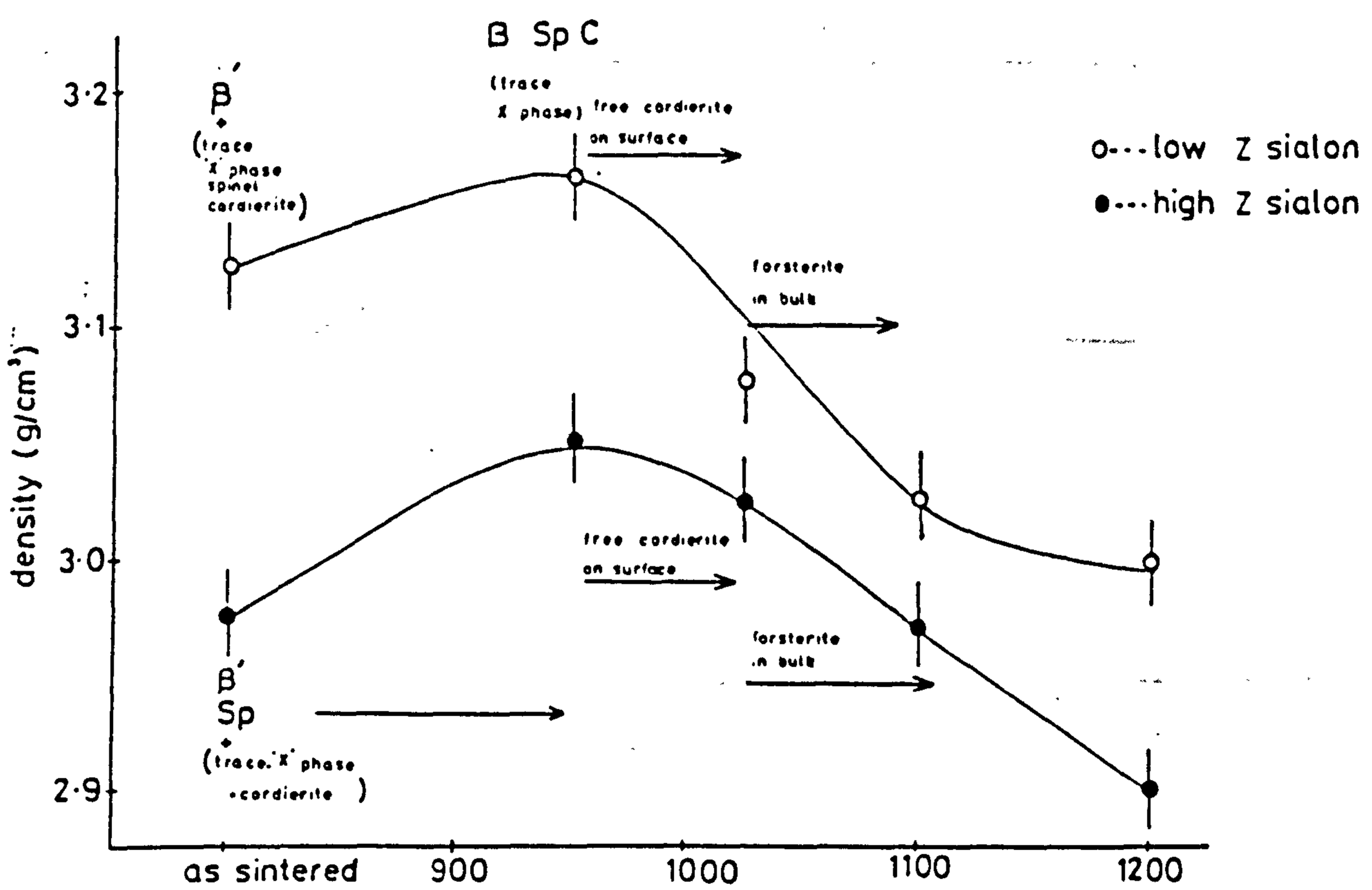

Figure 28: Density vs annealing temperature (for 24 hrs)

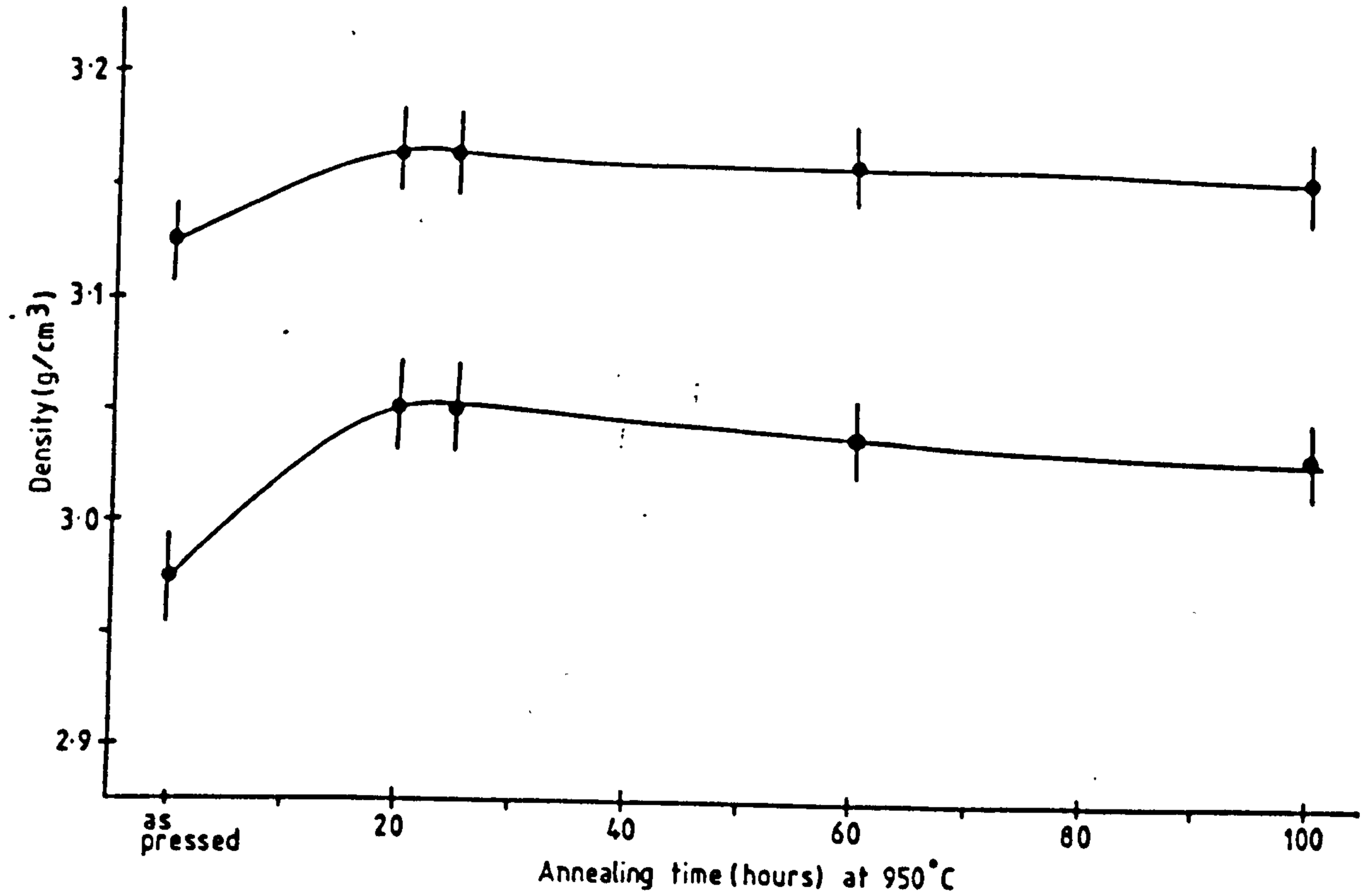

Figure 29: Density vs annealing time (at 950°C)

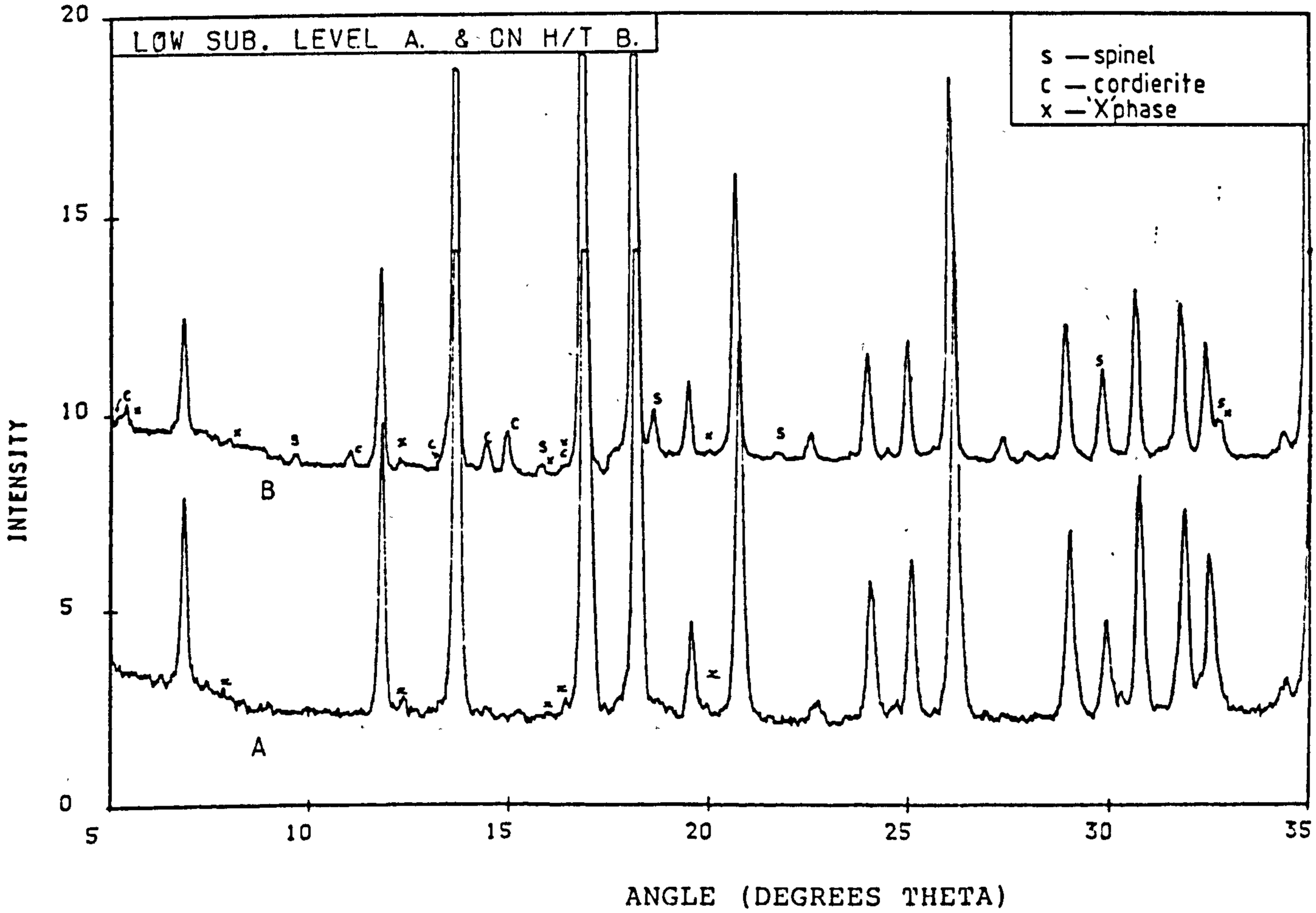

Figure 30: Heat-treatment products of ceramic A. (all unmarked peaks are β')

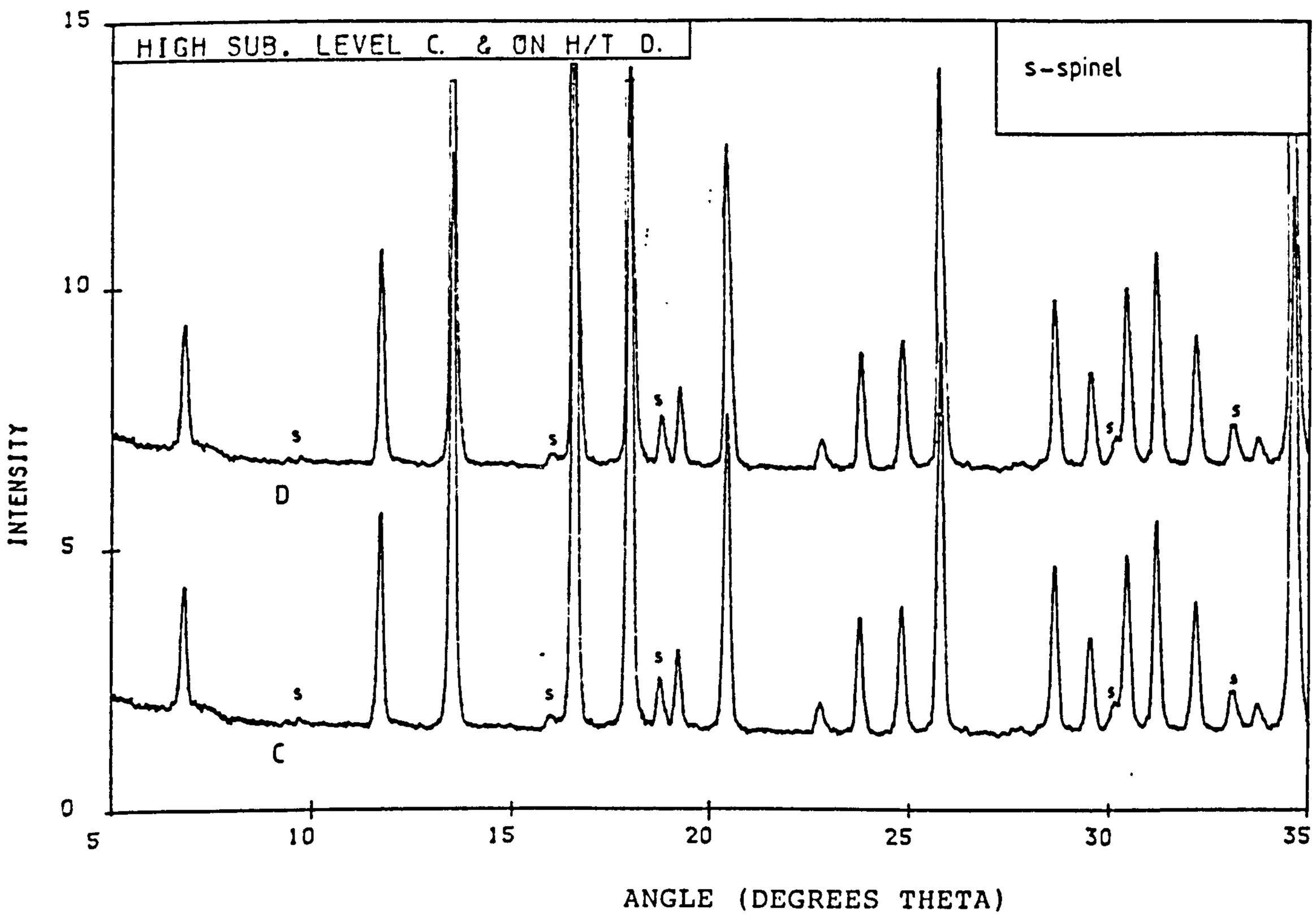

Figure 31: Heat-treatment products for ceramic C (all unmarked peaks are β')

forsterite formation, which is less dense than either spinel or cordierite, or more probably by the start of the glass out- diffusion. This is the cause of the density dropping below its initial value, at > 1000°C for A and > 1100°C for C.

The effect of heat-treatment on the microstructure of A and C is shown in Figures 32 and 33. These heat-treated ceramics have undergone the optimum sintering schedule of 24 hrs at 950°C. The micrograph of B shows almost total crystallization of the grain boundary glassy phase to produce spinel and cordierite. There is a little 'X' phase and only very occasionally is glass seen in the grain boundary triple point regions. The highly faceted B' crystals observed in A in Figure 24 have been replaced by a more rounded morphology indicating that reactions between the B' crystals and the grain boundary phases have taken place. Indeed there is a partitioning of silicon and nitrogen from the grain boundary phase into the β' phase as stated in Chapter Two lowering the z level from z = 1.2 to z = 1.0. The production of corderite and spinel accounted for most of the magnesium present and explains why the remaining glass becomes very silica rich, Figure 35.

The microstructure of the heat treated high z ceramic D shown in Figure 33 indicates that crystallization of spinel and 'X' phase had continued from the as-sintered condition. The z level of the β' remained constant at 2.5 and the residual glass was observed in triple point regions more frequently than for β (Figure 34). The analysis of these glassy regions is shown in Figure 35. The presence of this glass is detrimental to the high temperature mechanical properties of

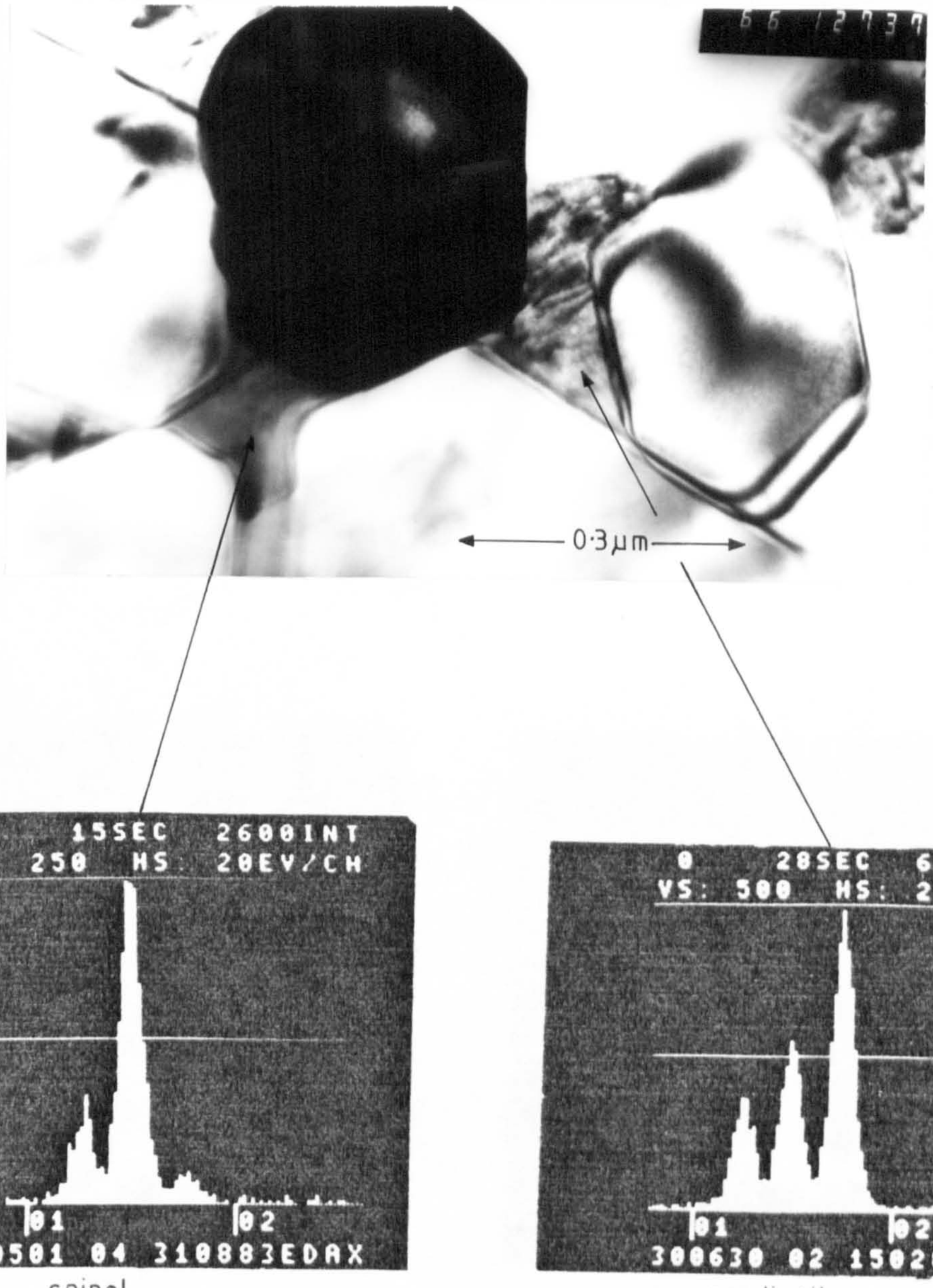

Figure 32: Heat treated ceramic B showing complete crystallization of grain boundary phases.

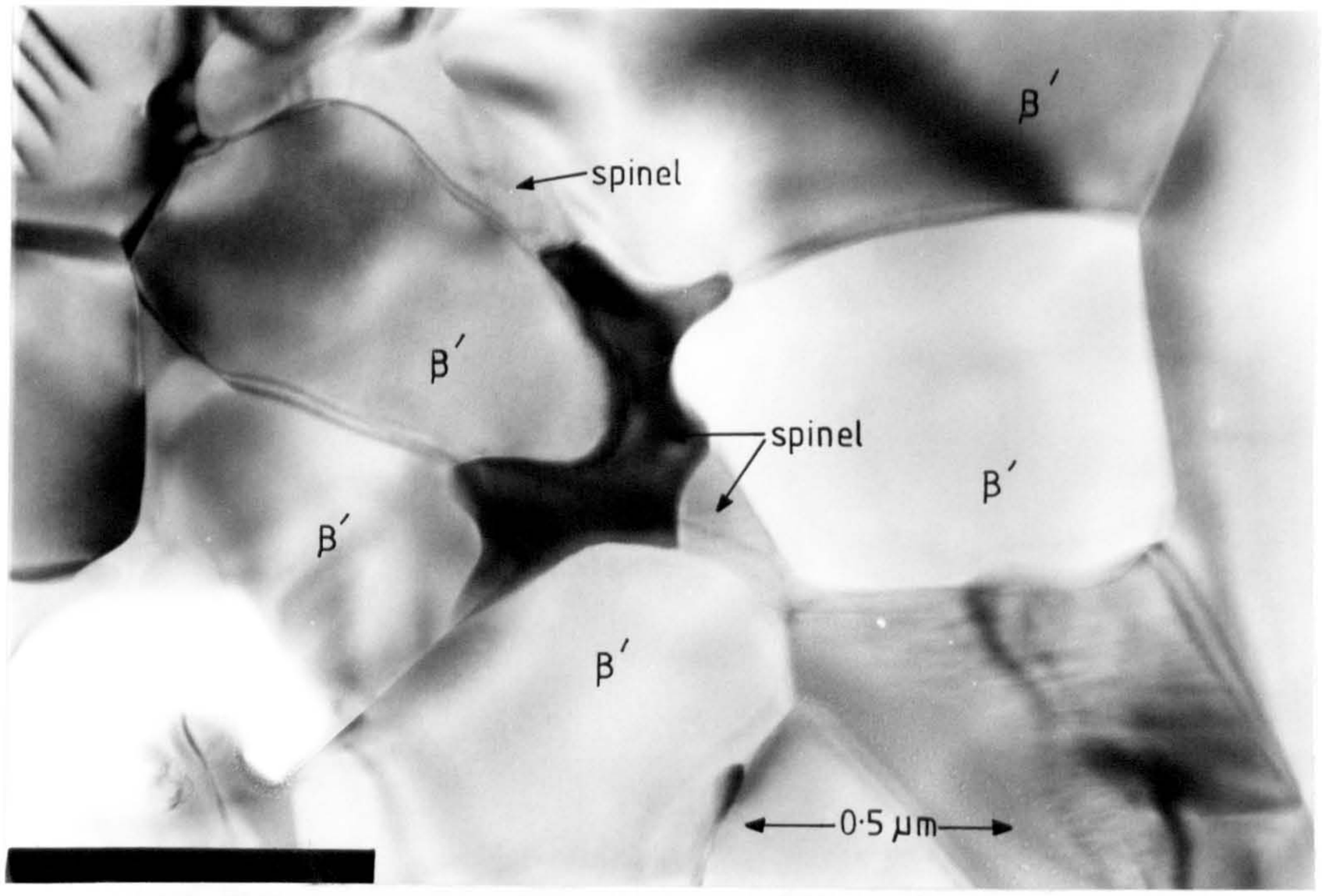

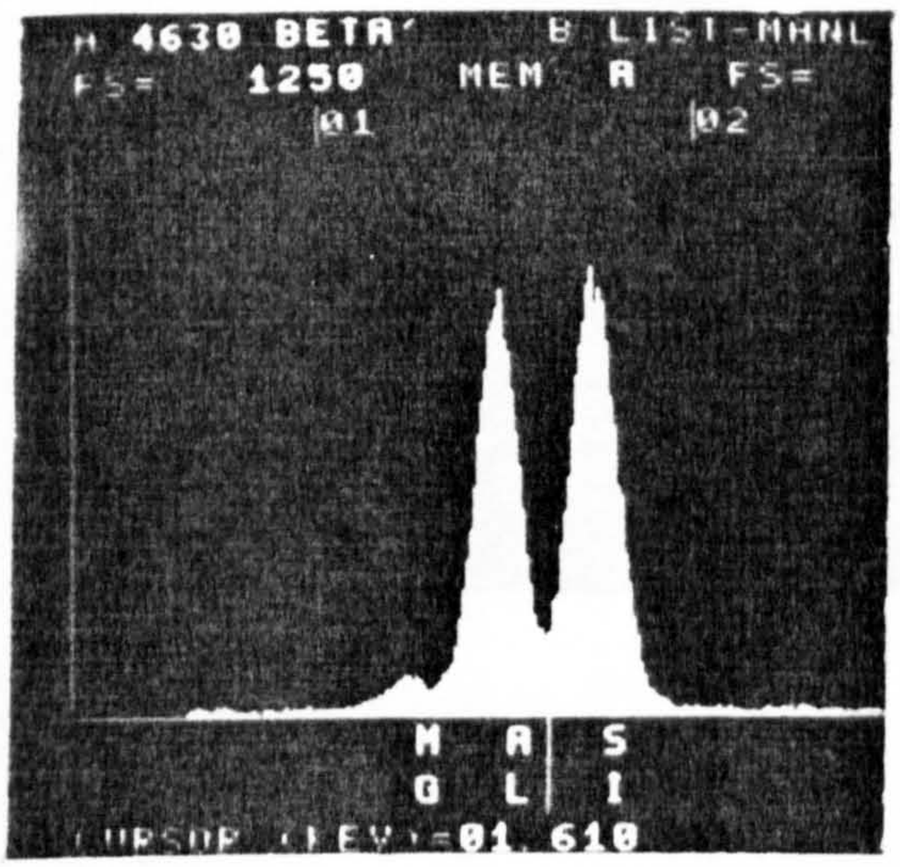

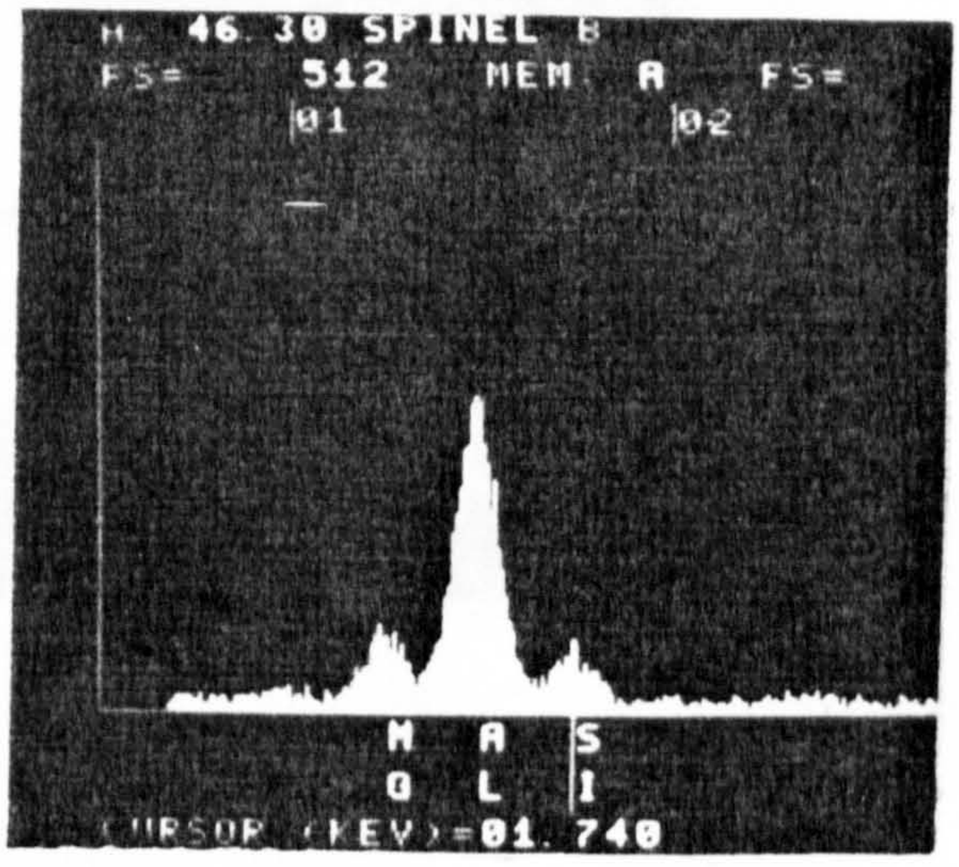

Figure 33:Microstructure of high z ceramic D:
crystallized spinel in the grain boundaries is discontinuous indicating homogenous nucleation.

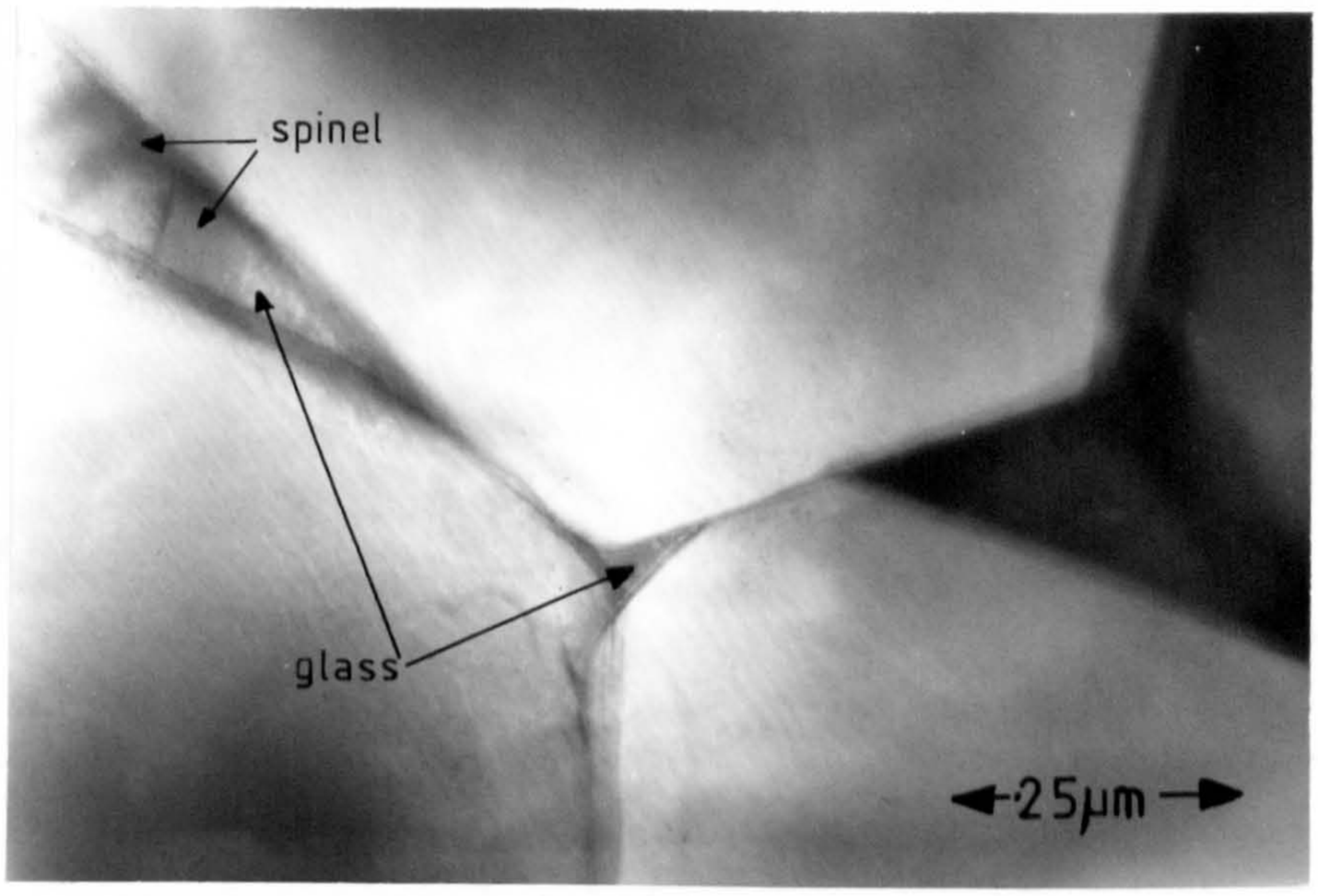

Figure 34: Small areas of glass remaining in triple point regions of ceramic D.

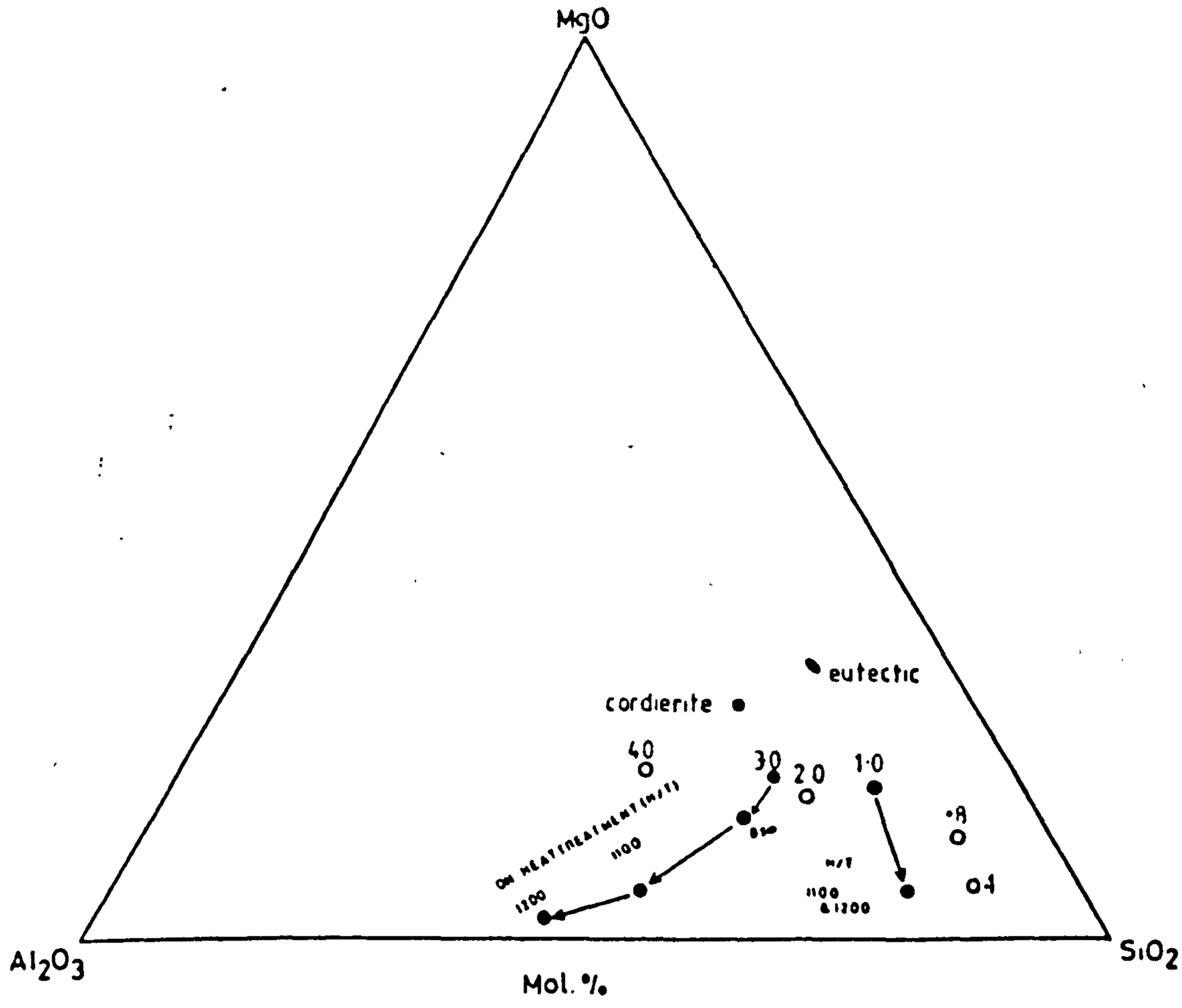

Figure 35: Glass analysis for A, B, C and D and some other heat-treated samples.

the high z ceramic as will be shown later. The reaction products in D prevent both the glass from becoming silica rich or the z level of the β' phase from decreasing as in the low z case.

An anomaly is that the amount of β' and 'X' phase found in ceramic A does not account for all the nitrogen added as silicon nitride and 21R polytypoid in the initial starting compositions. This discrepancy could be due to losses during sintering although this was performed in a nitrogen atmosphere in a 'sealed' crucible to help stop such losses but a probable solution is that the glass is nitrogen rich. Hendry et al[118] had found only crystalline phases in the Si_3N_4-Al_2O_3-MgO system but it has been shown by Jack[15] and others[37] that nitrogen-containing glasses in the MgSiAlON system can be formed. Despite the advantages of a nitrogen enriched glass expressed in Chapter Two by Loehmann[27], the fluidity is still very high. When low z ceramics were heat-treated at > 1000°C they were coated by this glass which had out diffused. High z ceramics are expected to have a lower nitrogen content glass due to the presence of less silicon nitride, but it has been shown to be partially crystallised on sintering so the problem of glass out-diffusion is much less severe.

The heat-treatment temperature used in the present work was very low compared to that used by Lewis et al[20], who used temperatures of approximately 1200°C. Spinel was the major grain boundary phase and was of constant orientation over 20-30 β' grains. Here in contrast spinel, or any other grain boundary phase, is discontinuous, much less than one β' grain in size although the spinel is slightly silicon substituted, in agreement with Lewis et al[20].

At only 50°C above the optimum sintering temperatures regions of high z ceramic showing severe bloating have been noted in Chapter Three.

The main cause of this is believed to be losses of nitrogen, silicon in the form of SiO and Al_2O (as suggested by Kuwabara [58] in Chapter Two above). The reason is that adjacent to those regions there are areas where the β' crystals are hexagonal, highly faceted and have an z level ~ 2.5 and where the grain boundary phases appear to be totally crystallised to spinel and 'X' phase. The microstructure of a high z ceramic in this condition is shown in Figure 36.

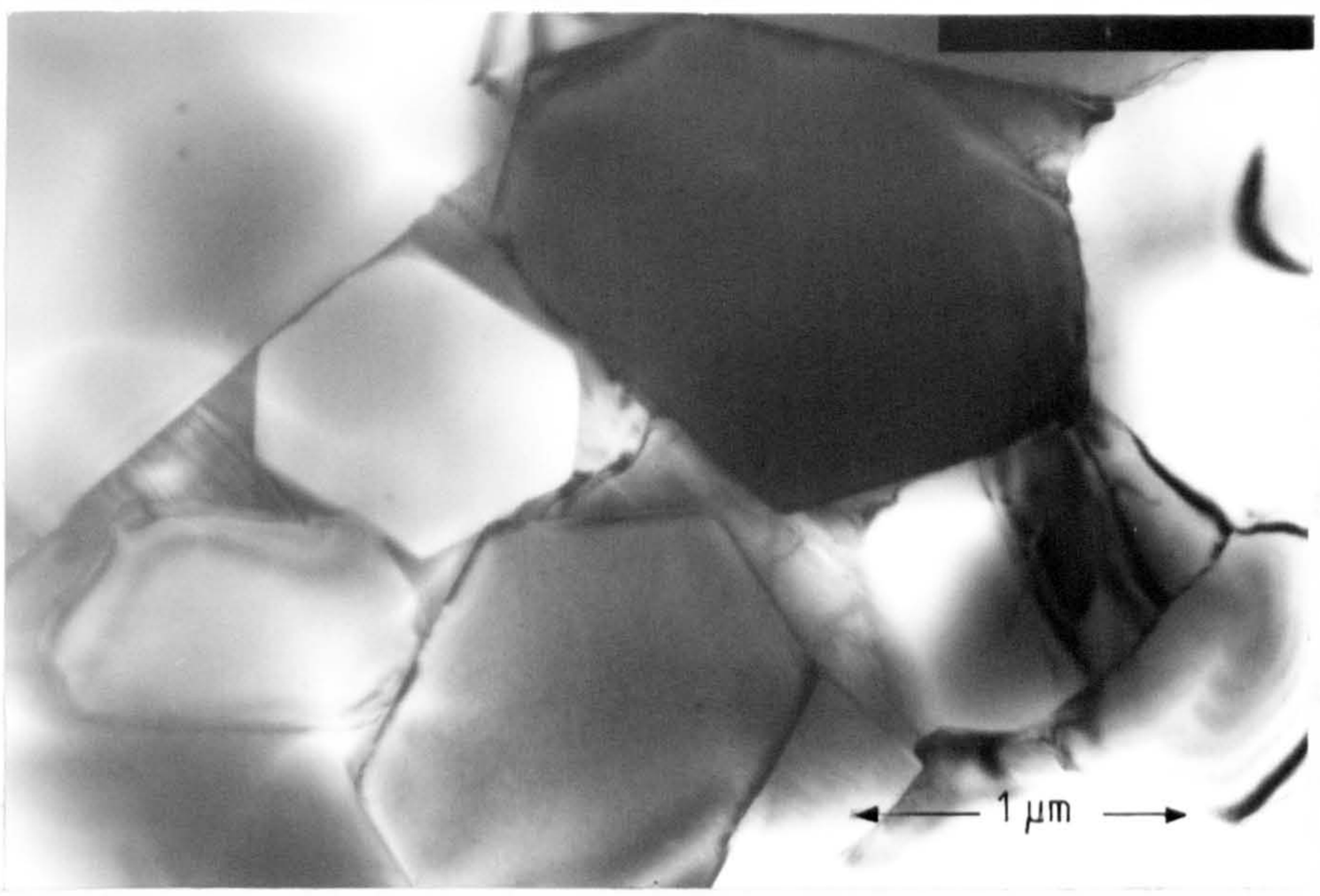

Figure 36: Microstructure of a high z ceramic after sintering at 1800°C for 1 hour (adjacent to bloated region shown in Figure 23).

4.2.3 Effect on Microstructure of Heating in an Oxidising Environment

The thermal stability of A, B, C and D in an oxidising environment was tested by heating samples in an open table furnace. Polished bars of approximately 3x3 mm or 5x3 mm cross section were supported on a platinum wire cradle and heated for up to 100 hours at temperatures of up to 1300°C. Examination of the samples was by optical microscopy, TEM, SEM, EDAX and XRD. The increase in resistance to oxidation of samples after heat-treatment is shown in Figure 37 where all samples have been subjected to a temperature of 1200°C for 56 hours.

Ceramic A and to a lesser extent C suffered from out-diffusion of the grain boundary glass which coated the surfaces of the samples. This occurred at temperatures > 950°C and produced a 'diffusion' zone beneath the surface which is visible in A and C in Figure 37. The microstructure of A and C within this zone indicated grain boundary phase reactions had taken place (Figure 38). A series of analyses from the surface inwards involving XRD and EDAX was undertaken to try to determine the cause of this zone; these are shown for A and B in Figure 39 and C and D in Figure 40.

For ceramic A the depth of the zone was 1 mm after 56 hours and 1.2 mm after 100 hours at 1220°C. Within the zone both the z level and the magnesium content of the β' crystals were reduced to the levels found for heat-treated ceramics. Spinel, cordierite and a little 'X' phase were crystallised in the grain boundaries shown in Figure 38, which became severely affected because of glass out diffusion. In the subsurface region both magnesium and silicon were lost from the β' crystals. Cordierite was the dominant oxide phase above 1000°C and the dominant surface phase above 1200°C. After 56 hours at 1300°C

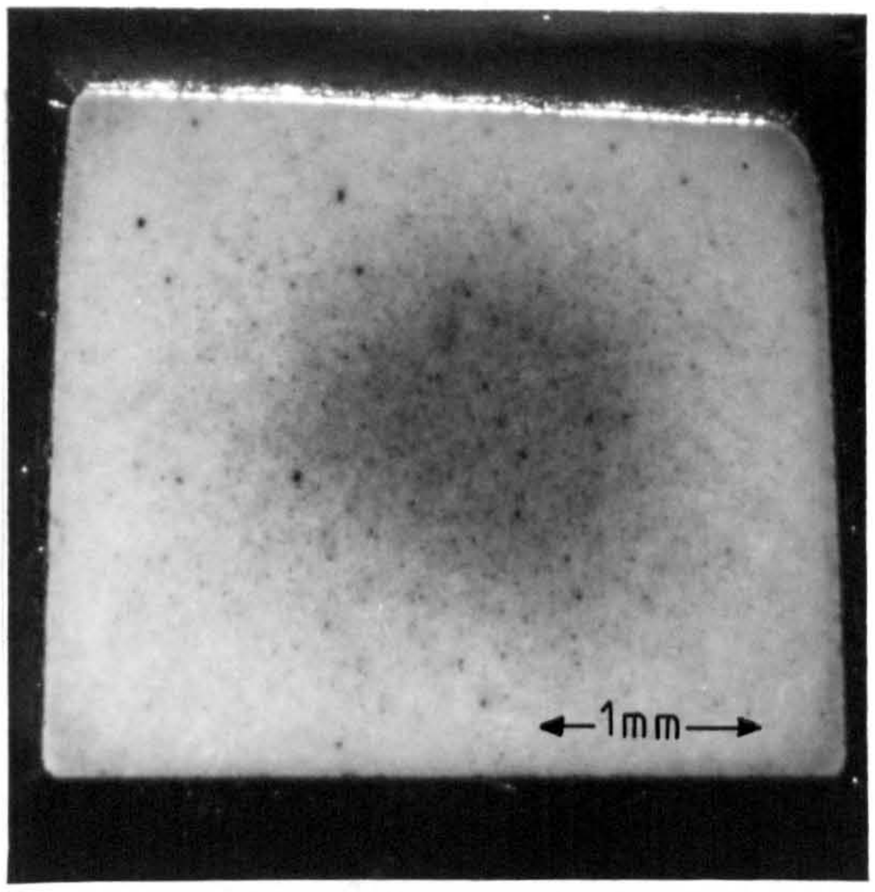

A

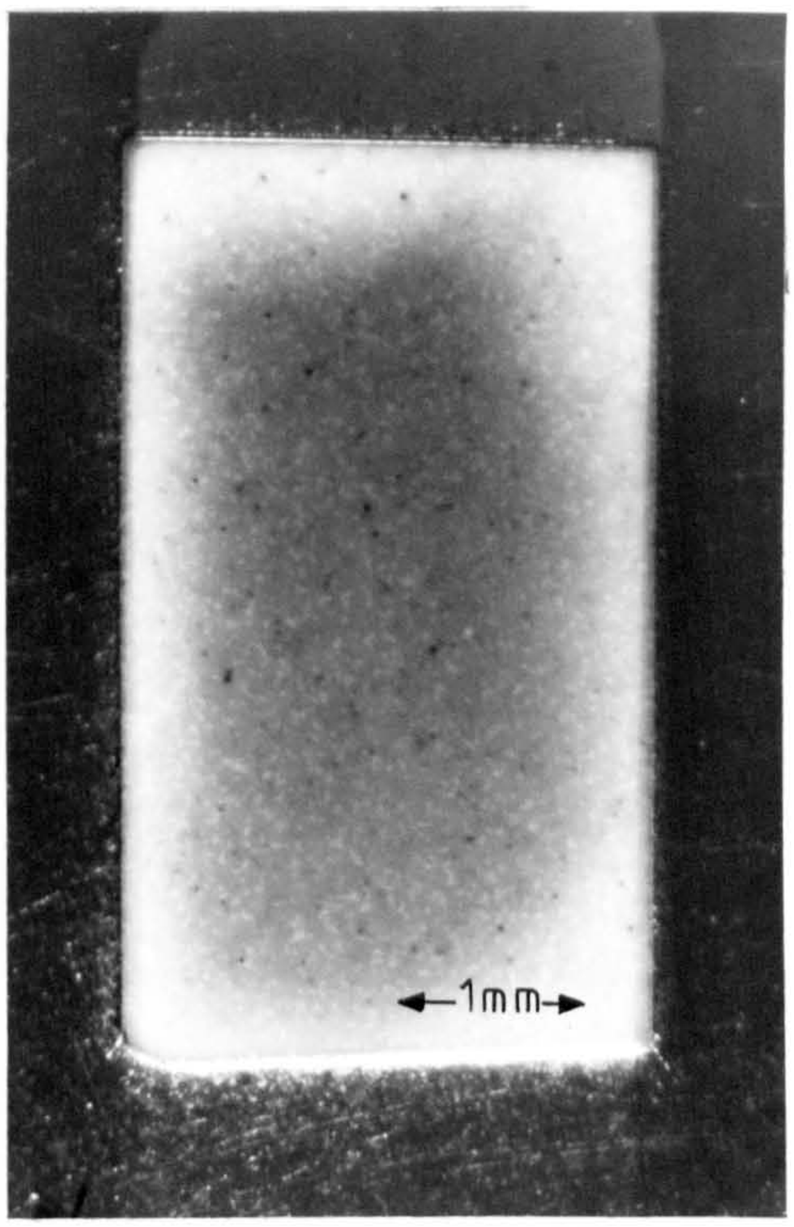

C

B

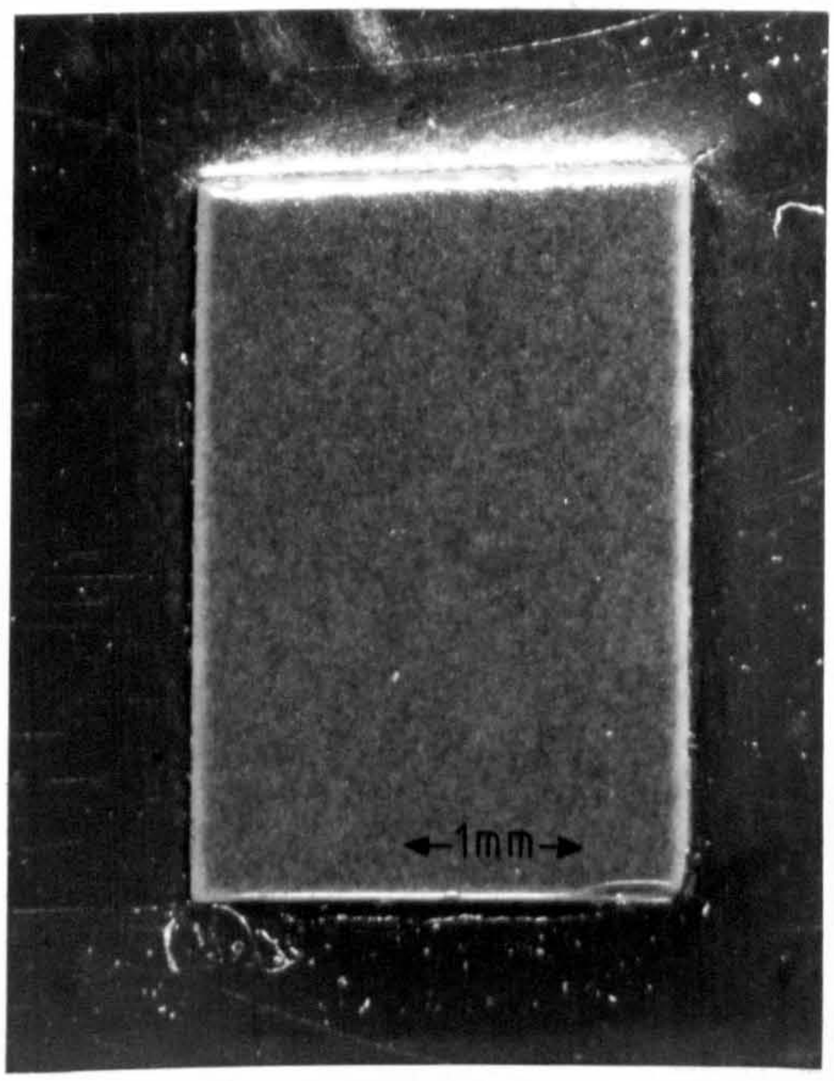

D

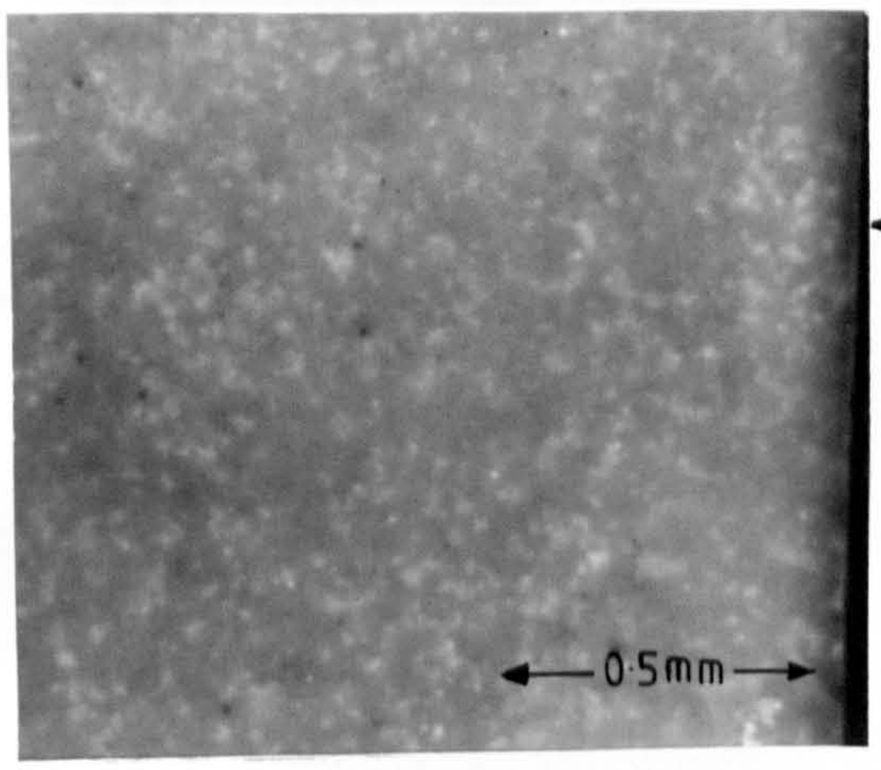

Figure 37: Thermal stability of A, B, C, and D showing increase after heat-treatment.

Samples have been heated for 56 hours at 1200°C.

The depth of the diffusion zone is much reduced after heat-treatment.

(b)

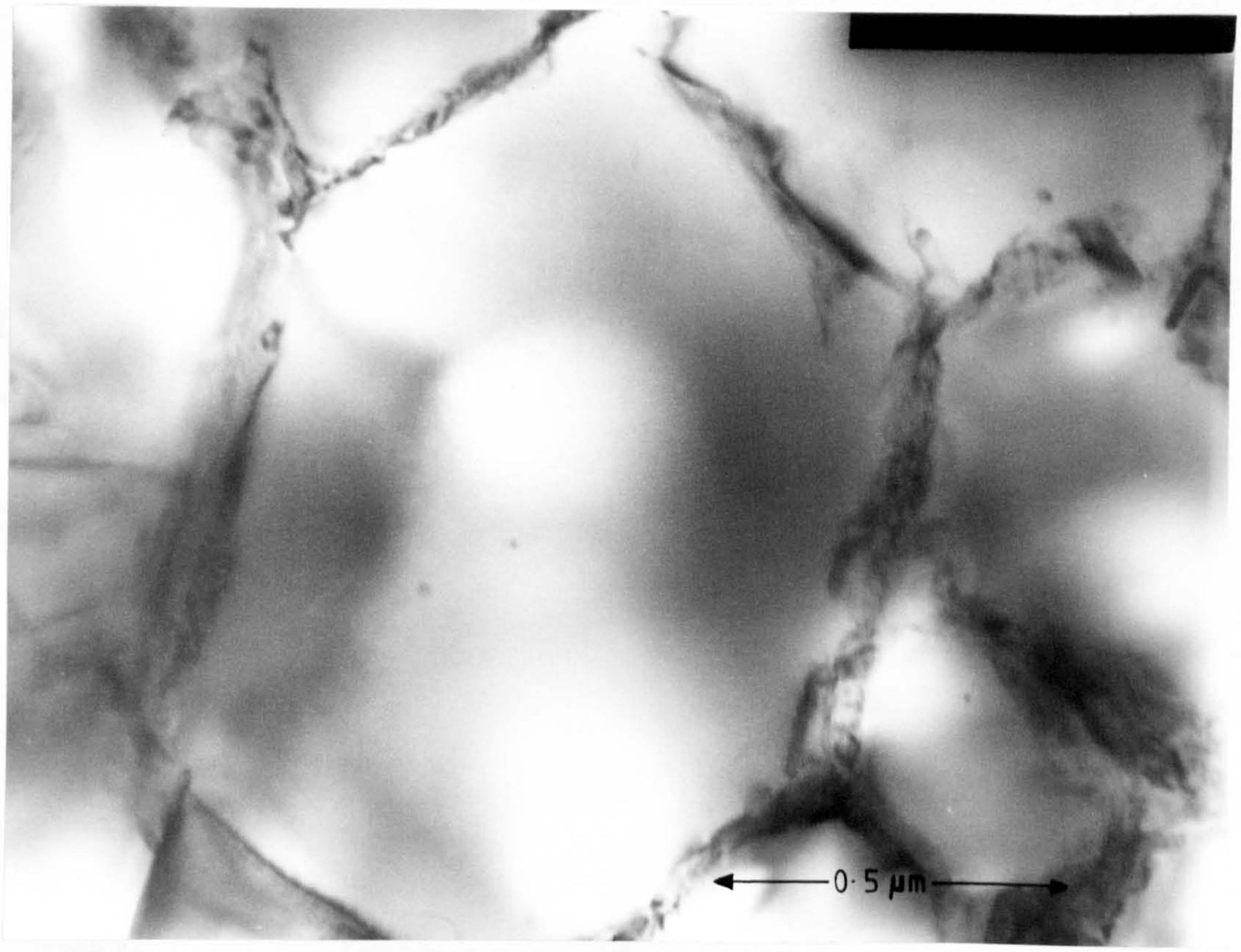

(a)

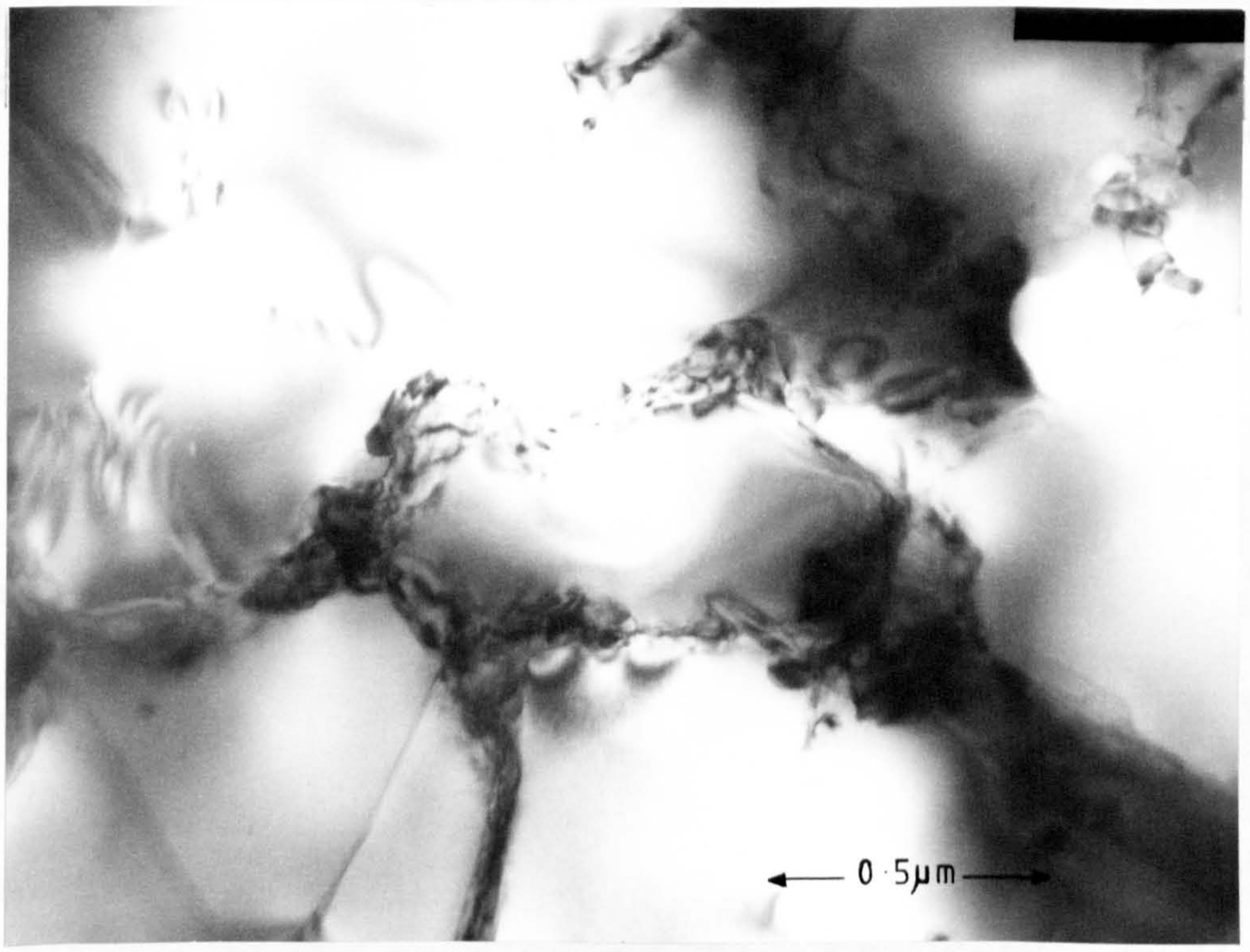

Figure 38: Microstructure of the ceramic in the diffusion zone

(a) low z ceramic A (b) high z ceramic C

Similar microstructure in both ceramics caused by grain boundary reactions and out-diffusion of glass.

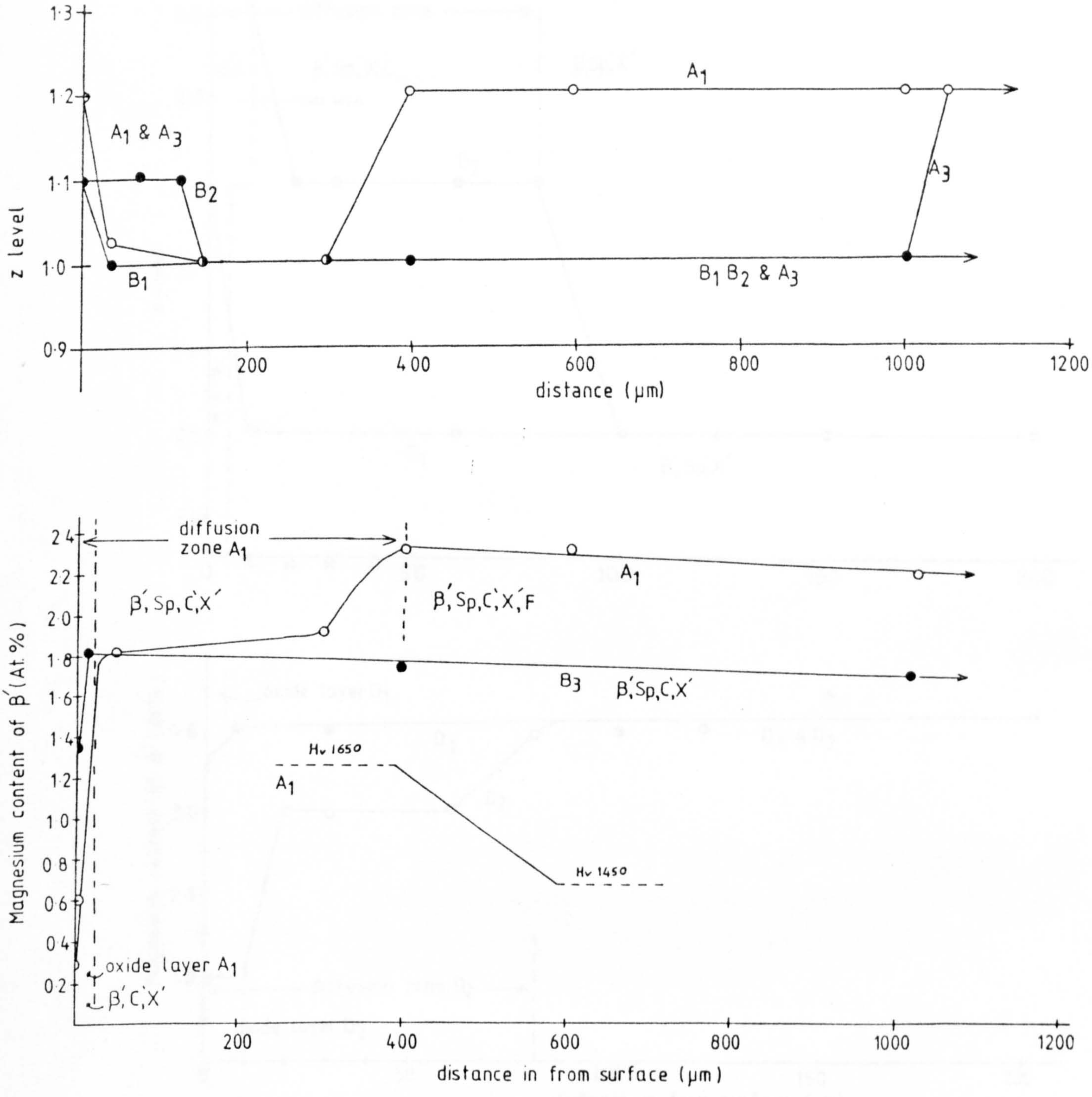

Figure 39: Effect on z level and magnesium level of β' crystal for A and B after heating in an oxidising environment.

The subscripts 1, 2, 3 are

(1) oxidised for 24 hours at 1100°C

(2) oxidised for 36 hours at 1200°C

(3) oxidised for 56 hours at 1200°C

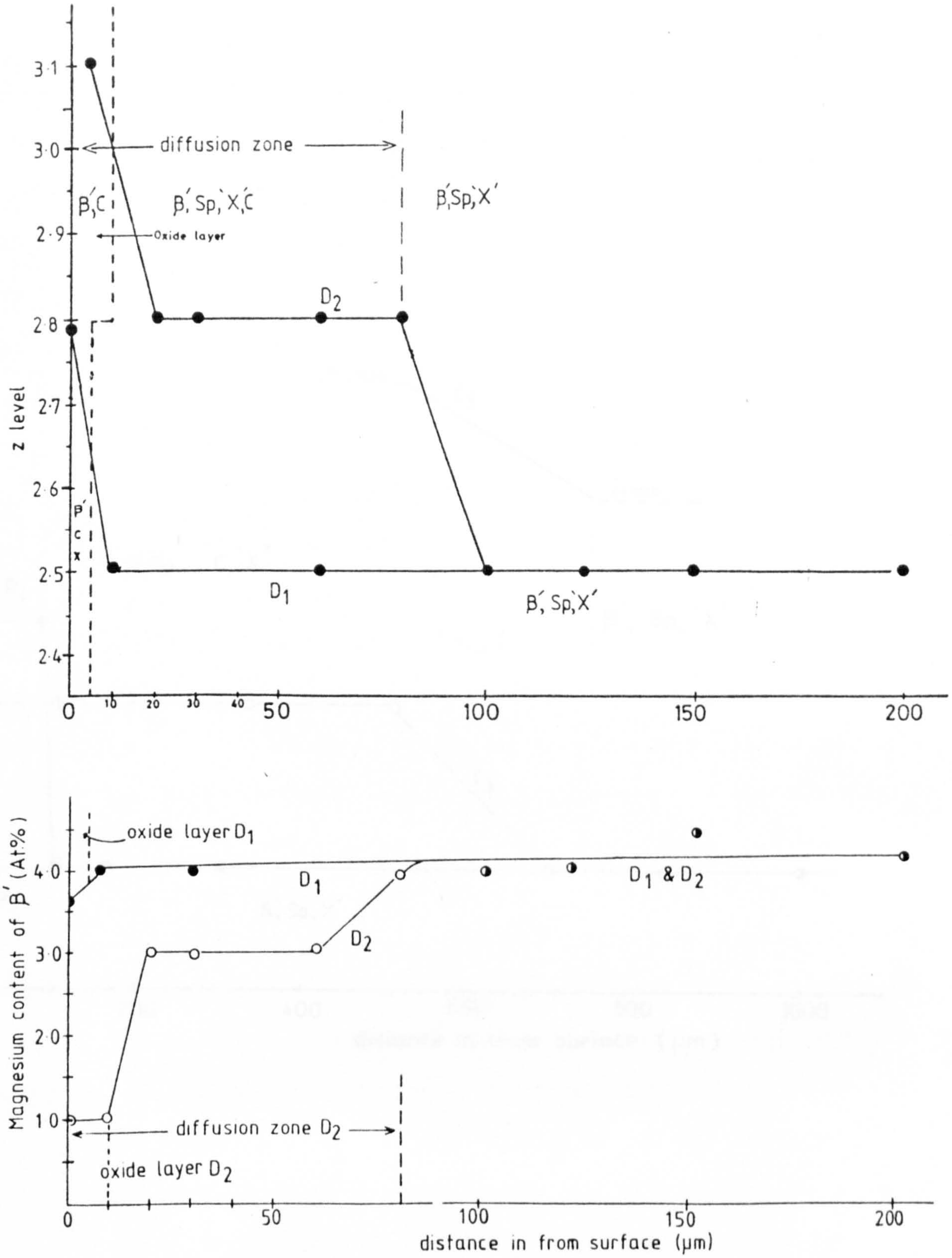

Figure 40(a) Effect on z level and Mg level of β' phase for D after heating in an oxidising environment.

Subscripts are defined in Figure 39.

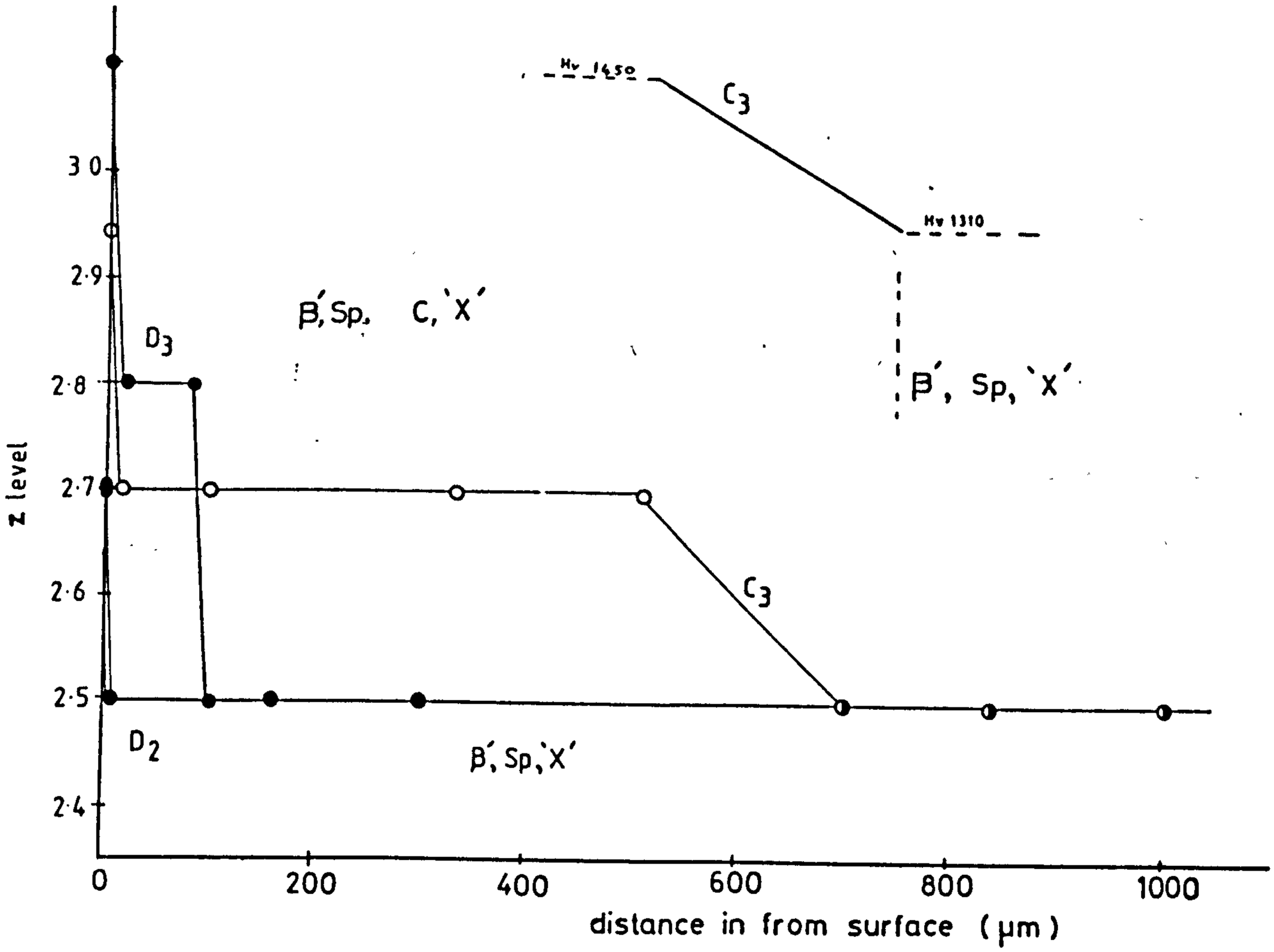

Figure 40(b): Effect on z level for C and D after heating in an oxidising environment.

Subscripts 2 and 3 are defined in Figure 39.

the thickness of the cordierite layer was 1 mm deep and nitrogen evolution thought to be from the glass caused bloating to the rest of the sample. Upto temperatures of 1220°C the core structure remains relatively unaffected. Crystallisation occurs as in the heat treated samples although forsterite is crystallised in addition to the heat-treated products found in the grain boundaries. The microstructure of the core of A is shown in Figure 41.

For ceramic B the diffusion zone is much reduced in depth, see Figures 39 and 42. There is a rise in z level and decrease in magnesium content of the β' crystal below the surface which indicates both silicon and magnesium losses. Cordierite is the major oxide phase and above 1000°C no spinel is observed on free surfaces.

In ceramics C and D, above 1000°C cordierite is formed in the diffusion zone. The silicon and magnesium for this may have originated from the β' crystals since there was an observed increase in z level and decrease in magnesium content. Glass out-diffusion for C was less than for A and the resulting diffusion zone was much smaller, see Figure 42. This is due to the fact that this glassy phase was partially crystallized in the as-sintered state. The microstructure of C within this zone is similar to A, see Figure 38, also indicating grain boundary reactions had taken place. In the core of C forsterite formed, as in A, along with spinel and 'X' phase. On the surface only β' 'X' phase and cordierite were found in C and D above 1000°C, and as with the low z ceramics no spinel was observed. The depth of this oxide layer was quite small, even after 1000 hours at 1220°C it was only a few microns deep.

The extent of the diffusion zone for A, B, C and D after heating to 1220°C for various times are shown in Figure 42 along with times at

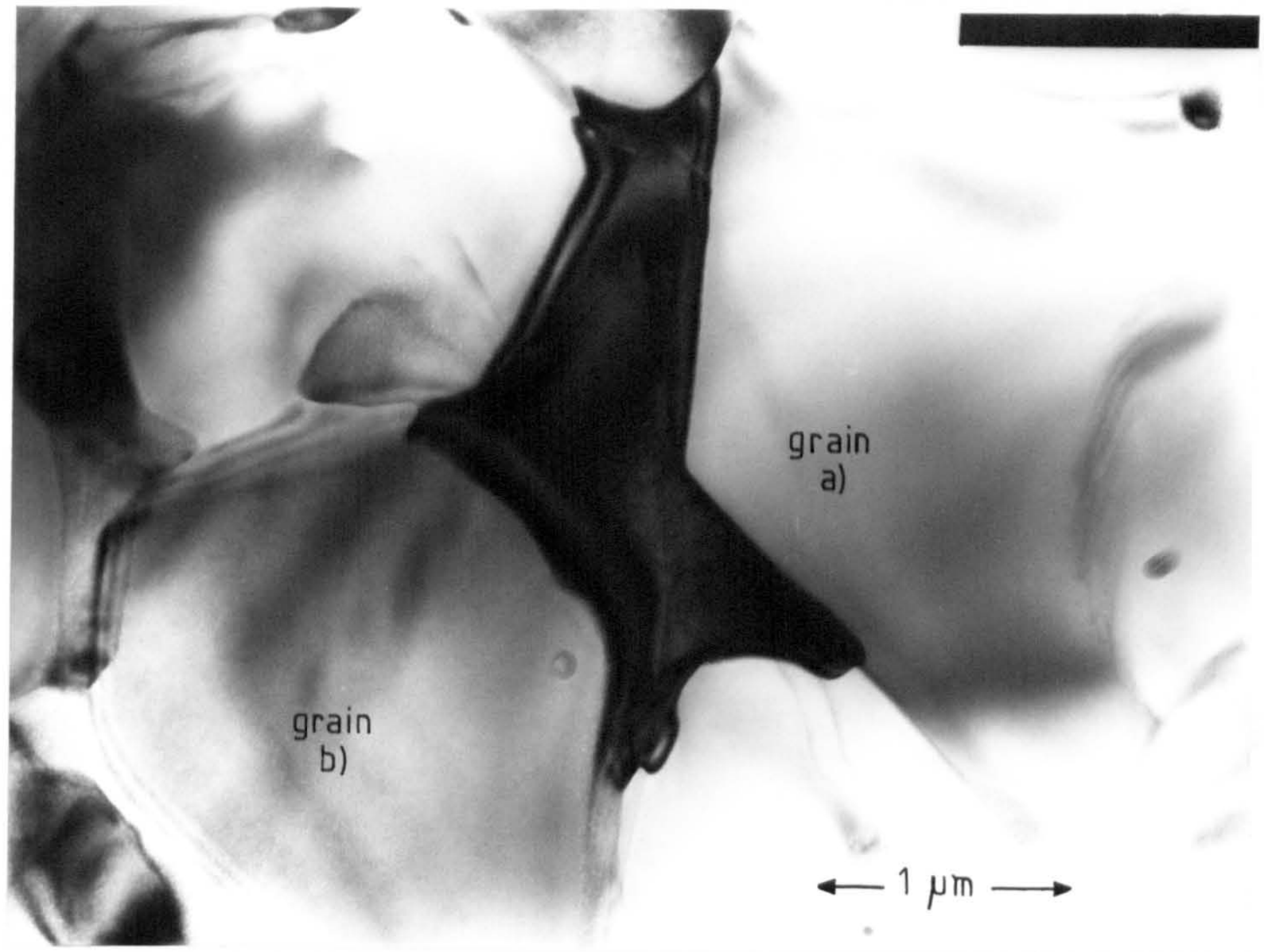

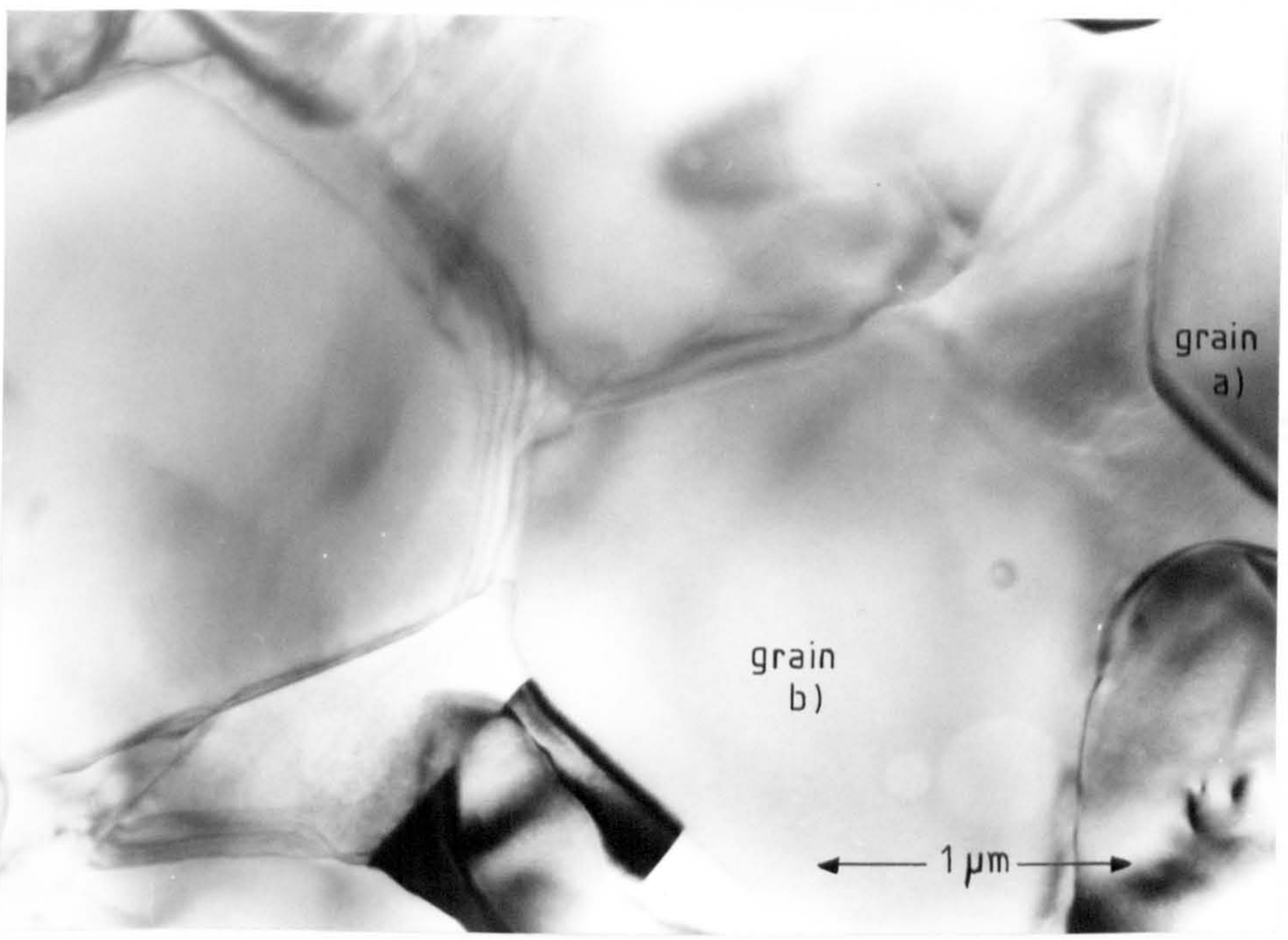

Figure 41: Microstructure found within the core of a low z SiAlON A after heating in an oxidising environment for over 50 hours at 1200°C.

The grain boundary phases include forsterite as well as the more commonly observed phases spinel, cordierite and 'X' phase.

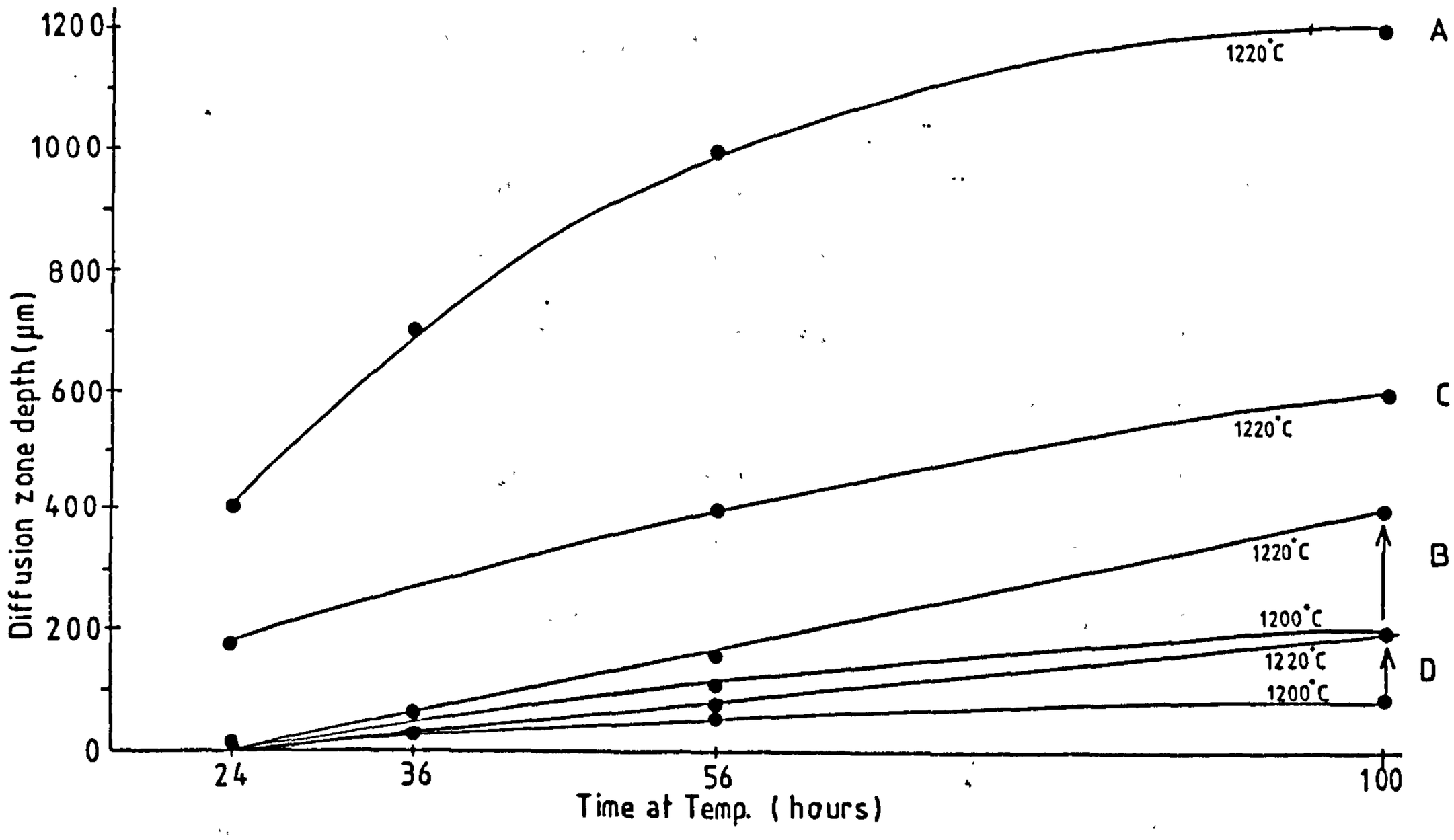

Figure 42: Graph of diffusion zone depth vs time at testing temperature

1200°C for B and D. Generally the high z ceramics C and D showed improved stability over low z ceramics A and B. There appeared to be a logarithmic reaction rate for A and a parabolic rate for C. Intermediate reaction rates were observed for B and D below 1200°C. Above 1200°C the reaction rate for B and D appeared to have a linear dependence, (these relationships were determined using least squares fit analysis). Reasons for the change in reaction mechanism of B and D could be due to dissociation of 'X' phase, which was not observed on the surface above 1200°C, the nitrogen from this reaction could make the protective cordierite layer porous. From the data it is observed that heat treated high z ceramic D is the most thermally stable in an oxidising environment with the stability decreasing in the order D > B > C > A. Without a heat-treatment schedule, use of these ceramics is limited to less than 900°C for A and 950°C for C, due to problems of glass out-diffusion. After the heat-treatment, use of ceramics up to 1200°C for D and slightly lower than this for B is envisaged. Despite the low value of the temperature used for heat-treatment, compared to those used by other workers, it has been shown to lead to a distinct improvement of the high temperature properties of these materials.

To summarise: as-sintered ceramics have been produced and subjected to various isothermal heat-treatments to crystallise grain boundary glassy phases. Cordierite and spinel, with a trace amount of 'X' phase are produced in the low z ceramics. In the high z ceramics the grain boundary glassy phase is already partially crystallised, but more spinel and 'X' phase are produced leaving some residual glass in grain boundary triple points.

During this heat treatment the z level of the low z ceramics decreases, as predicted, but the z level of the high z ceramics remains constant.

Both as-sintered and heat-treated ceramics were subjected to thermal stability testing. The as-sintered low z ceramics performed badly at temperatures above 1000°C due to glass out-diffusion to form cordierite on the surface. For the high z ceramic, the diffusion front moves only half the distance that the low z front moves under similar conditions. The increase in stability is due to the fact that the grain boundary phase is partially crystallised on sintering. Heat-treatment improves thermal stability of both low and high z ceramics due to further crystallization of the grain boundary glassy phases, the depth of the oxide layer as well as the sub-surface diffusion zone are much reduced. The temperature of the heat-treatment used in the project was 950°C, this was found to give a upper working limit in air of 1150-1200°C for the high z ceramics. Low z ceramics were less stable in an oxidising environment. The increase in working limit (approximately 200°C) over the as-sintered ceramic may be improved by altering the isothermal heat-treatment which was used in this project and would form an interesting topic for future work.

Thermal stability in an oxidising environment is important in relation to high temperature mechanical behaviour, one of the topics discussed in Chapter Five.

CHAPTER FIVE

MECHANICAL PROPERTIES' SURVEY

This chapter analyses some mechanical properties of the MgSiAlON ceramics. At low temperatures fracture toughness and hardness were determined and at high temperatures some creep properties were examined. This survey describes the effects of stress and oxidising environment on the MgSiAlONs to determine the maximum working limits of these ceramics in engineering applications.

5.1 Experimental Techniques

5.1.1 Fracture Toughness and Hardness Testing

The dimensions of the samples of A, B, C and D (defined in Chapter Two) used for the room temperature SENB fracture toughness testing were standardised[75] and are shown in Figure 43.

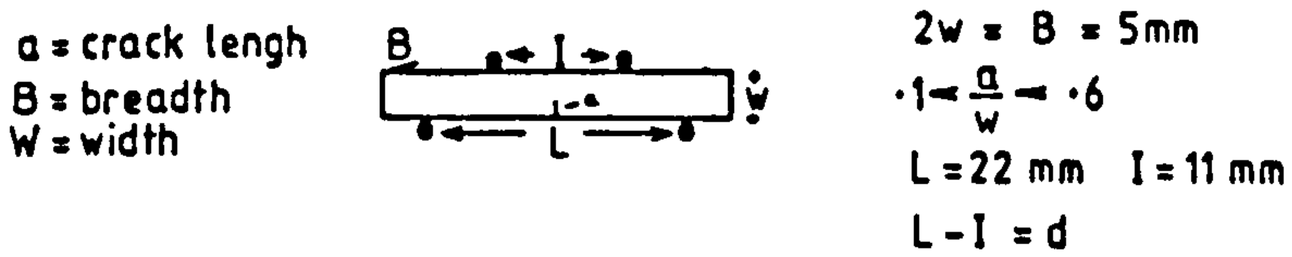

Figure 43: Dimensions of SENB test bar and loading knife edges.

Both the sides and the tensile face (lower surface) of the bar had been ground and polished using 6 and 1 μm diamond paste respectively. These bars were then notched to a recorded depth using

a diamond-edged saw and then fractured in air at ambient temperature on a four point bend jig using an Instron tensile testing machine (type 1122). The formula used in the present work for the determination of fracture toughness, was derived by Smith and Piper[76] and is:

$$K_C = \frac{3P_f}{Bw^2} a^{\frac{1}{2}} \left[3.86 - 6.15 \frac{a}{w} + 2.17 \left(\frac{a}{w}\right)^2\right]^{\frac{1}{2}}$$

where P_f is the load at fracture. The definitions of a, B and w are shown in Figure 43.

Other samples of A, B, C and D were indented by a Vickers diamond to known loads and the crack system developed was then used as a critical flaw. They were then fractured as in the SENB method. The formula for this method is[80]:

$$K_C = \frac{(\sigma_m P l/3)^{\frac{1}{2}}}{1.69} \cdot \left(E/H\right)^{1/8}$$

where P is the indenting load

σ_m is the fracture stress

E is Young's modulus

H is the Vickers hardness.

The stress σ_m is given by[82]:

$$\sigma_m = \frac{3}{2} \frac{(L-I)}{Bw^2} P_f$$

where P_f is the fracture load

L, I, B and w are as defined previously in Figure 43.

Samples of A, B, C and D were also Vickers Hardness tested using the Instron. Loading and unloading rates of .1 mm s^{-1} were used and a fixed hold-time of thirty seconds ensured standard testing conditions.

The results of the SENB and indentation fracture toughness and hardness testing are shown in Table 6. They show that low z ceramics are both harder and tougher than their high z counterparts in both the as-sintered and heat-treated conditions.

Sample	Indentation K Testing MPa $m^{-\frac{1}{2}}$	Corrected K (x1.4) MPa $m^{-\frac{1}{2}}$	SENB MPa $m^{-\frac{1}{2}}$	Vickers Hardness kg mm^{-2}
A	2.26 ± .02	3.16 ± .03	3.57 ± .02	1450 ± 40
B	2.72 ± .07	3.81 ± .1	3.95 ± .06	1650 ± 20
C	1.72 ± .05	2.41 ± .02	3.22 ± .02	1310 ± 15
D	1.74 ± .06	2.44 ± .08	3.22 ± .03	1450 ± 40

Table 6: Fracture toughness and hardness results

In an attempt to define the fracture mode, the fracture surfaces were examined in the SEM. The results, Figures 44 to 47, show that for A and B the fracture mode is mixed (transgranular + intergranular) but for C and D it is predominantly transgranular.

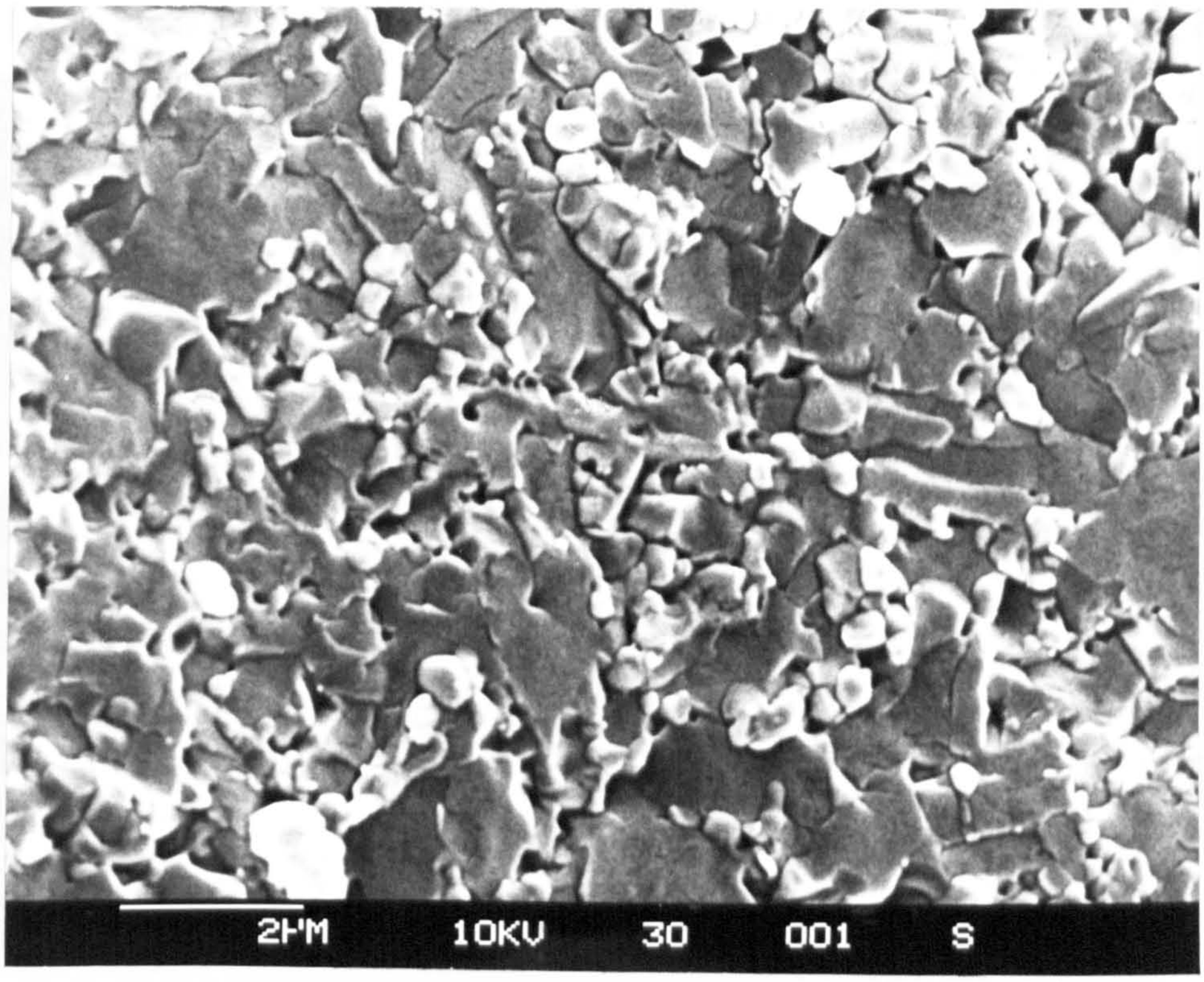

Figure 44: Fracture surface of ceramic A

Showing mixed mode fracture i.e. both intergranular and transgranular fracture.

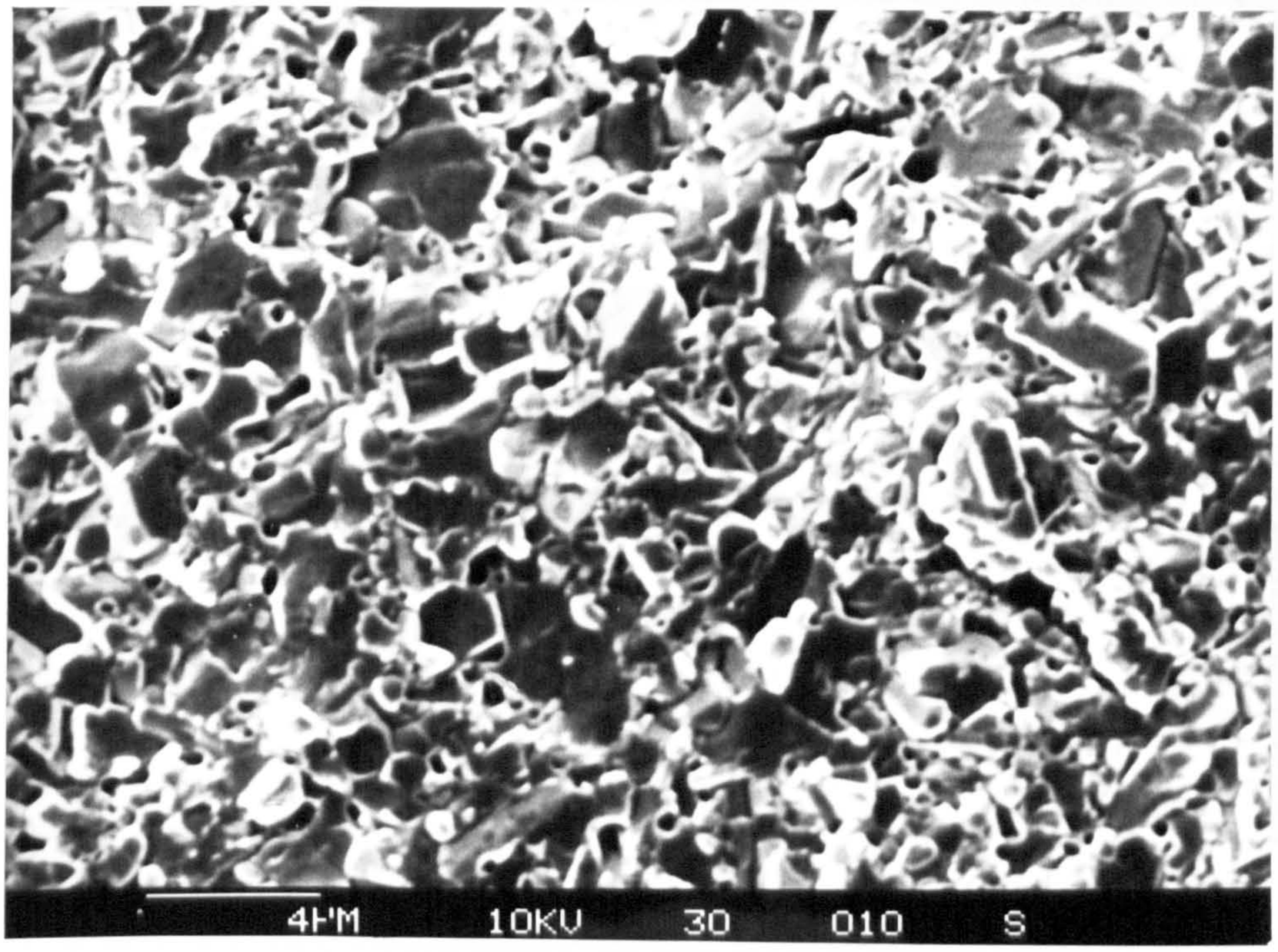

Figure 45: Fracture surface of ceramic B

Showing mixed mode fracture as found in ceramic A.

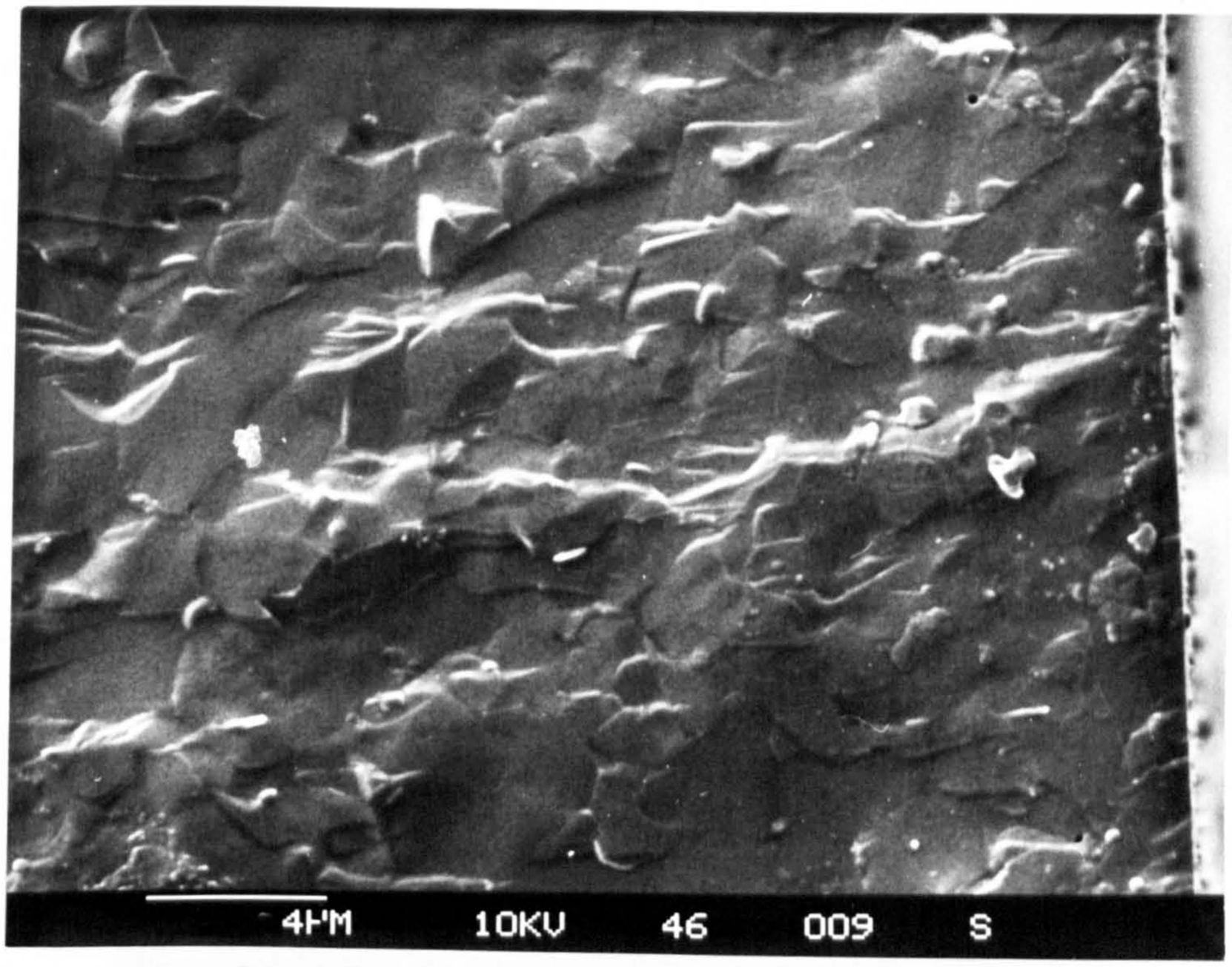

Figure 46: Fracture surface of ceramic C

Showing predominately transgranular fracture which is in complete contrast to that found for low z ceramics in the as-sintered or heat-treated condition (Figures 44 and 45).

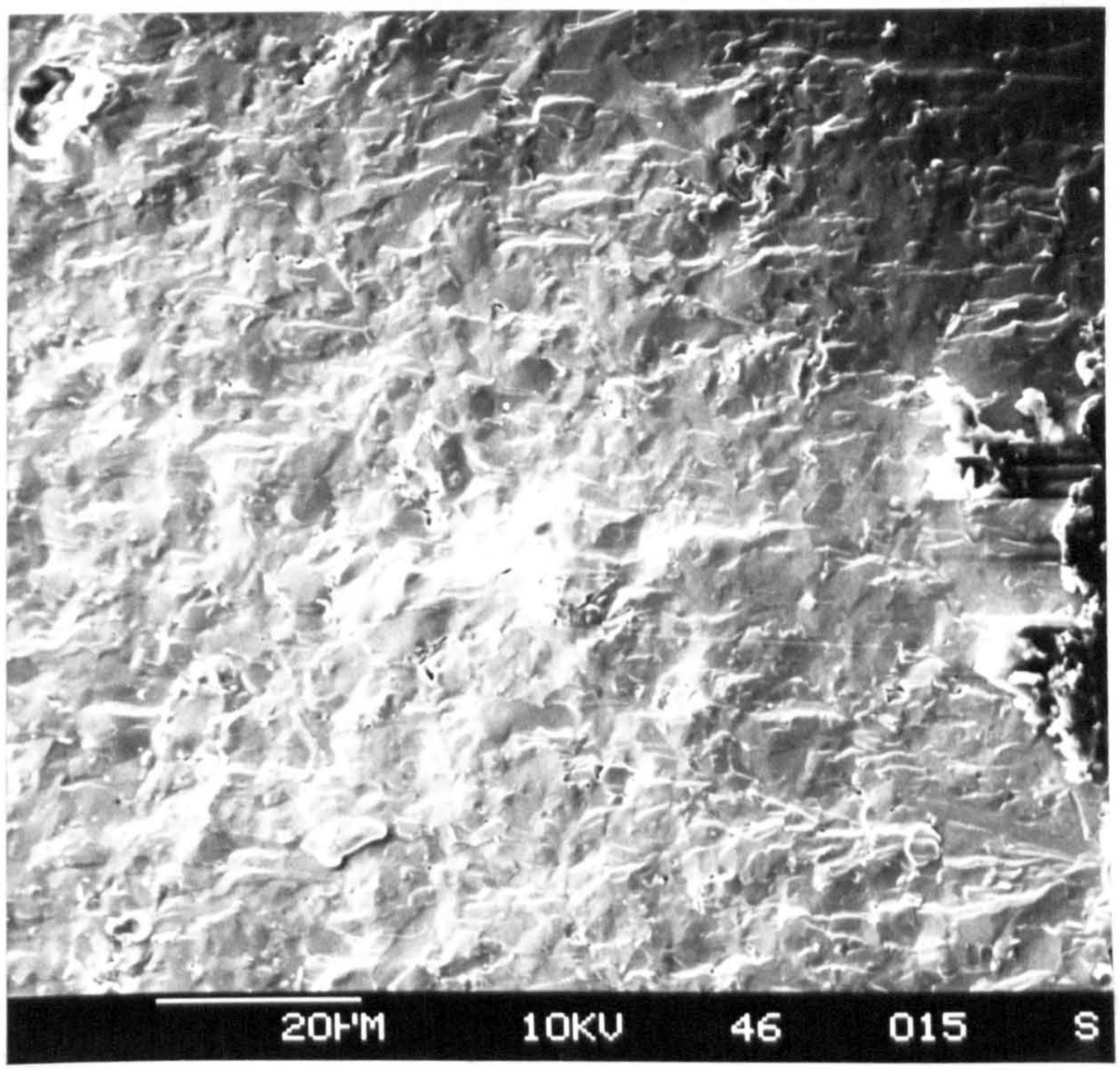

Figure 47: Fracture surface of ceramic D

Showing predominantly transgranular fracture, as found for Ceramic C.

5.1.2. Creep Testing

Four point bend testing of the creep samples was chosen for the following reasons: (a) it has the advantage over three point bend testing of constant bending moment between the inner knife edges of the loading jig. The loading arrangement can therefore be less precise, (b) the area of the specimen in which cavity formation is expected would be more easily detected than in a compressive creep experiment where these tensile and shear regions are less localised and therefore less easily observed[119] and (c) a suitable four point loading jig was already available.

The vertical movement of the bending specimen which was required to calculate the outer fibre tensile strain was measured using a Linear Variable Differential Transducer (LVDT). This was calibrated with feeler gauges prior to and after the creep testing.

The formula to calculate the tensile creep strain[105] is:

$$\varepsilon = \frac{6yb}{(L-I)(L+2I)}$$

where y = vertical movement
b = specimen height
L = lower support width
I = upper support width

The formula used to calculate the stress was that used for the fracture toughness testing shown above.

Testing was performed in air in a furnace which could hold the sample temperature to $\pm$ 5°C. A Eurotherm power controller (Type 070) regulated the temperature using the output from a Pt/Pt 13% Rh

thermocouple placed close to the sample. To aid temperature control an air conditioner was installed in the testing room, which helped to keep the ambient air, and hence the cold junction of the Eurotherm and LVDT, at an almost constant temperature. This removed daily thermal fluctuations and the observed fluctuations in creep rate associated with them. The furnace shown in Figure 48 consisted of two separable halves which allowed easy access for sample alignment and maintenance. Each half consisted of three silicon carbide heating elements: in the fixed half the loading arrangement was contained. This comprised alumina rods and tubes, Figure 48 and also the loading head and sample, Figure 49. Single phase SiAlON knife edges were used to prevent bonding with the test bar.

Samples of B and D were cut to approximately 5 x 2.5 x 25 mm and then polished. On raising either the temperature or the load several days were allowed to enable the sample to reach steady state conditions and to ensure transient creep had been completed[110]. The results of the creep testing in the form of log (creep rate (ε)) versus log (stress) graphs are shown in Figures 50 and 51 for B and D respectively and in the form of log (ε) vs $^{1}/T$ for both B and D in Figure 52. The results show that different mechanisms apply to B and D but generally the stresses and working limit are rather low when compared to yttrium SiAlON ceramics. The microstructures of the ceramics using optical and transmission microscopy are shown for B in Figures 53 to 55 and for D in Figures 56 to 59. Cavitation was observed in B above 1225°C and in D above 1175°C and shown in Figure 58. Values of the activation energy Q for the creep process could not be determined for B due to the non-linear plot of log ε vs $^{1}/T$ in Figure 52, but Q for D up to 1200°C was determined to be of the order of 125 ± 10 kJ mol^{-1}.

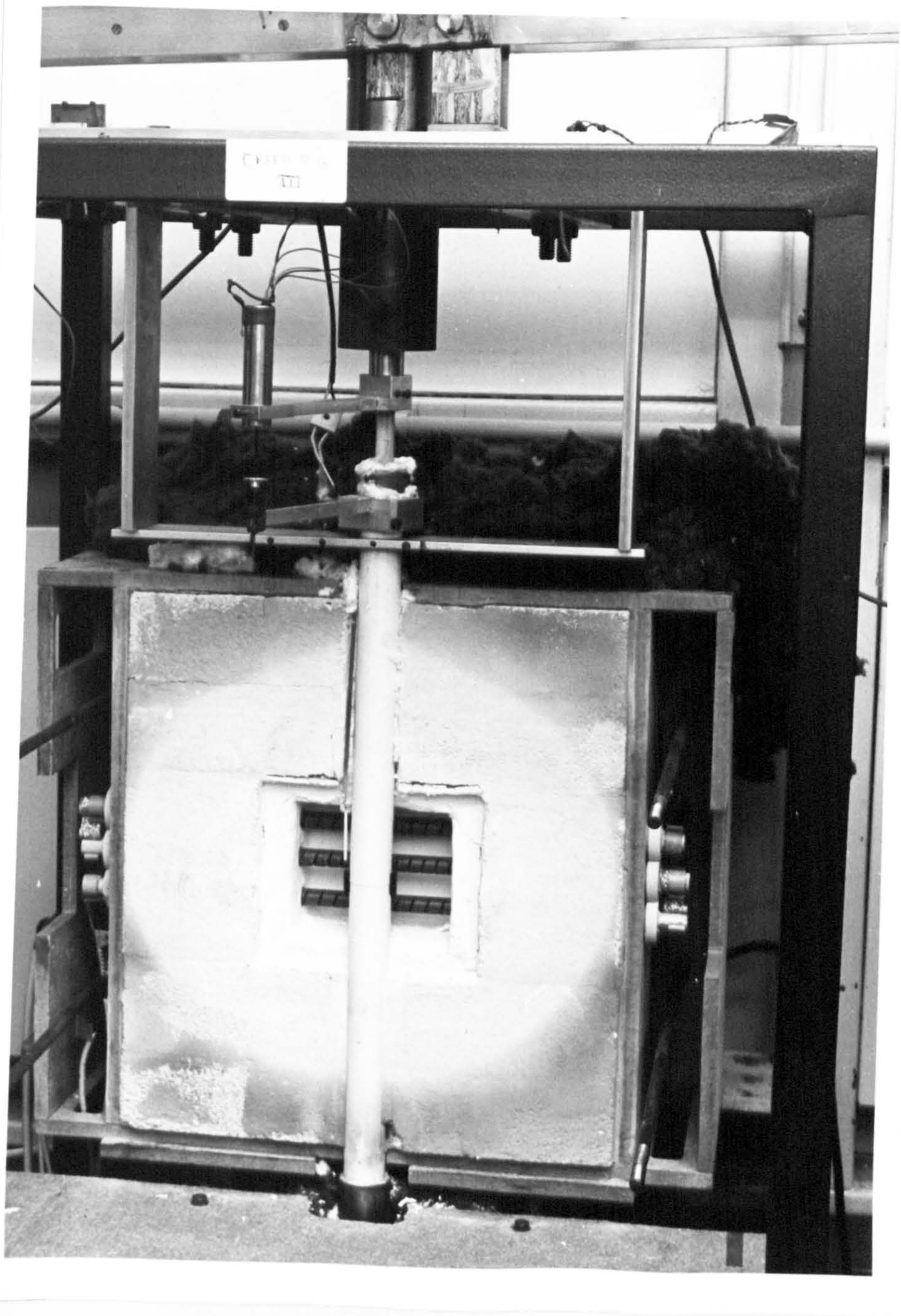

Figure 48: Creep furnace

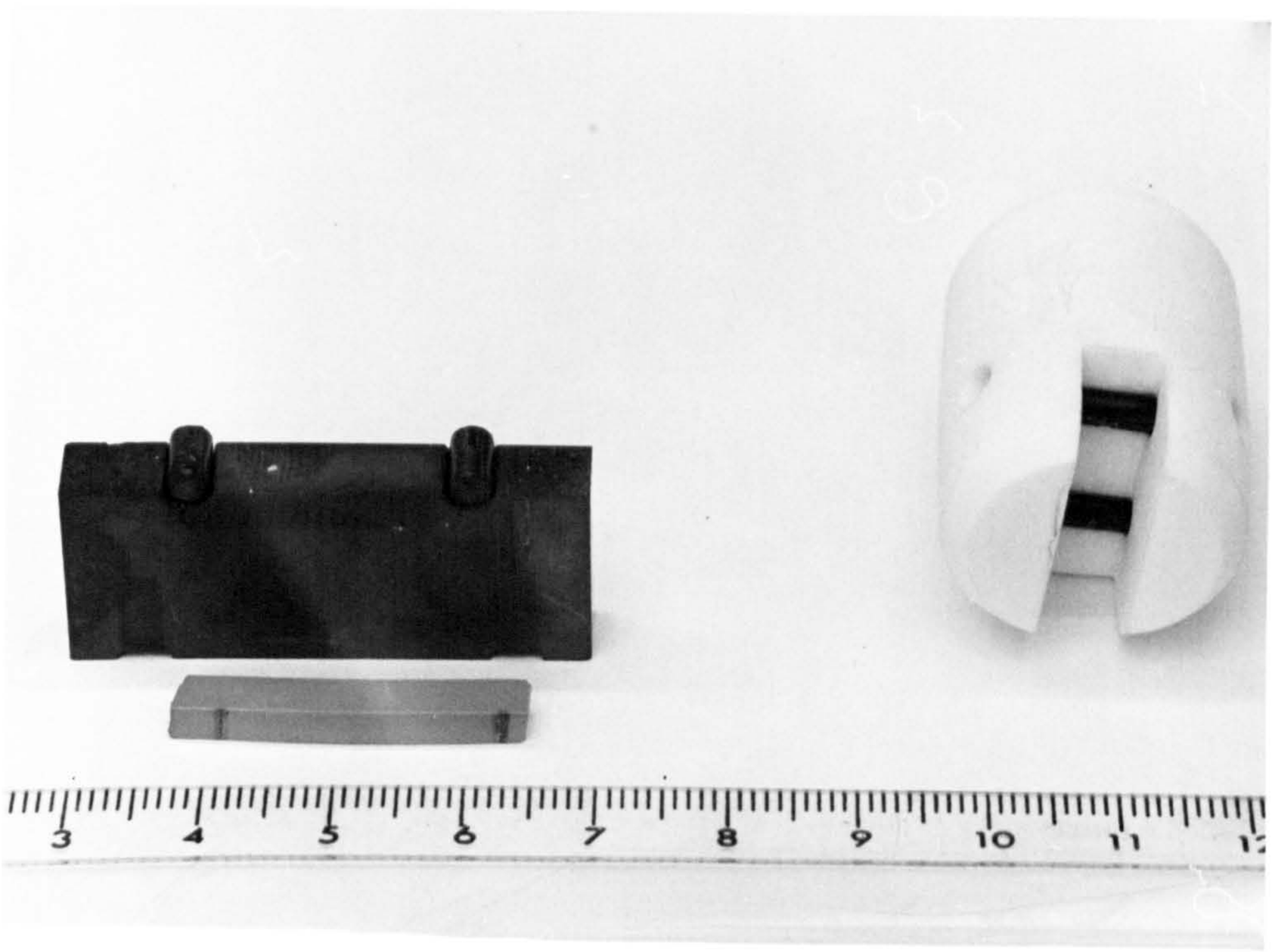

Figure 49: Loading head and sample.

The loading head was machined from an alumina bar and has single phase SiAlON knife-edges. The lower support is made from silicon carbide has similar knife-edges which prevents bonding of the sample to the supports.

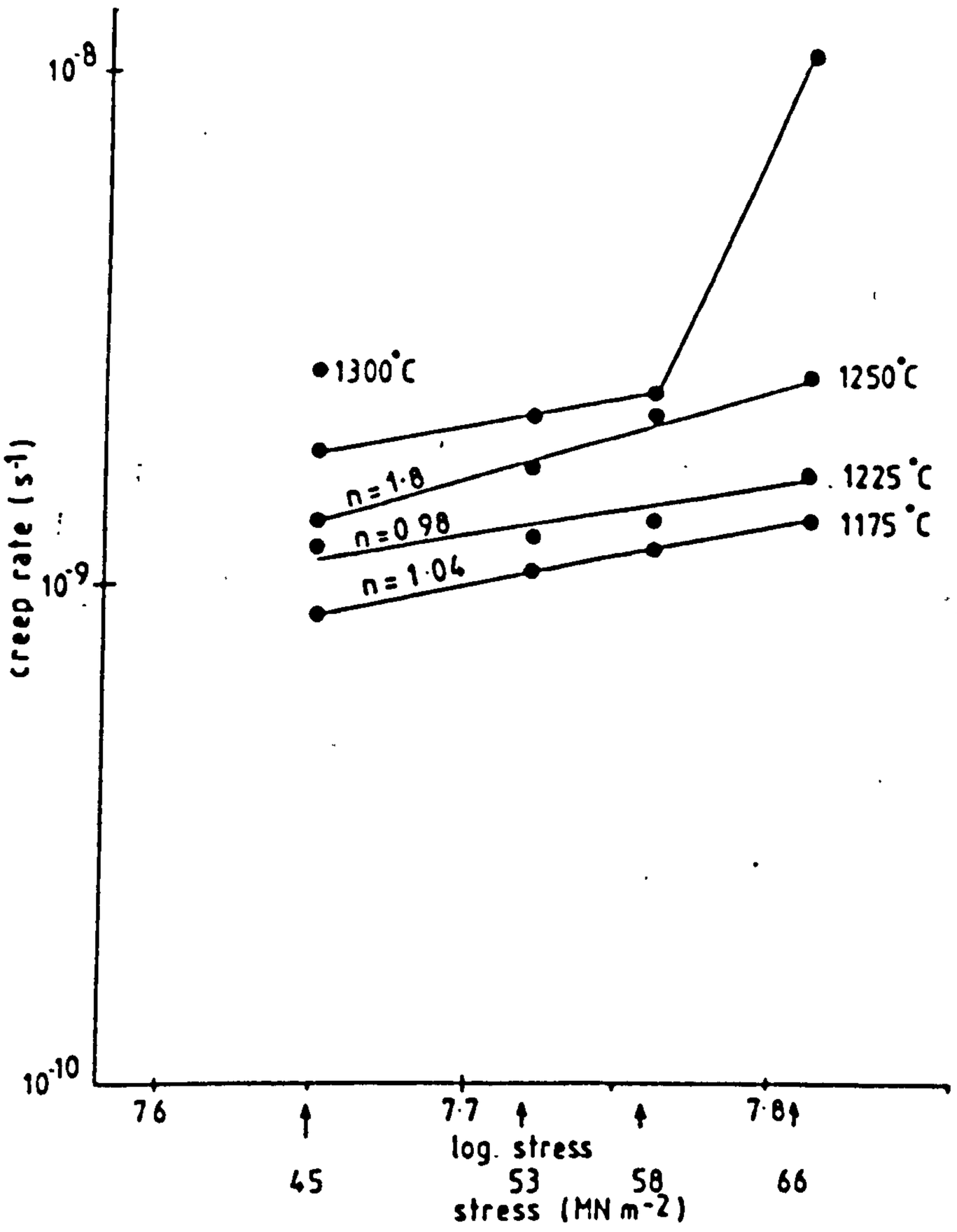

Figure 50: Log (creep rate) vs log (stress) for ceramic B

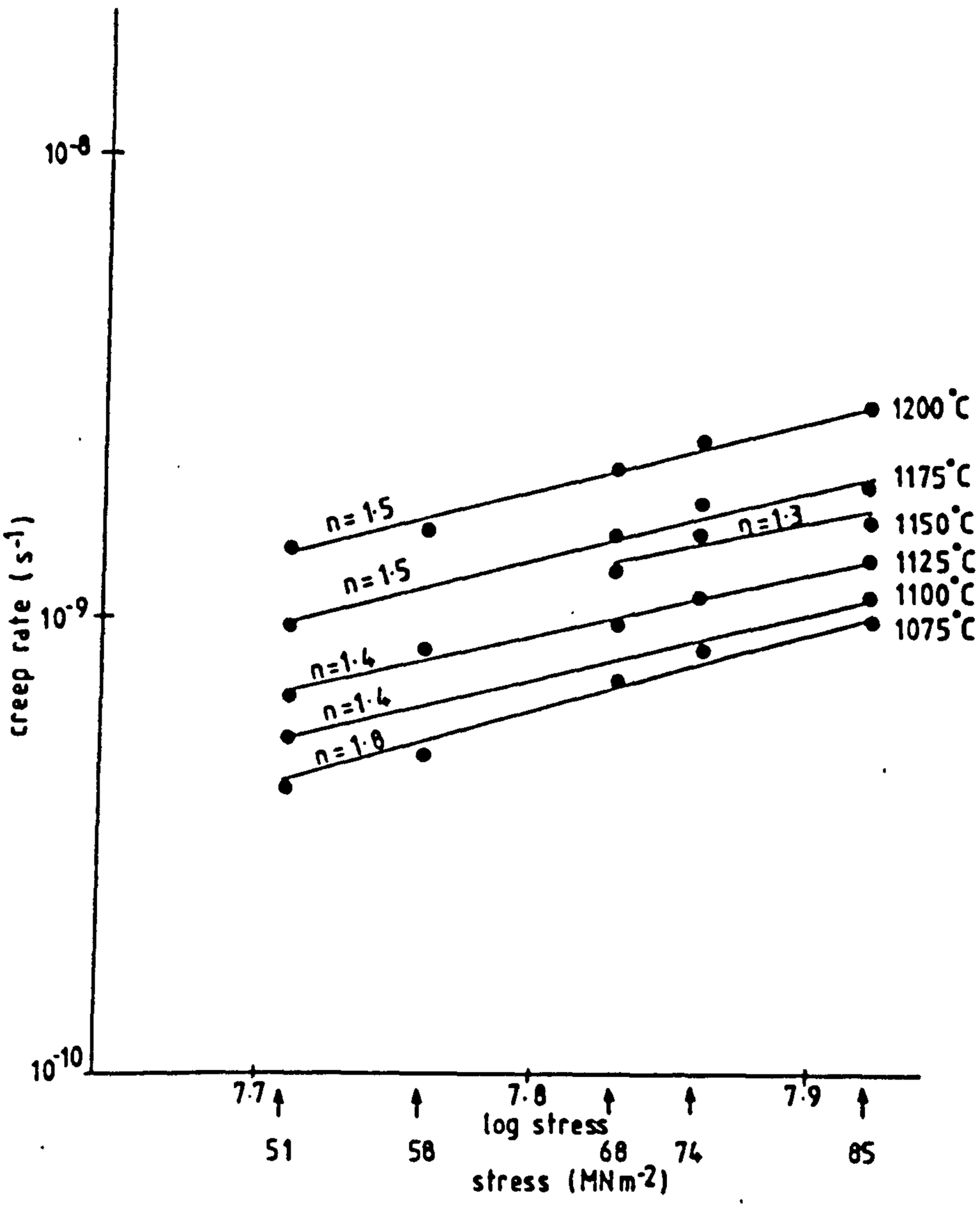

Figure 51: Log (creep rate) vs log (stress) for ceramic D

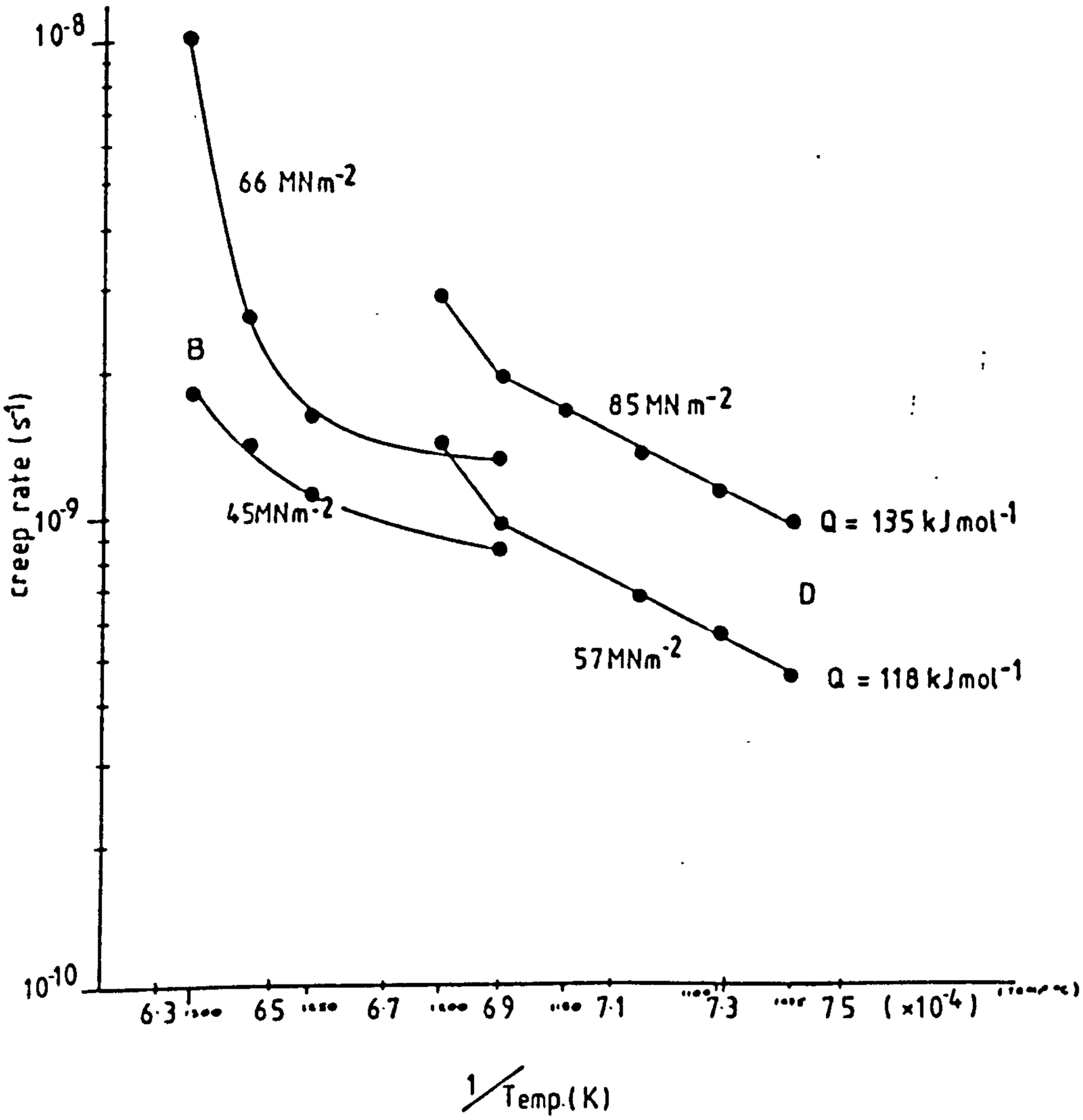

Figure 52: Log (creep rate) vs $\frac{1}{\text{test temperature}}$ for both B and D for the determination of Q.

(a)

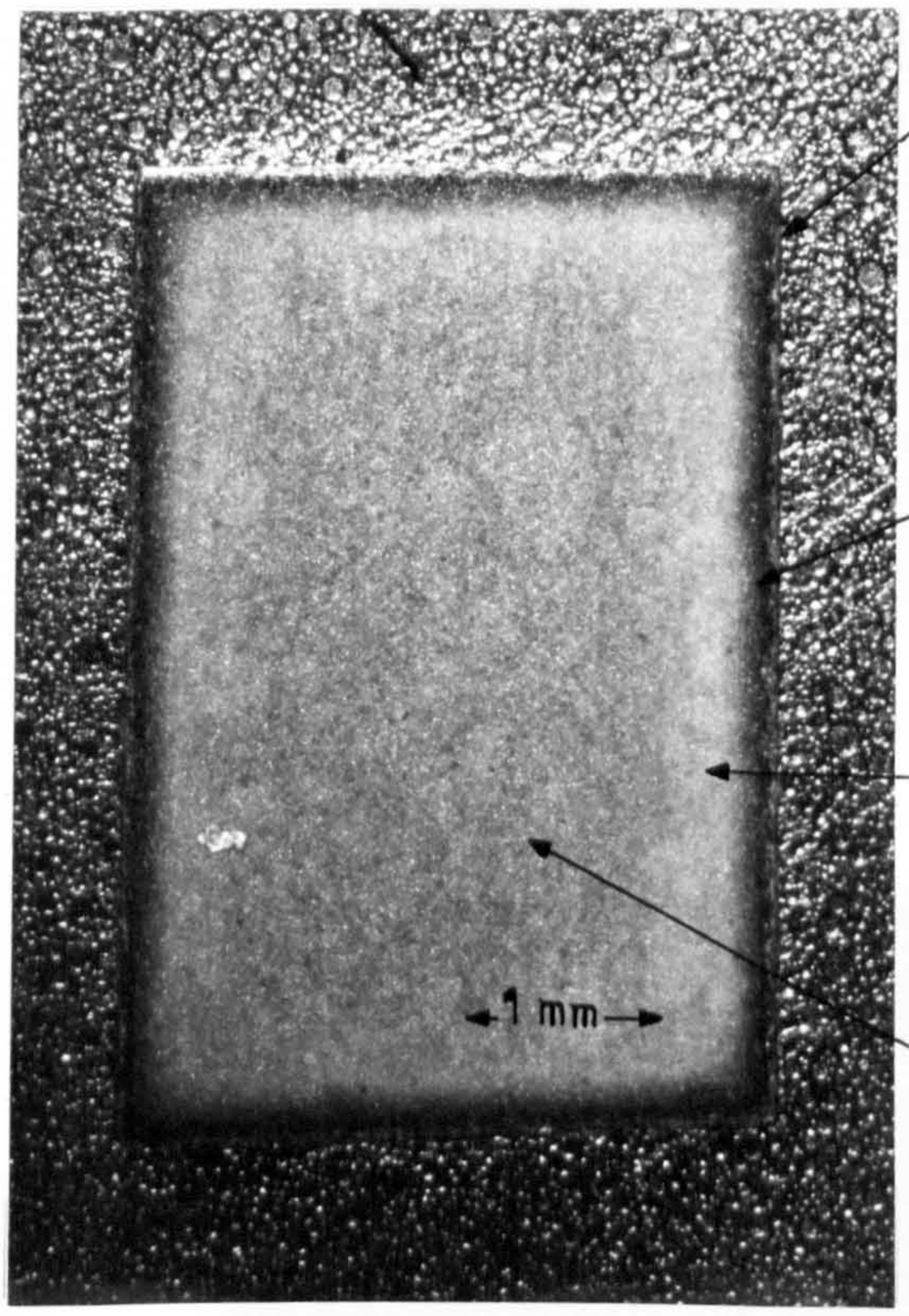

Oxide layer: cordierite, β', spinel and silicon oxynitride

Black layer: cordierite, β', spinel and sapphirine

Grey layer: cordierite, β', spinel and mullite

Core: cordierite, β', spinel mullite and silicon oxynitride

(b)

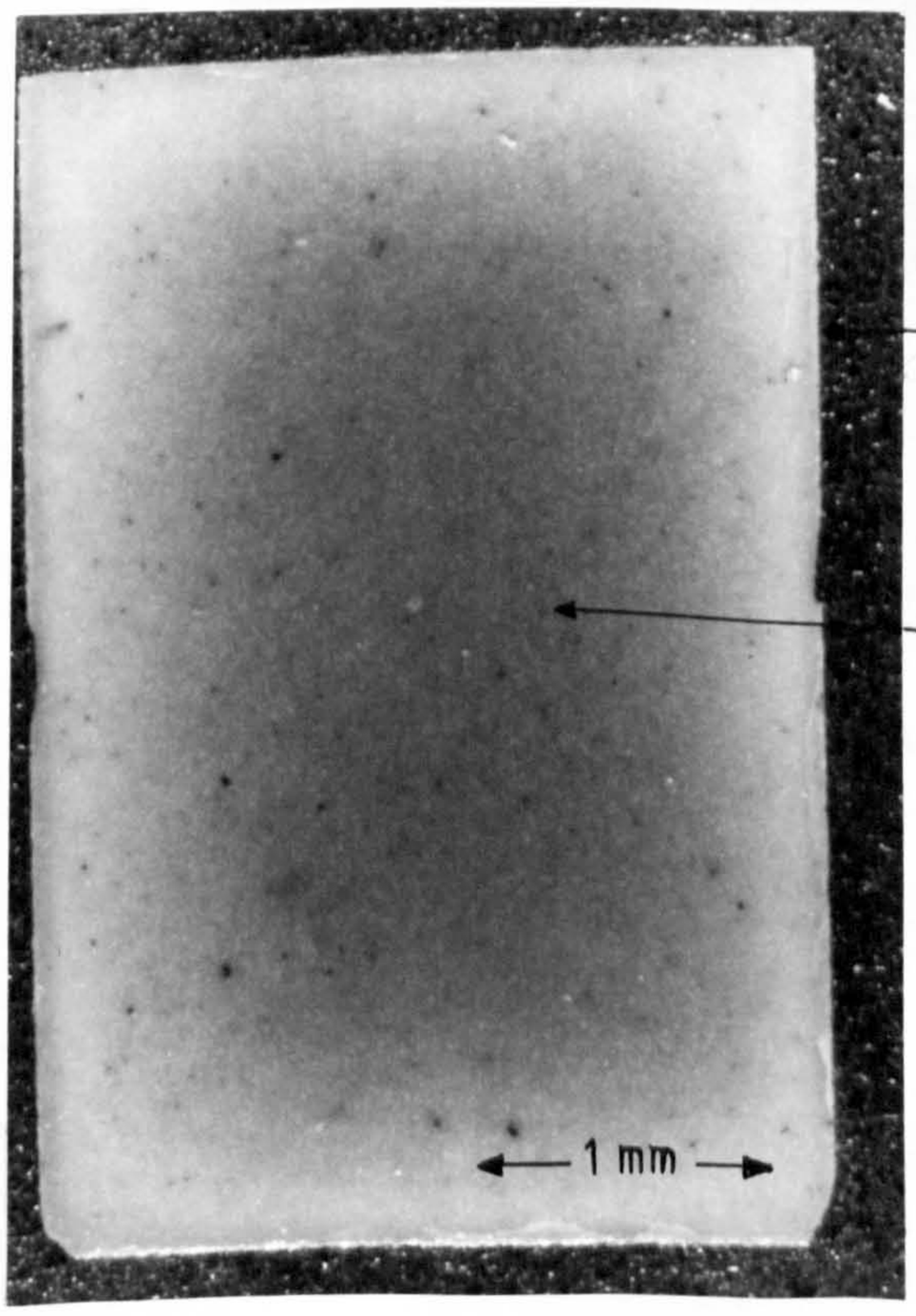

Oxide layer: cordierite, β', spinel and 'X' phase

Core: β' cordierite spinel and 'X' phase

Figure 53: Effect of creep testing on ceramic B

(a) after 150 hours at 1300°C

(b) after 150 hours at 1200°C

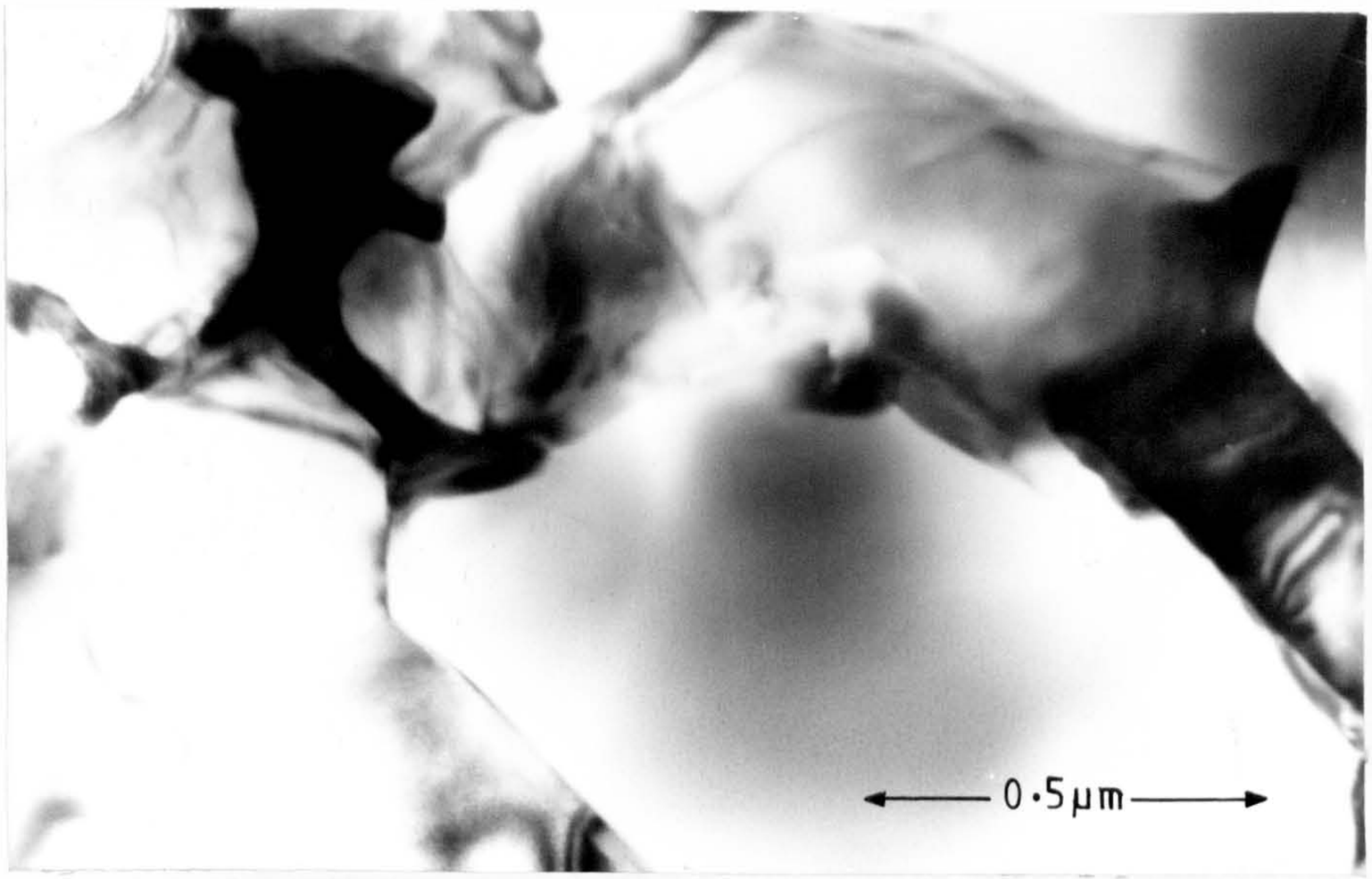

(a)

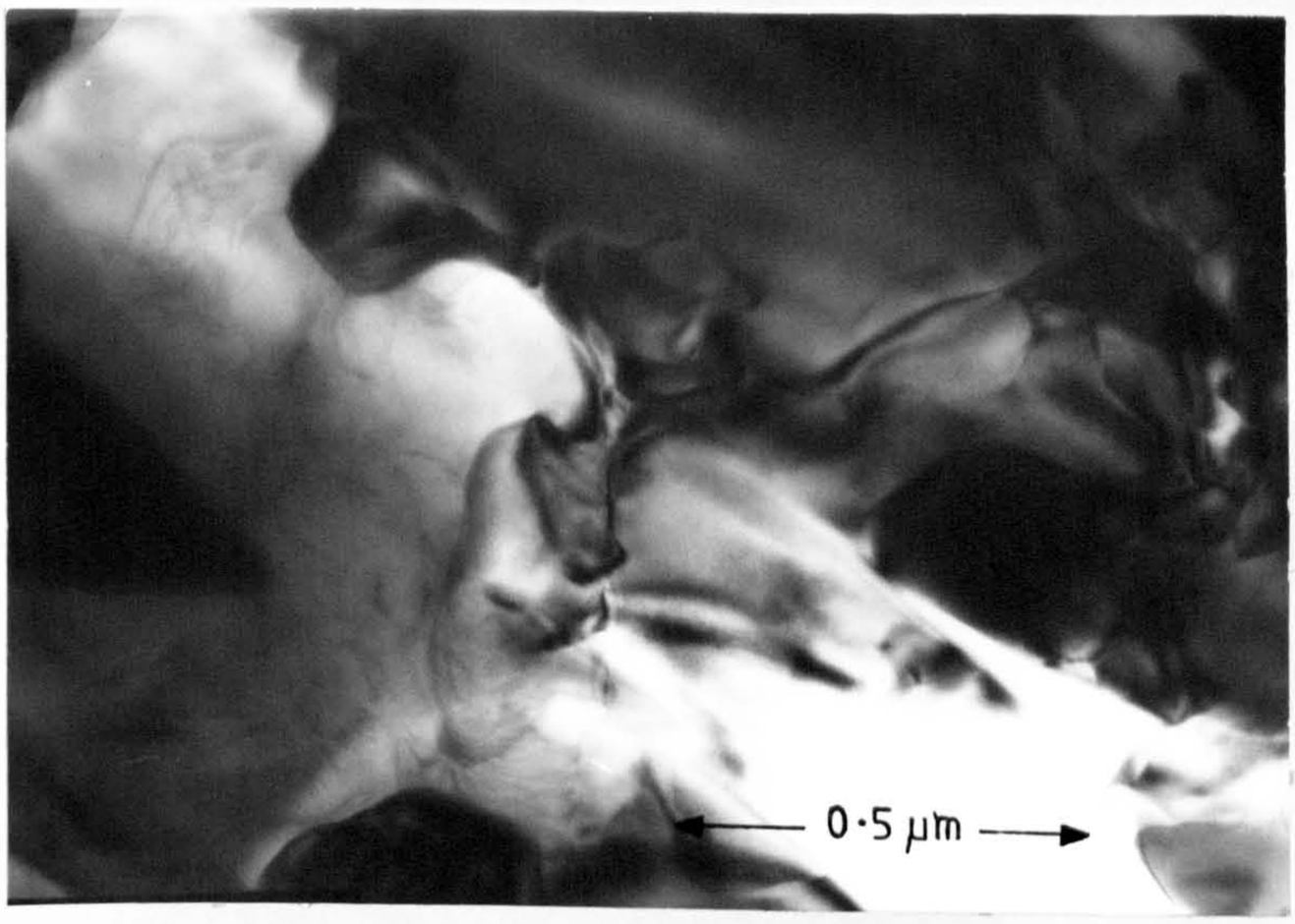

(b)

Figure 54: Microstructure of ceramic B after creep testing for 150 hours at 1300°C

(a) outer 'black' layer

(b) within the core

Despite different phases identified - the microstructures appear similar, probably due to liquid formation during the creep testing - either residual glass or cordierite re-melting. This is why no cavitation was observed.

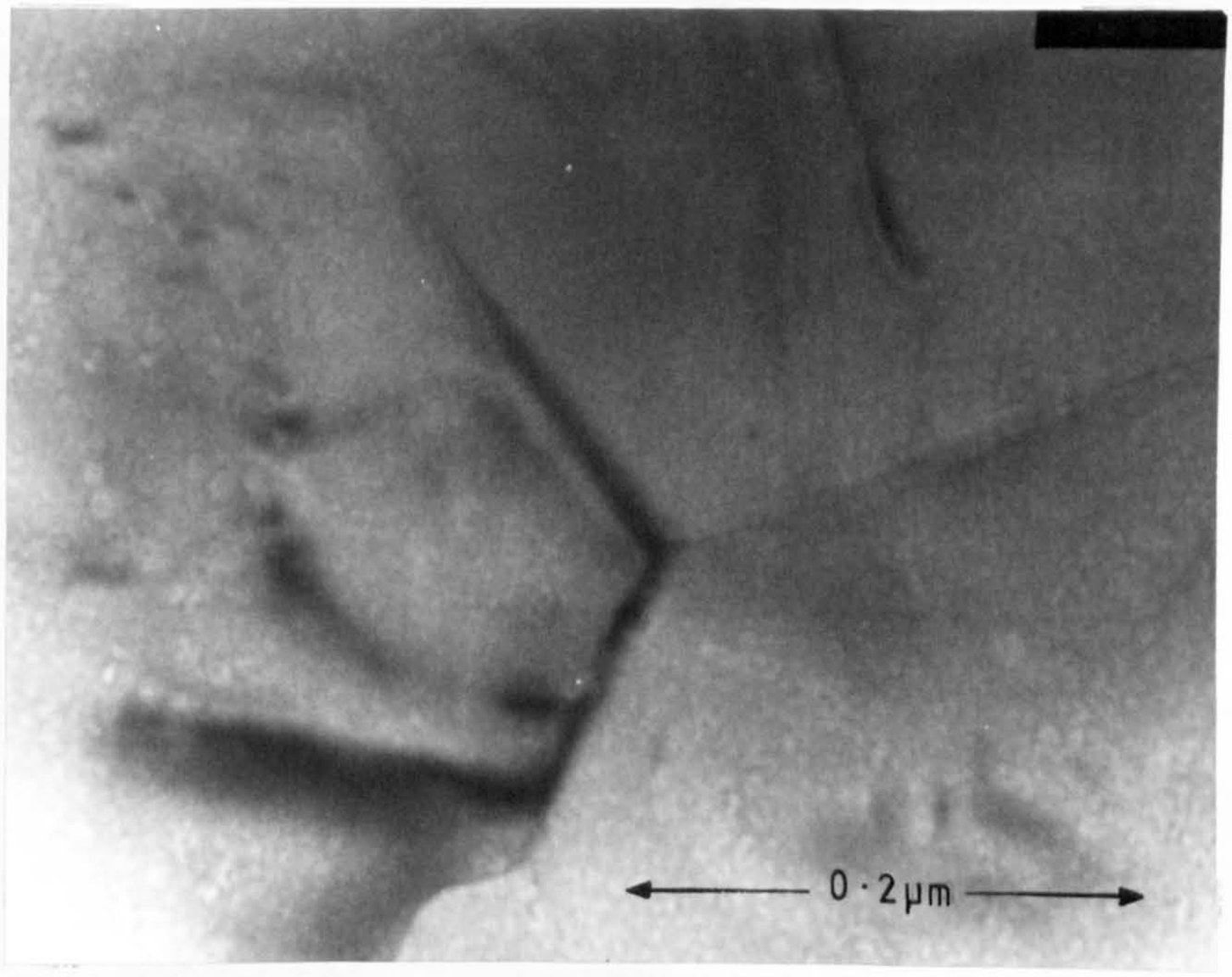

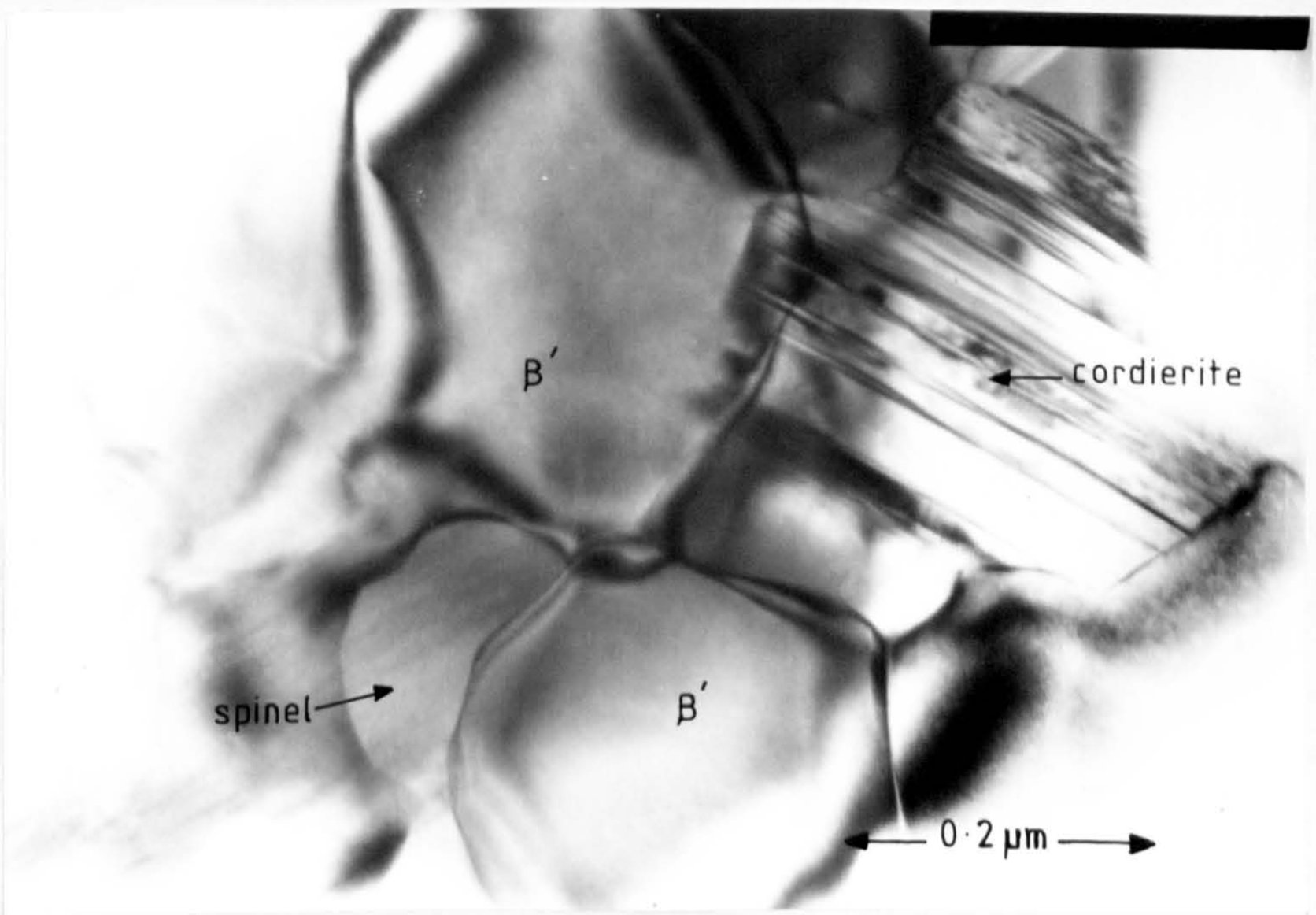

Figure 55: Microstructure of ceramic B after creep testing at 1200°C

No cavitation was observed upto 1225°C but increased faulting in cordierite phase was identified.

(a)

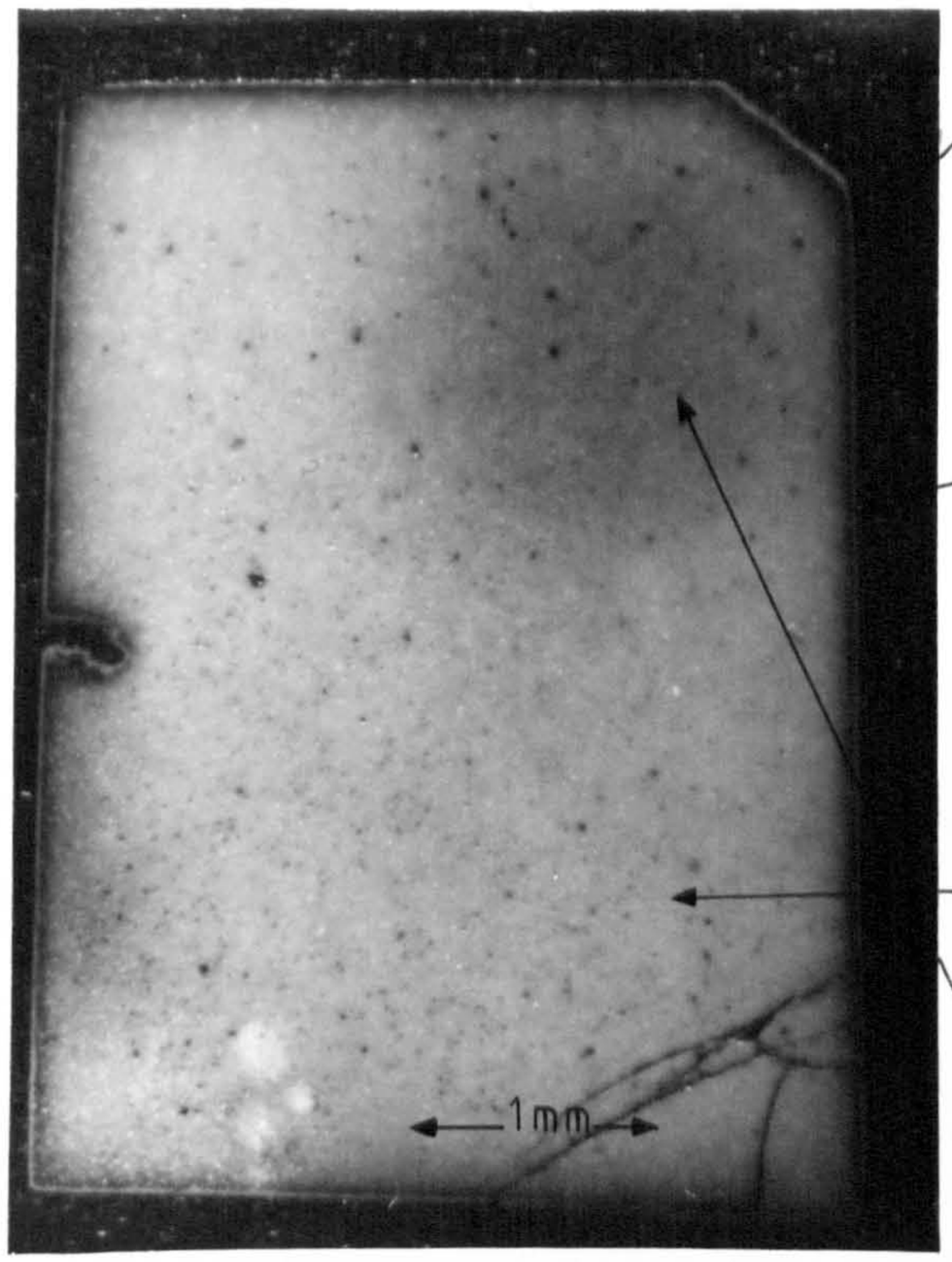

Oxide layer: cordierite, β', spinel and silicon oxynitride

Black layer: β', 'X' phase, cordierite and spinel

Bulk: β', spinel, cordierite and 'X' phase

Core: β', spinel, 'X' phase and trace cordierite

(b)

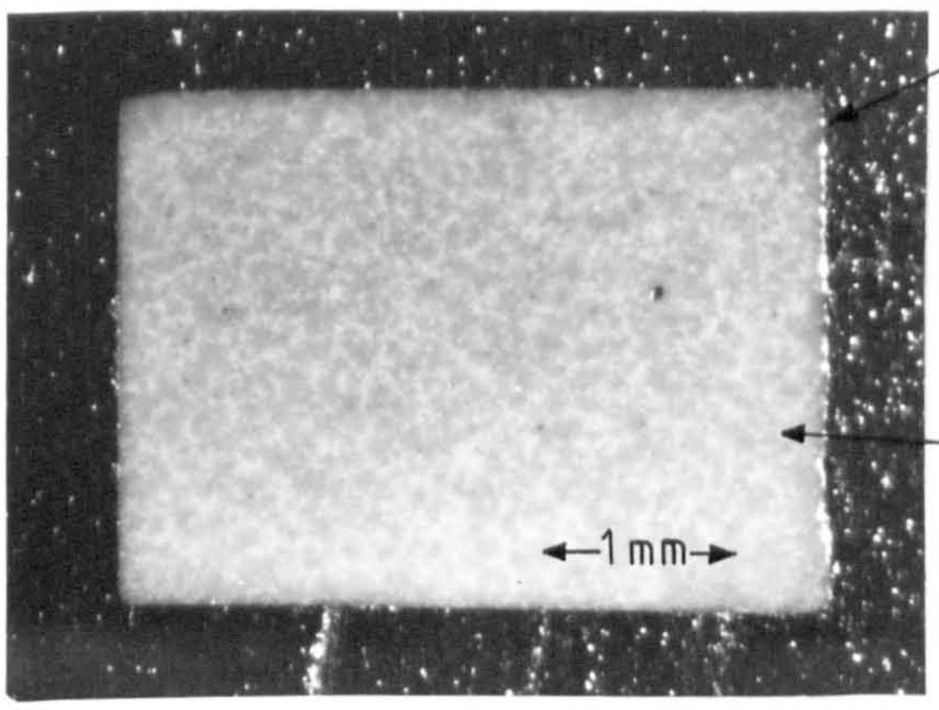

Oxide layer: β', cordierite, spinel and 'X' phase

Core: β', spinel, 'X' phase and trace cordierite

Figure 56: Effect of creep testing on ceramic D

(a) after 150 hours at 1280°C

(b) after 150 hours at 1200°C

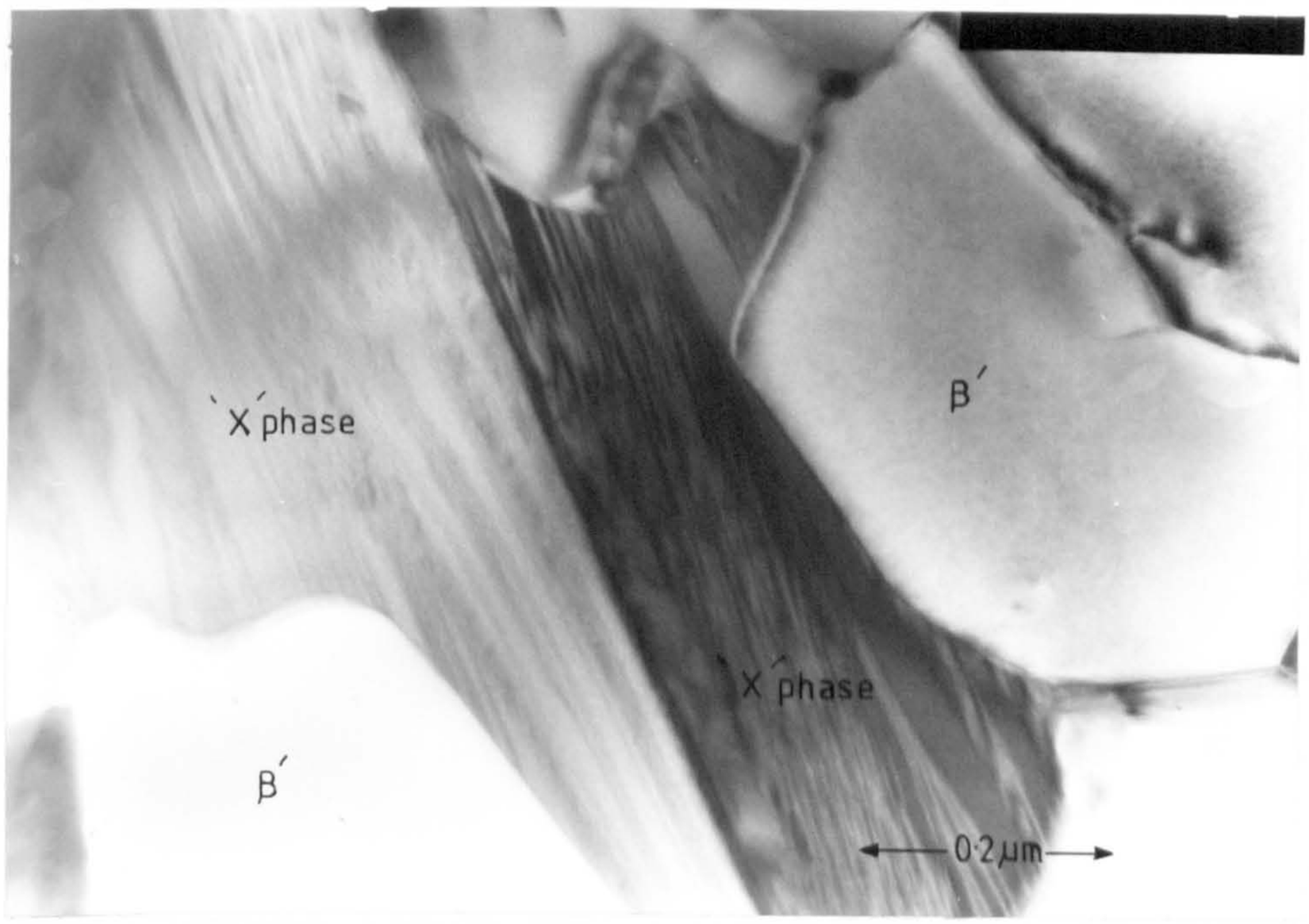

Figure 57: Microstructure of ceramic D after creep testing at 1200°C showing areas of 'X' phase which were heavily faulted. This was only observed in samples that had undergone creep testing.

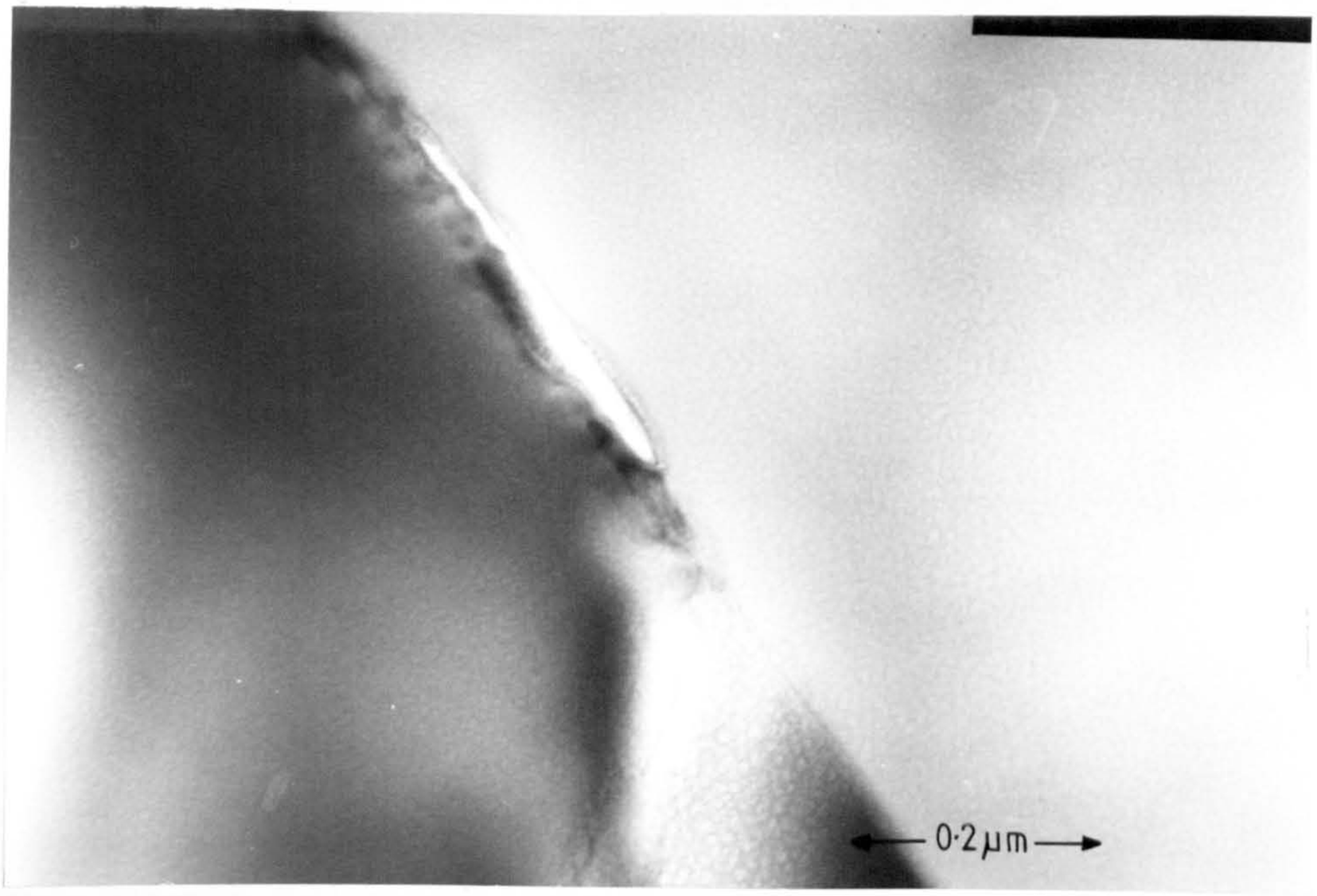

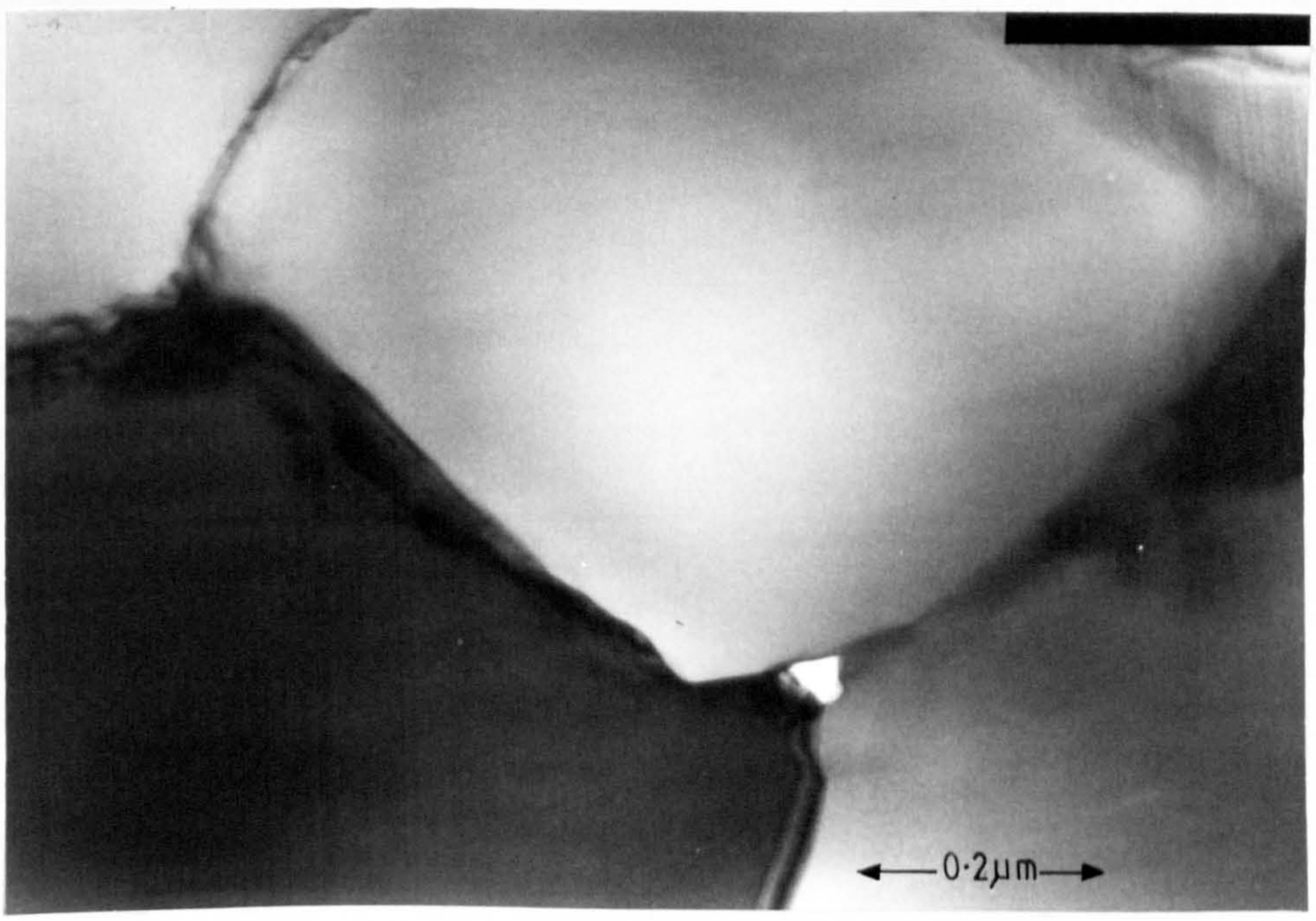

Figure 58: Microstructure of ceramic D after creep testing at 1200°C showing cavity formation.

Cavities were found in triple point region (b) or between adjacent β' grains where there was little grain boundary phase present.

Figure 59: Microstructure of ceramic D after creep testing for 150 hours at 1280°C.

Liquid formation due to grain boundary phase remelting is indicated by a reaction between this liquid and the β' phase.

5.2 Discussion

5.2.1 Fracture Toughness

The results (Table 6) show a substantial increase in fracture toughness after heat-treatment of A to B from 3.57 ± .02 MPa $m^{-\frac{1}{2}}$ to 3.95 ± .06 MPa $m^{-\frac{1}{2}}$. For the high z ceramics the value of fracture toughness remained constant on heat treatment at 3.22 ± .03 MPa $m^{-\frac{1}{2}}$. Values obtained by the indentation method were much lower and even after inclusion of a factor of 1.4[86] only the values for B corresponded well, the results for A, C and D were lower than expected. A factor of 1.7 would produce figures for the 'corrected' indentation method which would more closely match those found for the SENB method. The difference in values of fracture toughness may be explained by a residual stress field. The equation used was derived to take into account this residual stress caused by indentation and avoid the need of an annealing treatment[120]. It is thought that the condition required to use the equation i.e. no residual stresses prior to indentation was achieved in the as-sintered material since for the high z ceramic there was no increase in toughness observed by either indentation or SENB test method. The indentation method must therefore be used with caution.

The range of values found[89] for the fracture toughness of Mg SiAlONs is 3-3.5 MPa $m^{-\frac{1}{2}}$ and the results obtained here are in accord with this and are the same as that found for equiaxial β' grained material produced via hot-pressing. Grain anisotropy measurements is required to determine whether this is the cause of the relatively low value of fracture toughness observed for these MgSiAlONs when compared to the yttrium material.

The fracture surfaces of A, B, C and D are shown in Figures 44 to 47. For the low z ceramic a slight increase in transgranular fracture was observed on heat treatment. There was still a high percentage of intergranular fracture observed, which was suggested as beneficial in order to obtain a high K_C material[99]. The fracture mode for the high z ceramics was predominantly transgranular and this did not change on heat treatment. This, coupled with the fact that high z ceramics are less tough than low z ceramics, is explained by (a) the increased inhomogeneity and grain size associated with high z ceramics, or (b) the intrinsic properties of the β' phase are a function of z level. This will be discussed together with the hardness results in the next section.

5.2.2 Hardness

The increase in hardness after heat-treatment of A and C has been shown in Table 6. This was due to the crystallization of the 'soft' glass to 'hard' spinel or cordierite in the low z ceramics, and to spinel in the high z ceramic. Only limited crystallisation subsequently took place on heat-treatment of C to D and this accounted for the smaller increase in hardness than was observed with the low z ceramics, in which a high percentage of the grain boundary phase was initially glassy and was then crystallised by the heat-treatment. Lower values of hardness were observed for ceramic C compared with A as well as D compared with B. This indicated that the hardness of the β' phase of high z ceramics was lower than for low z β' phase since the grain boundary of C was partially crystallized on sintering. These results and those from fracture toughness testing indicate that the intrinsic properties of the β' phase are a function of z level,

with the higher z ma terial less hard and less tough. This is in contrast to earlier work by Lumby[121] who found that hardness increased with z level: no explanation was given for this trend. The decrease in hardness and toughness with increasing substitution level observed in the present work is thought to be due to a decrease in bond strength within the silicon nitride lattice as it is expanded to accommodate large alumina additions. This would account for the difference in hardness and toughness observed and the difference in fracture surface topology shown in Figures 44 to 47.

5.2.3 Creep

Creep tests were carried out on B and D only, due to the problems of the crystallisation of the second phase on testing. Log (creep rate) versus log (stress) data for ceramics B and D have been shown in Figures 50 and 51 and log (creep rate) versus 1/T data in Figure 52. From these results and from density and grain size determinations and microstructural observations, creep mechanisms and upper working temperature limits are suggested below.

For ceramic B, a diffusional creep mechanism (n=1) was found to operate up to 1225°C. The density after this creep test was found to be 3.16 g cm^{-3} i.e. identical to that of the heat-treated ceramic, and indicates the absence of cavitation. The grain diameter in the tensile region was found to be slightly smaller than in the heat-treated ceramic, 0.75 μm compared to 0.85 μm. This could indicate a solution precipitation mechanism as suggested by Tsai and Raj[111] where a grain elongation and narrowing occurs on stressing. (The method of measurement of the diameter of the β' crystal involved measurement of the largest circle diameter which would fit in the β'

crystal. Measurement of grain anisotropy, which would have been a more precise determination is a possibility for future work). The value of the activation energy Q was not determined since the graph of log (creep rate) versus 1/T was not linear. Above 1225°C there was a change in mechanism to one involving cavitation. The density of B had decreased to 2.85 g cm^{-3} after testing at 1300°C. The effect of cavitation on the microstructure is shown in Figure 60.

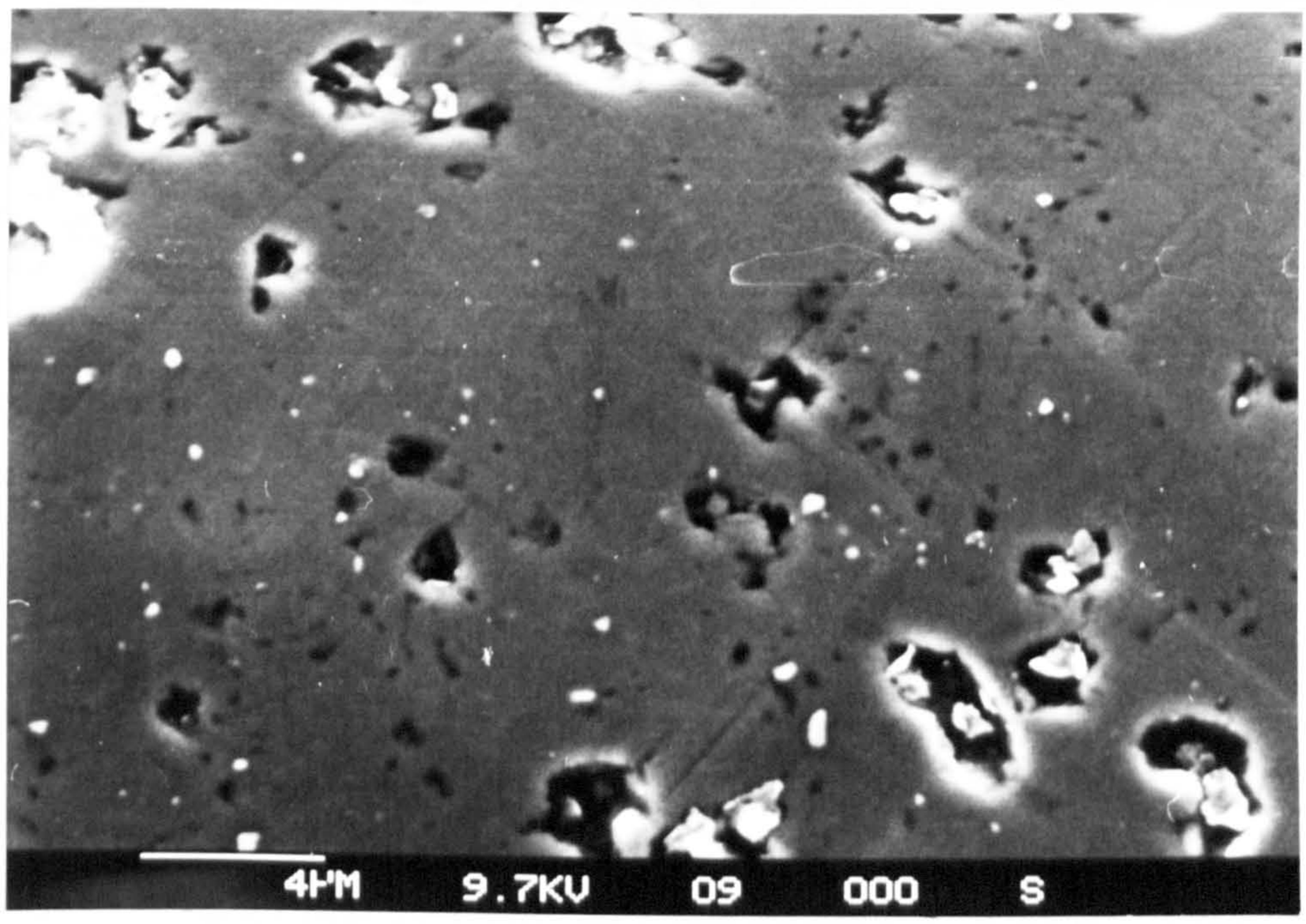

Figure 60: Extent of cavitation observed in a creep sample, after testing at 1300°C. Compare this to the fracture surface shown in Figure 45.

The effect on the microstructure of creep testing was examined by optical and transmission microscopy Figures 53-55. A cross section of B after creep testing up to 1300°C showed that after 1 week severe oxidation had taken place (Figure 53 (a)). XRD analysis indicated mullite and silicon oxynitride were present in the core in addition to

the normally observed phases. In the sub-surface "black" layer sapphirine was also identified. Transmission microscopy of both the core and black layer showed extensive reactions between the β' crystals and the grain boundary phase with possible liquid formation, Figure 54. Below 1225°C only minimal out-diffusion of cations in the grain boundary phase occurred to form a thin layer of cordierite on the surface (Figure 53 (b)). The creep mechanism could also have involved dislocation movement within the cordierite grain boundary phase. Increased faulting was observed compared to the oxidised state: an example is shown in Figure 55, though this is not thought to be rate controlling. There was no evidence of residual glass or of cavitation in the grain boundaries for temperatures up to 1225°C.

For ceramic D, the creep mechanism operating at 1200°C was indicated by dislocation movement in 'X' phase found in the microstructure, Figure 57 and by cavity formation. This was identified by the density decrease from 3.02 g cm^{-3} to 2.96 g cm^{-3} during testing. Effect of the cavities on the microstructure is shown in Figure 58. The activation energy Q for this process was determined from Figure 52 to be Q = 125 ± 10 kJ mol^{-1} which is low compared for processes suggested earlier[107] which had activation energies of > 500 kJ mol^{-1}. The values of Q obtained in the present work correspond better to that for silicon diffusion in a silicate eutectic glasses. Diffusion data for $CaO-SiO_2-Al_2O_3$ system[122] indicate a decrease in Q from 290 kJ mol^{-1} for diffusion in SiO_2 glass at 1000°C to 230 kJ mol^{-1} for diffusion in a 40 wt% SiO_2, 40 wt% CaO, 20 wt% Al_2O_3 glass. There is no available data for silicon diffusion in $MgO-Al_2O_3-SiO_2$ glasses so an absolute determination of the creep mechanism is not possible, but silicon diffusion in the near eutectic glass is

indicated. Unfortunately there is a problem that the value found for the activiation energy for diffusional creep may not be meaningful since steady-state conditions did not appear to occur (Figure 51, n=1.8) and the ceramic was cavitating.

The only region which indicated diffusional creep was by ceramic B between 1175°C and 1225°C. This gave two points in the graph of log (creep rate) vs $\frac{1}{\text{Test temperature}}$ and the value for the activation energy found was of the same order of magnitude as that found for the high z material although obviously it is not quoted.

Oxidation of the high z ceramics was not as acute as the low z ceramics Figure 56, but cordierite was identified in the core in small amounts and on the surface in larger amounts. Above 1200°C there appeared to be a change in mechanism but though no further measurements were possible to enable identification, observations were made. After creep testing at 1300°C the tensile region was heavily oxidised with a large diffusion zone visible, Figure 56. Cordierite was found in this region. The sample had an asymmetrical structure and this is explained by the fact that the sample had been loaded incorrectly, hence no stress results were obtained but oxidation accelerated by the applied stress was observed. Extensive liquid formation was also observed and as the temperature was only 50°C below the ternary oxide eutectic, this could have been cordierite or more probably residual glass remelting. This liquid is believed to be capable of dissolving with or reacting with the β' phase, evidence for this is shown in Figure 59.

There was no effect of creep testing on the z level of the β' phase of either B, or D (up to 1200°C). Above this temperature grain boundary phase reactions are probably more important than silicon partitioning or out-diffusion which were observed in the stability study (Chapter Four).

To summarise: hardness, fracture toughness and creep testing were carried out on both low and high z level ceramics. As-sintered low z ceramics were found to be both harder and tougher than high z ceramics and it is probable that the intrinsic properties of the β' phase are a function of the substitution level. This effect may be more important than the composition and structure of the grain boundary phases. After heat-treatment, hardness values increased in both cases but those for the high z ceramics were smaller due to the fact that the grain boundary phase was already partially crystallised on sintering. The value of K_c also increased on heat-treatment of A to B from 3.5 to 3.9 MPa $m^{-\frac{1}{2}}$. For the high z ceramic after heat-treatment of C to D the value remained constant at 3.2 MPa $m^{-\frac{1}{2}}$. These values were of the order found when the β' grains are equiaxed i.e. in hot-pressed material.

Creep testing was performed on heat treated samples B and D only, due to the problems of crystallisation on testing. The creep rates were acceptable at the low stresses and temperatures used (< 70 MPa and < 1200°C) but this represented the maximum limit of operation. For the low z ceramics below 1225°C solution- precipitation or another diffusion control and dislocation movement in the cordierite phase should be included in the overall creep mechanism. Above 1225°C cavitation was observed. For the high z ceramics cavitation and dislocation movement in 'X' phase were observed above 1175°C which would limit the use of these ceramics. This was unexpected since testing involving heating in an oxidising environment had suggested that the higher z ceramics would be the more creep resistant because it was indicated that there was less residual glass present in these ceramics.

In the next chapter the mechanical properties of these ceramics will be compared to those of the yttrium system together with the conclusion of the project.

CHAPTER SIX

SUMMARY, COMPARISON AND CONCLUSIONS

This chapter briefly summarises the results from this work and compares them with those obtained from the yttrium SiAlON ceramic system. Conclusions are made of the results obtained and the thesis ends with some suggestions for future work.

6.1 Summary of Results

6.1.1. Sintering and Microstructural Observations

The low temperature of the melting point of the ternary eutectic composition was advantageous in sintering the higher z ceramics where the residual grain boundary phase approached this composition. For the low z ceramics the glassy phase was more silica rich and therefore had a higher viscosity and melting point. This resulted in a much smaller grain size for the low z ceramics as well as a much higher sintering temperature requirement. The liquid phase observed at the start of stage I for both low and high z ceramics was identified as a magnesium 21R polytypoid. At the start of stage II the collapse of the α framework occurred with the formation of a new β framework and as sintering proceeded alumina was removed from the liquid phase which implied that the z level of the β' crystal was initially low and then increased.

High z ceramics were found to be the most easily sintered due to the lower viscosity of the residual grain boundary phases at the sintering temperature. A sintering schedule of 1750°C for one hour was required to produce a high density ceramic of z level = 3.0.

Low z ceramics of z = .75 were sintered using temperatures up to 1850°C for one hour followed by one hour at 1750°C which produced high density ceramics of similar relative density to the high z ceramics. For even lower z ceramics (z = 0.10) temperatures in excess of 1900°C were required to achieve similar results.

The as sintered low z ceramics contained highly faceted β' crystals in an almost totally glassy grain boundary phase and there was a little 'X' phase indicated. As the z level was increased inhomogeneity also increased: this was thought to be caused by the production of spinel on cooling. This occurred throughout the sintering process indicating an inhomogeneous liquid. Also the low viscosity of the residual phase enabled more rapid grain growth in some regions. The z level prediction was good with the higher z ceramics, but with the low z ceramics the production of a silica-rich phase kept the z level of the β' crystals higher than initially expected.

An optimum heat treatment schedule was determined from density-time and density-temperature data to be 24 hours at 950°C. The effects of this on the low z ceramics were (a) a decrease in z level of the β' as predicted and (b) the crystallization of the glassy phase to spinel and cordierite. For the high z ceramics the z level remained constant but the grain boundary crystallization of both spinel and 'X' phase continued. The highly faceted β' crystals observed in the as sintered state were replaced with more rounded grains on heat-treatment. Grain growth also occurred in both high and low z ceramics which had previously been reported[123].

The effect on the microstructure of thermal stability testing was examined. As-sintered low z, and to a much lesser extent the high z also, suffered from glass out-diffusion at temperatures above

950°C. After heat-treatment in nitrogen the stability of both improved due to crystallisation of the glassy grain boundary phase. The working limit was raised to approximately 1200°C. Cordierite formed the major oxidation phase on the surface above 1000°C and in the core above 1200°C in both low and high z ceramics.

6.1.2. Mechanical Properties

The Vickers hardness of the as sintered MgSiAlON ceramics was determined to be 1450 kg mm^{-2} for the low z and 1310 kg mm^{-2} for the high z ceramics. After heat-treatment the values were increased to 1650 kg mm^{-2} and 1450 kg mm^{-2} respectively. Fracture toughness for these ceramics was determined through SENB testing. As sintered low z ceramics had a value 3.5 MPa $m^{-1/2}$ and high z ceramics a value of 3.2 MPa $m^{-1/2}$. After heat-treatment the toughness for low z increased to 3.9 MPa $m^{-1/2}$ whilst that for the high z remained constant. The fracture mode was mainly intercrystalline for the as sintered low z ceramics, and for the high z ceramics mainly transcrystalline. This was not altered by heat treatment. Vickers hardness and fracture toughness values did appear to be dependent upon the z level. This is in contrast to that reported by previous workers[123] who had found that values of hardness for hot-pressed SiAlON were independent of z level. The trend was also the reverse of that found by Lumby[121].

Bend creep testing was performed to determine creep rates and mechanisms. Testing of heat-treated low z ceramic indicated an upper working limit of 1220°C, above this cavitation was observed. High z ceramics were found to cavitate above 1175°C due to incomplete glassy phase crystallization. Other creep mechanics were observed, in

cordierite and 'X' phase both involving dislocation movement. The main mechanism for the low z ceramics below 1220°C involved diffusion of material along grain boundaries, i.e. Coble creep, or solution-reprecipitation.

6.2. Comparison with the Yttrium SiAlON Ceramics

It has recently been found[124] that care must be taken in the choice of α Si_3N_4 source powder. This work, completed at Lucas Cookson Syalon, suggests that materials made from Starck LC10 powder had impaired high temperature properties due to residual contaminants from the manufacturing process. Subsequently a change of α Si_3N_4 source powder led to improved creep resistance and fracture toughness, as recent work at Warwick University is now showing[125]. The Starck powder was used in the production of all material in the present work so the properties of these will be compared to older yttrium SiAlONs made from a similar source rather than to the new yttrium SiAlONs which are very impressive.

6.2.1. Sintering and Microstructure Comparison

Reports indicating advantages when using magnesium oxide rather than yttrium oxide to aid the α→β transformation are conflicting. Generally a temperature of approximately 1700°C is required during pressureless sintering of SiAlON ceramics to allow this reaction to proceed. The higher z Mg SiAlONs offer a definite advantage when compared to the yttrium SiAlONs when considered from a sintering view point. To date there has been no publication on the sinterability of high z yttrium SiAlONs and this information is required before use of

high z Mg SiAlONs is recommended. The higher temperatures required by the lower z Mg SiAlONs are comparable to that used to sinter yttria additive materials.

The microstructure of the low z ceramics are similar, i.e. highly faceted β' crystals with a glassy grain boundary phase but the magnesium ceramics do contain a little 'X' phase, a phase not found in the yttrium SiAlONs. Values for the relative densities are also similar (97-98%). Heat-treatment of the magnesium ceramics was performed at a very much lower temperature than that used for the yttrium ceramics, 950°C compared with 1300-1400°C, both schedules being for 24 hours. The low temperature heat-treatment offered a considerable advantage in oxidation resistance. Thermal stability testing predicted that the upper temperature limit of the Mg SiAlONs would be approximately 1200°C for heat-treated high z ceramics and slightly lower than this for low z ceramics. Similar testing of yttrium ceramics are undertaken up to 1450°C. Reaction rates are usually near parabolic for the yttrium ceramics and similarly for the Mg SiAlONs below 1220°C.

Grain growth was observed on heat-treatment for both types of material; in the yttrium system this can isolate the YAG in the triple point regions. Inhomogeneous nucleation with these ceramics was indicated (a) by the presence of large rosettes (1-2 mm diameter) observed in the specimen and (b) by the fact that there was no change in density during heat-treatment[126]. In the magnesium SiAlONs there was an observed increase in density and the size of the spinel or cordierite grains was typically less than that of a β' grain.

6.2.2. Mechanical Properties Comparison

The values of fracture toughness of the yttrium SiAlONs are at least twice those found for the magnesium ceramics made for this

project. Heat-treatment of yttrium ceramics was found to be detrimental to the strength with Modulus of Rupture decreasing from 794 to 750 MN m^{-2} on heat-treatment[22]. This was caused by the inhomogeneous nucleation which increased porosity and development of the critical flaw. The fracture mode of the low temperature testing was predominantly transgranular and the high fracture toughness observed was thought to be due to the fine interlocking morphology.

Low z magnesium ceramics appeared to have this microstructure but grain anisotropy would have to be examined in detail to find whether this was the cause of the difference observed in K_c. Heat-treatment increased fracture toughness of the MgSiAlONs. Values of hardness for Mg SiAlON glass were quoted as being 'low' compared to the yttrium SiAlON and it is likely that hardness values for the respective ceramics follows the same trend.

Creep testing suggests that low z Mg SiAlONs can operate up to 1225°C before the onset of cavitation, with high z ceramics cavitating at a temperature lower than this. Creep rates appear similar to yttrium SiAlONs operating at 1300°C at twice the stress level used for the Mg SiAlON, i.e. 100 MN m^{-2}. (Testing of yttrium SiAlON at present is usually up to 1400°C and at even higher stress levels). The creep mechanism of the yttrium SiAlONs (in the as sintered condition) involved cavitation, although this changed to a Coble creep mechanism after heat-treatment. The activation energy Q for the creep process was increased by heat-treatment from 400 kJ mol^{-1} to 850 kJ mol^{-1}. For comparison the value of Q obtained for the cavitating Mg ceramic was Q = 125 kJ mol^{-1}. This was for the high z ceramics; values for low z material could not be calculated.

Early reports[107,123] of hot-pressed material implied that no change in material parameters, e.g. fracture toughness, and density had occurred subsequent to creep testing and that if cavitation was identified as a creep mechanism then this was acceptable provided that ε and Q for the ceramic were of the order of 10^{-8} s^{-1} and > 600 kJ mol^{-1} respectively. The change in density and the degree of cavitation observed with ceramics B and D at only modest stress and temperature levels and the low creep rate recorded implied that the earlier (also cavitating) ceramics would be affected quite badly by a decrease in density and hence load bearing capability. Since no changes in density or any other parameters, including toughness and hardness were reported[88] the performance of the earlier pressureless sintered ceramics at the high temperatures quoted may have been over-exaggerated. It is only very recently[125] that SiAlONs have been reported to have performances to match the early ceramics.

6.3. Conclusions

The conclusions of the project are:

(a) High z magnesium SiAlONs offer a possible low temperature alternative to the yttrium system, but low z magnesium SiAlONs are as difficult to sinter as the yttrium SiAlONs. This is due to the high temperature required for the $\alpha \rightarrow \beta$ transformation and also to the low viscosities of the silica rich residual phases.

(b) The mechanical properties of the β' crystal appear to be a function of the z level. As the z level is increased both hardness and toughness decreased. It would thus be possible to tailor these properties by varying the z level.

(c) Heat-treatment of the magnesium SiAlONs was performed at 950°C for 24 hours, which is a low temperature compared to that used for the yttrium system (1300°C). Although this led to a distinct improvement of the high temperature properties it was insufficient to crystallize totally the glassy phase of the high z ceramics.

(d) The high z magnesium SiAlONs appeared to be the more stable in an oxidising environment at the expense of a minor decrease in toughness. Low z SiAlONs were found to have better creep resistant properties. A diffusion control was identified up to 1225°C, but above this temperature cavitation was observed. For the high z ceramics cavitation was observed above 1075°C. The ceramics made for this project were generally out-performed by the yttrium SiAlONs, although the situation may be improved if a heat-treatment schedule can be determined to crystallise the grain boundary glass more fully.

Some interesting topics have arisen from this work and merit further attention; they include examination of the variation of properties of the β' crystal with z level to show whether high z ceramics are viable in the magnesium and yttrium SiAlON systems. Further testing is required of high z magnesium SiAlONs made from different α starting powder. A two stage heat treatment schedule is necessary to try to crystallize the residual glass more completely: a first stage at 950°C for 24 hours to prevent glass out-diffusion and a second stage at approximately 1200°C. Experiments should be undertaken varying the second phase content and also the sintering schedule to try to achieve more homogeneous high z ceramics. Grain

anistrop y calculations should also be carried out to determine why there is such a difference in toughness between high and low z ceramics and between magnesium and yttrium SiAlONs. An analysis of the creep mechanisms of both cordierite and 'X' phase is required to try to determine their contribution to the overall creep rate observed for the magnesium SiAlON ceramics. Finally the samples that have undergone creep testing should undergo further mechanical properties testing. This would ensure that the ceramic could be used at these temperatures and stresses rather than merely surviving a creep test.

Appendix One

A selection of the compositions used in the project are shown below. Each composition was designed to have spinel as second phase. 'Spinel' was added as magnesium oxide and aluminium oxide. Each composition was manufactured in batches of 100 grams, except for composition C (see page 66).

Sample No.	z level	Weight % Second phase	Si_3N_4	$SiAl_6O_2N_6$	Al_2O_3	MgO
1	0.10	10	88.47g	0.44g	8.29g	2.80g
2	0.25	10	86.18g	1.09g	9.93g	2.80g
3	0.50	10	82.37g	2.18g	12.65g	2.80g
4	1.00	10	74.76g	4.36g	18.08g	2.80g
5	2.00	10	59.62g	8.68g	28.90g	2.80g
6	3.00	10	44.57g	12.98g	39.65g	2.80g
7	4.00	10	29.62g	17.26g	50.32g	2.80g
8	.10	15	83.56g	0.41g	11.83g	4.20g
9	2.00	15	56.31g	8.20g	31.29g	4.20g
10	3.00	40	29.71g	8.66g	50.43g	11.20g
A	0.75	10	78.57g	3.27g	15.36g	2.80g
C	3.00	10	44.57g	12.86g	39.6	6.80g

Appendix Two

XRD spectra for samples during the sintering process are shown in the next few pages. These are for both low and high z material and the results are summarised in tables 3 and 4 in the text.

LOW Z 1200-1600°C

α and β Si_3N_4

A alumina

Sp spinel

X 'X' phase

m magnesium 21R polytypoid

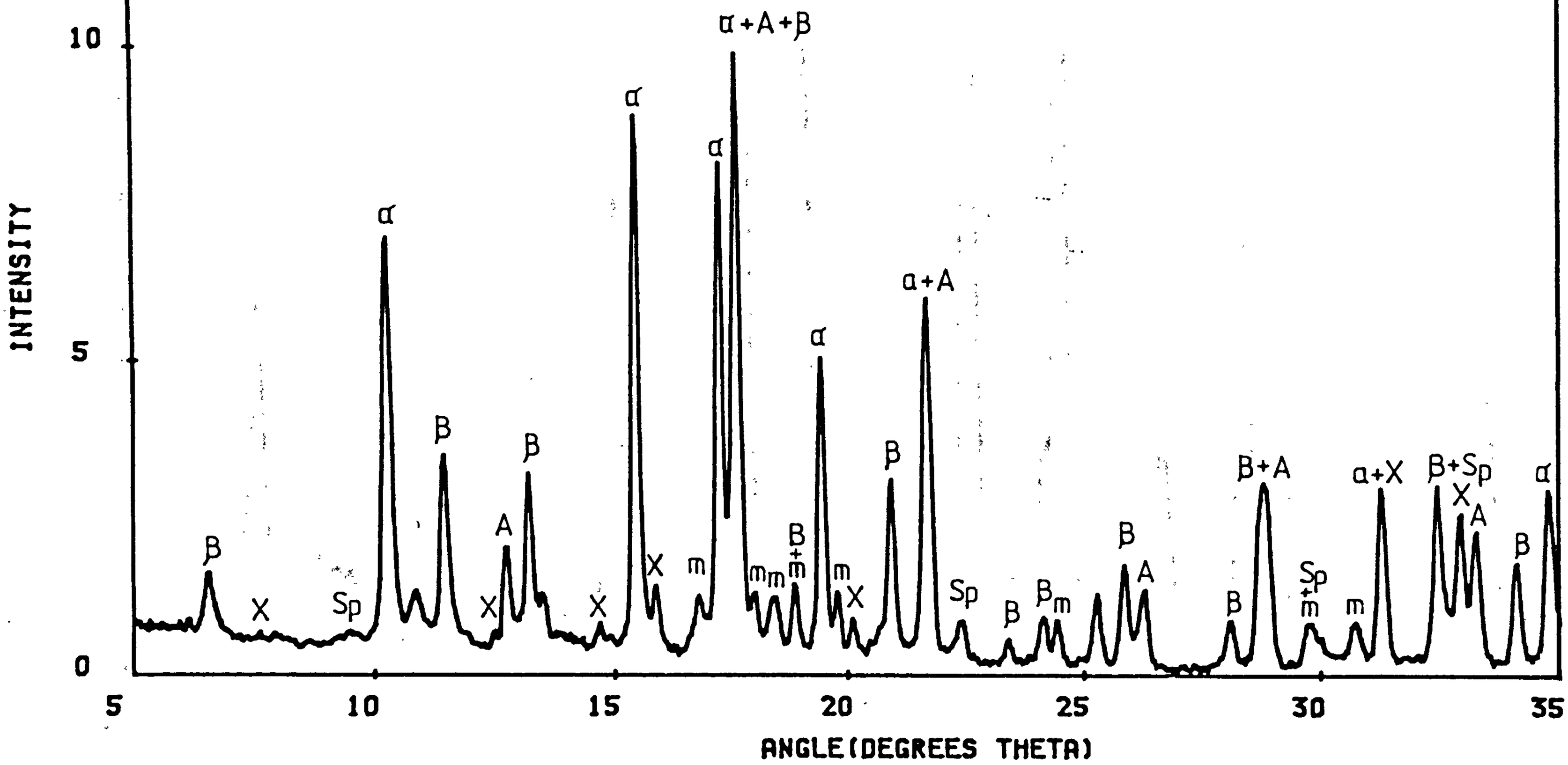

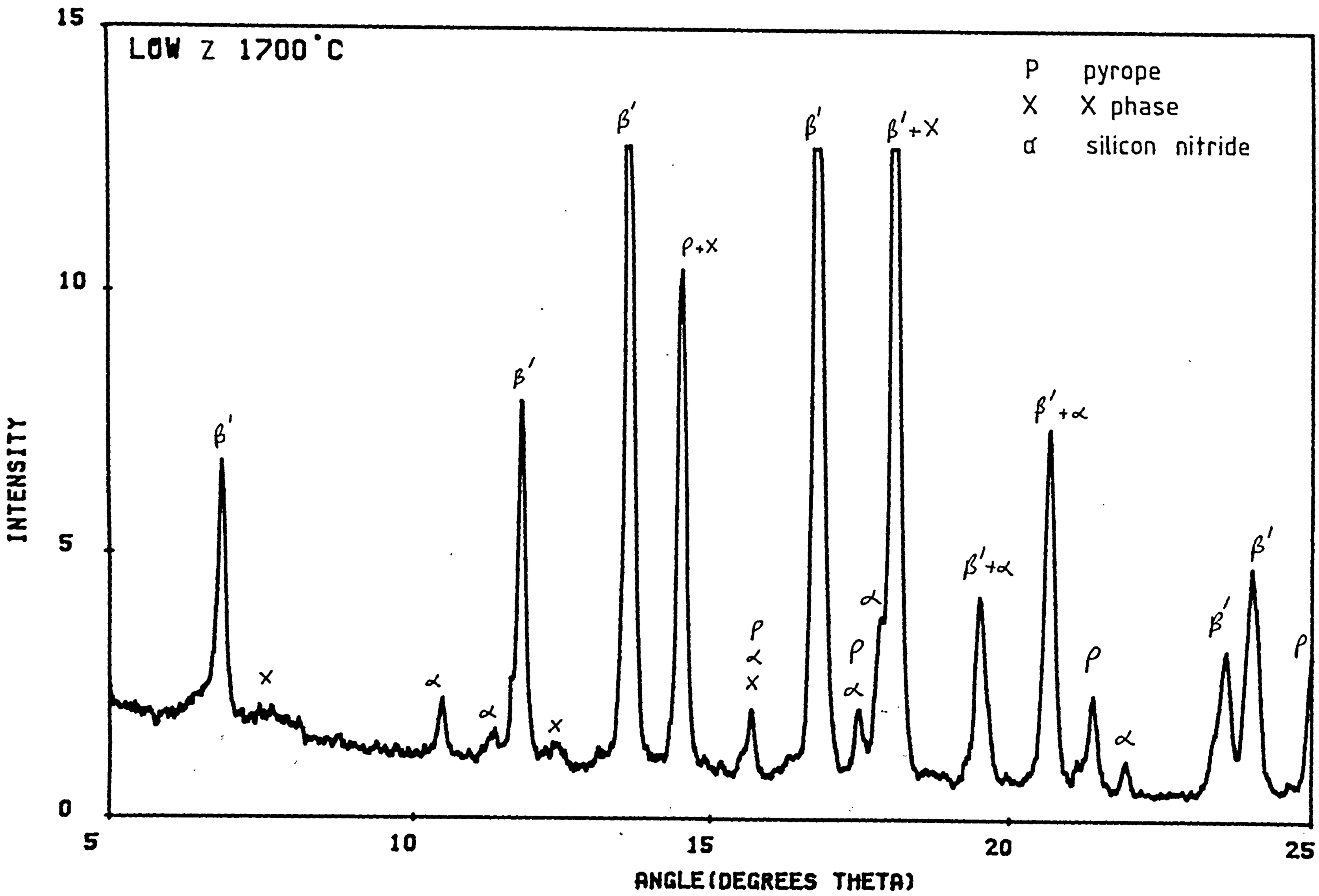
LOW Z 1700°C
P pyrope
X X phase
α silicon nitride
β'
β'+X
ρ+X
β'+α
ρ
α
X
INTENSITY
0
5
10
15
5
10
15
20
25
ANGLE(DEGREES THETA)

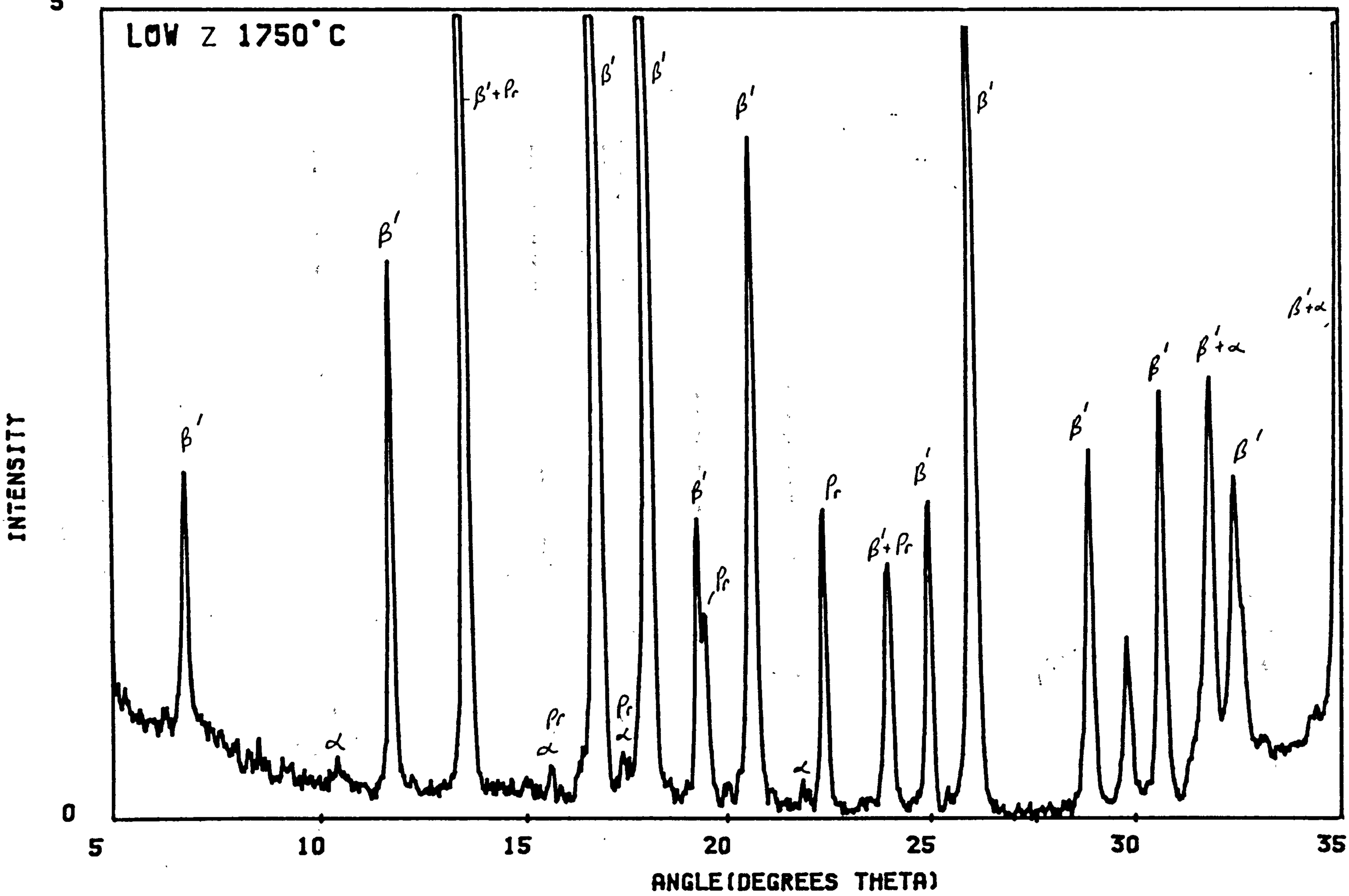
LOW Z 1750°C
INTENSITY
0
5
10
15
20
25
30
35
ANGLE (DEGREES THETA)
β'
β'+Pr
Pr
α
β'+α

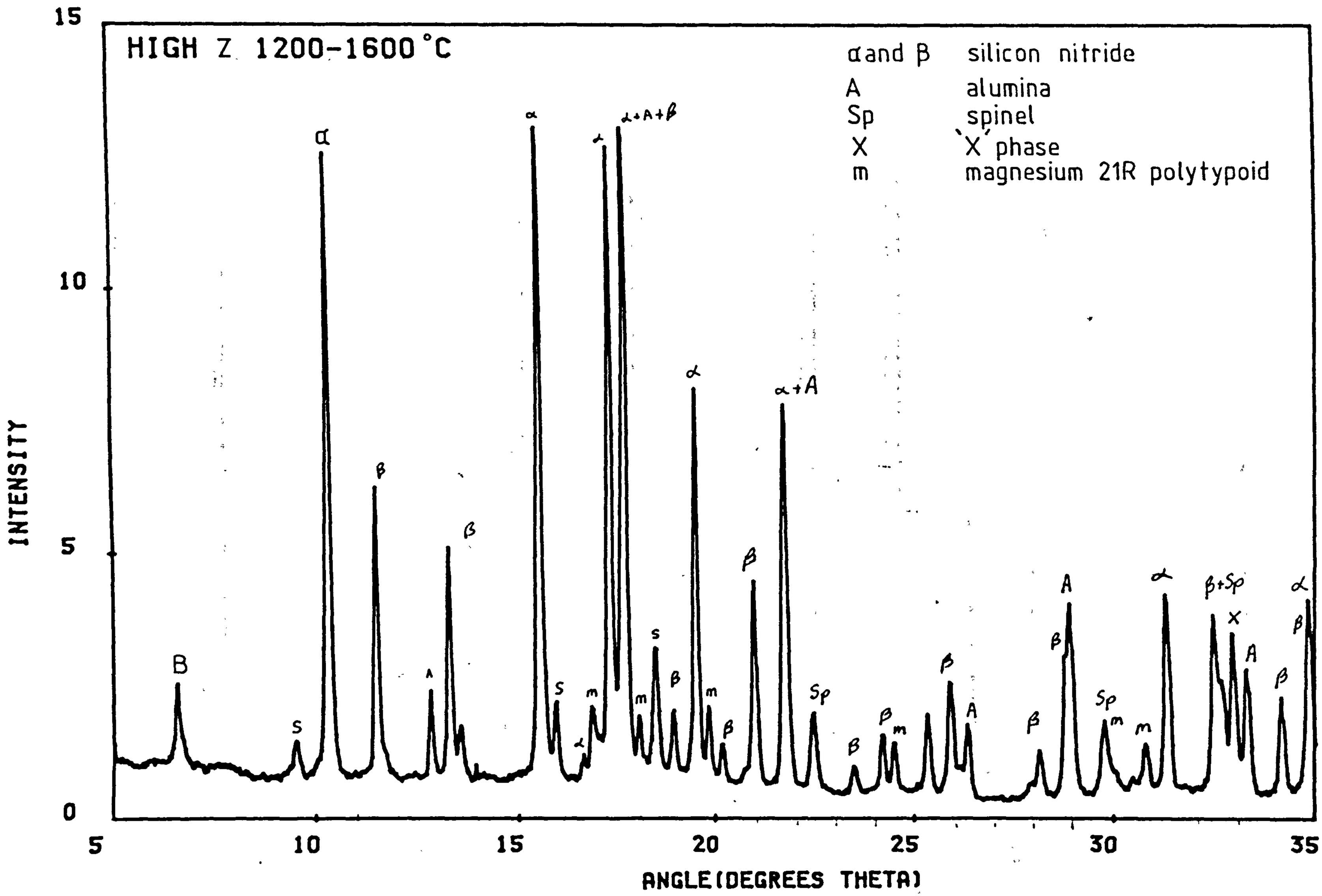
HIGH Z 1200-1600 °C
α and β silicon nitride
A alumina
Sp spinel
X 'X' phase
m magnesium 21R polytypoid
INTENSITY
ANGLE (DEGREES THETA)
0
5
10
15
5
10
15
20
25
30
35

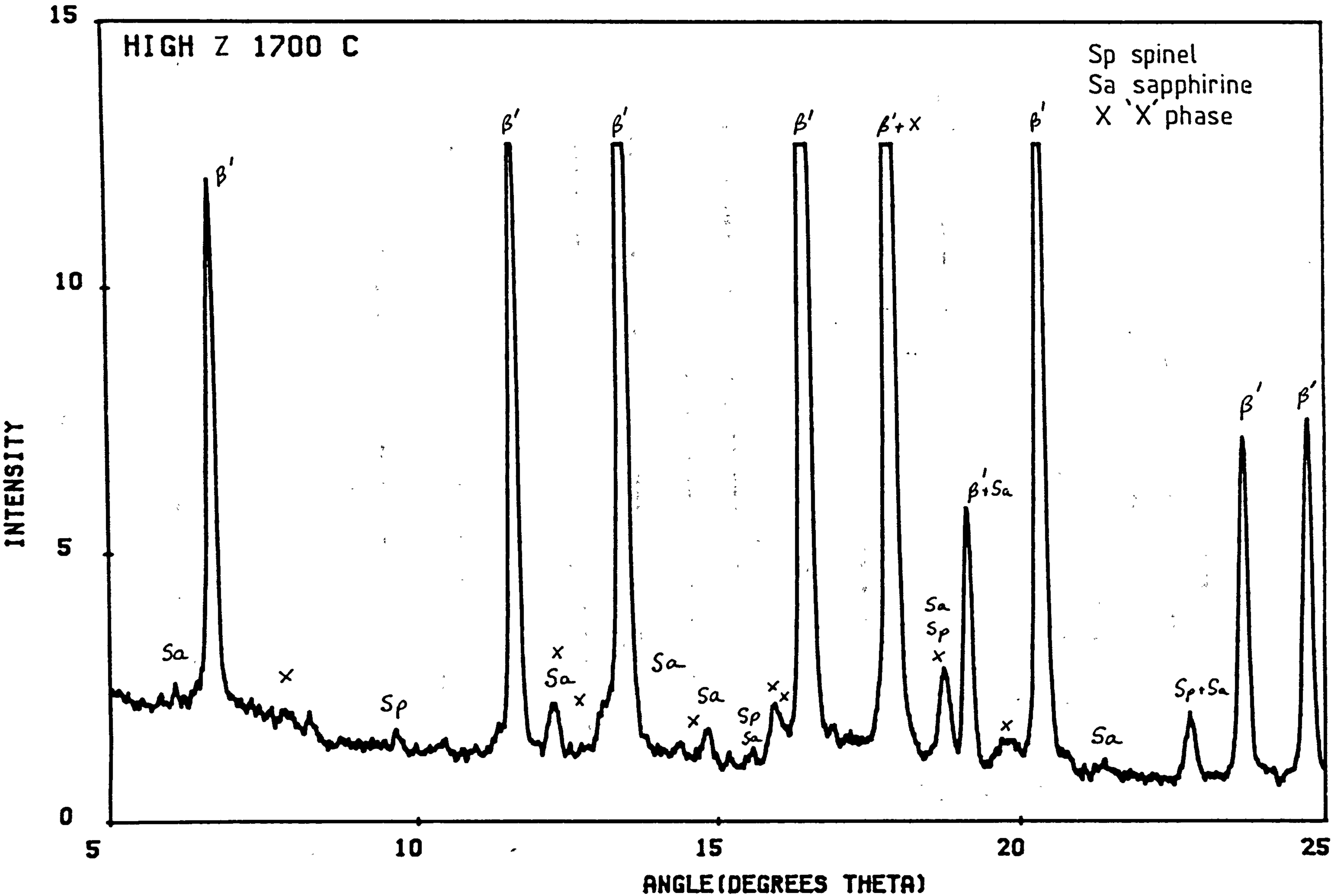
HIGH Z 1700 C
Sp spinel
Sa sapphirine
X 'X' phase
β'
β'
β'
β'+X
β'
β'
β'+Sa
β'
β'
Sa
X
Sp
X
Sa
X
Sa
X
Sa
Sp
Sa
X
X
Sa
Sp
X
X
Sa
Sp+Sa
15
10
5
0
INTENSITY
5
10
15
20
25
ANGLE(DEGREES THETA)

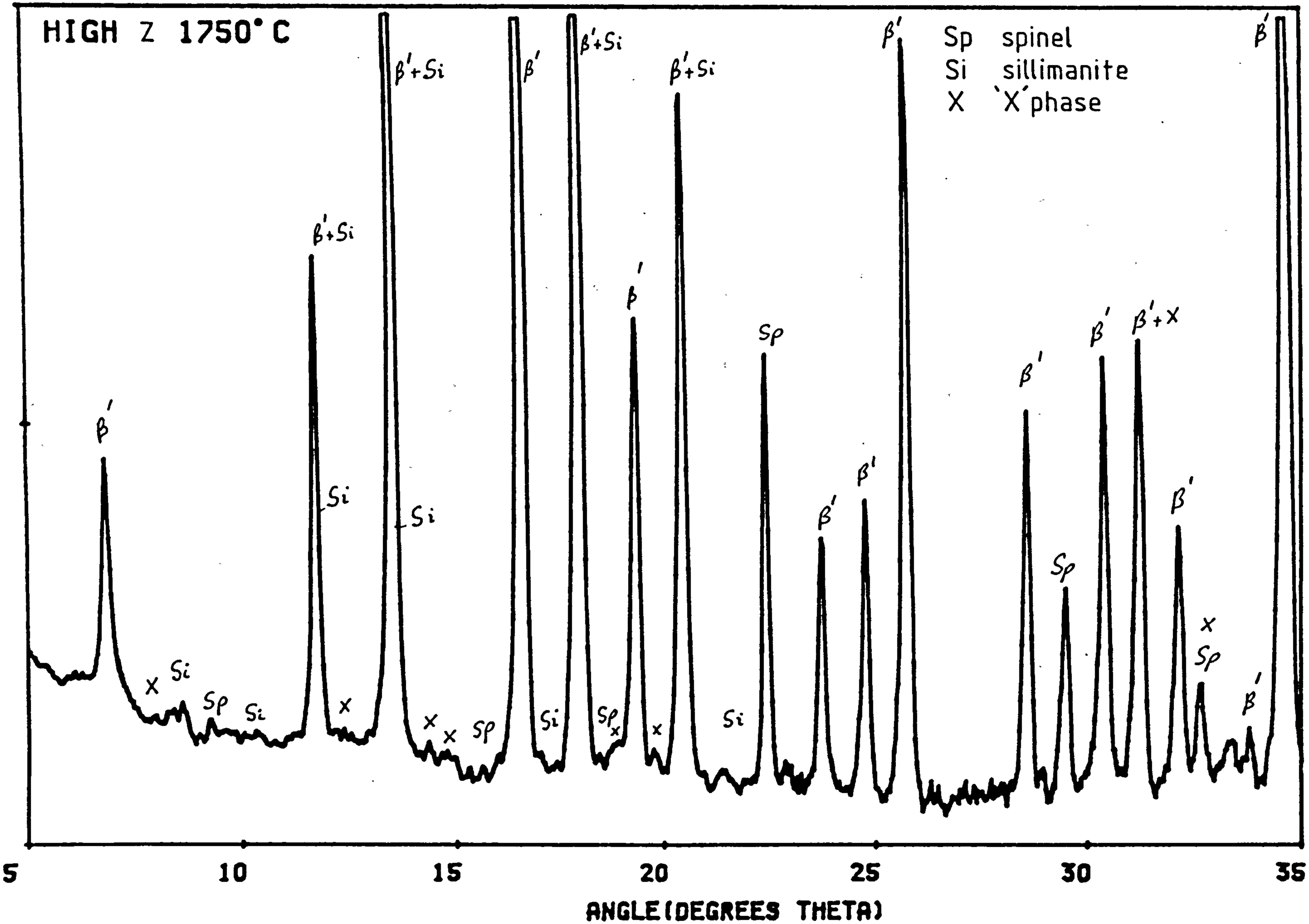
HIGH Z 1750°C
Sp spinel
Si sillimanite
X 'X' phase
INTENSITY
ANGLE(DEGREES THETA)
0
5
5
10
15
20
25
30
35

REFERENCES

1. Jack, K.H. and Wilson, W., Nature Phys. Sci. 238, (1972), p28.

2. Gauckler, L., Lucas, H. and Petzow, G., JACS, 58, (1975), p346.

3. Lumby, R.J., North, B. and Taylor, A.J., Special Ceramics 6, Ed. P. Popper, Academic Press, (1974), p283.

4. Hohnke, H. and Tien, T.Y., Progress in Nitrogen Ceramics, Ed. F.L. Riley, Martinus Nijhoff, (1983), p101.

5. Wild, S., Grieveson, P. and Jack, K.H., Special Ceramics 5, Ed. D. Taylor and P. Popper, Academic Press, (1972), p385.

6. Messier, D.R., Riley, F.L. and Brook, R.J., JMS 13, (1978), p1199.

7. Weiss, J., Am. Review Mat. Sci., 11, (1981), p381.

8. Jack, K.H., Progress in Nitrogen Ceramics, Ed. F. L. Riley, Pub. Martinus Nijhoff, (1983), p54.

9. Thompson, D. P. and Korgul, P., ibid., p375.

10. Jack, K.H., JMS 11, (1976), p1135.

11. Drew, P. and Lewis, M.H., ibid, 9, (1974), p1833.

12. Zangvil, A., ibid, 13, (1978), Letters 1370.

13. Oyama, Y., J.J. App. Phys. Soc., 11, (1972), p670.

14. Land, P.L., Wimmer, J.M., Burns, R.W. and Choudhury, N.S., JACS 61, (1978), p56.

15. Jack, K.H., Progess in Nitrogen Ceramics, Ed. F.L. Riley, 2nd NATO ASI, (1983), p41.

16. Tien, T.Y., Petzow, G., Gauckler, L. and Weiss, J., ibid, Ed. F.L. Riley, Martinus Nijhoff, (1983), p84.

17. Jack, K.H., ibid, Noordhoff, (1977), p257.

18. Hofmann, S. and Gauckler, L., Powder Met. Int., 6, (1974), p2.

19. Gauckler, L., Weiss, J. and Tien, T.Y., JACS 61, (1978), p397.

Note JMS denotes Journal of Material Science

JACS denotes Journal of the American Ceramics Society.

20. Lewis, M.H., Bhatti, A.R., Lumby, R.J. and North, B., JMS 15, (1980), p438.

21. Gazza, G.E., Bull. Am. Ceram. Soc., 54, (1975), p778.

22. Lewis, M.H., Bhatti, A.R., Lumby, R.J. and North, B., JMS 15, (1980), p10.

23. Drew, R.A.L., Hampshire, S. and Jack, K.H., Progress in Nitrogen Ceramics, Ed. F.L. Riley, Martinus Nijhoff, (1983), p323.

24. Boskovic, S., Gauckler, L. Petzow, G. and Tien, T.Y., Powder, Met. Int., 11, (1979), p169.

25. Harding, F. and Ryder, R., Glass Tech., 11, (1970), p54.

26. Shillito, K., Wills, R. and Bennet, R., JACS 61, (1978), p537.

27. Loehmann, R., JNCS 42, (1980), p433.

28. Wusurika, R. and Crynga, G., ibid. 38/39, (1980), p39.

29. Drew, R.A.L., Hampshire, S. and Jack, K.H., Special Ceramics, 7, Ed. D. Taylor and P. Popper, Proc. BCRA, (1980), p119.

30. Richerson, D., Bull. Am. Ceram. Soc., 52, (1973), p560.

31. Levin, E.M. and McMurdie, H.F., Phase diagrams for Ceramicists, Pub. Am. Ceram. Soc., 1969.

32. Nathan-Katz, R., Progress in Nitrogen Ceramics, Ed. F.L. Riley, 2nd NATO ASI, (1981), p3.

33. Raj, R., JACS 61, (1981), p245.

34. Clarke, D.R., Zaluzec, N.J. and Carpenter, R.W., ibid, p608.

35. Roy, B.N., and Narrotsky, A., ibid, 67 (1984), p606.

36. Shaw, T.M., Thomas, G. and Loehmann, R.E., ibid, p43.

37. Leng-Ward, G., Wild, S., and Lewis, M.H., JMS Letters, 3, (1984), p83.

38. Leng-Ward, G., Wild, S., and Lewis, M.H., JMS Letters, 19, (1984), p1726.

39. Momery, J. and McGarry, D.L., JACS 67, (1984), C225.

40. Kriegel, W.W., Peetner, H. and Choi, D.M., Special Ceramics 4, Ed. P. Popper, Academic Press, (1964), p167.

41. Lumby, R.J., Butler, E. and Lewis, M.H., Progress in Nitrogen Ceramics, Ed. F.L. Riley, Martinus Nijhoff, (1983), p683.

42. McMillan, P.W., Glass Ceramics, Academic Press, (1979), p100.

43. Deeley, G., Herbert, J. and Moore, N., Powder Metallurgy, 8, (1961), p103.

44. Terwilliger, G.R., Lange, F.F., JACS 57, (1974), p252.

45. Loehmann, R.E. and Rowcliffe, D.J., ibid, 63, (1980), p144.

46. Kingery, W.D., J. App. Phys. 30, (1959), p301.

47. Happmann, W.J., and Riegger, H., Acta Met. 23, (1975), p965.

48. Wiess, J. and Kaysser, W.A., Progress in Nitrogen Ceramics, Ed. F.L. Riley, Martinus Nijhoff, (1983), p169.

49. Popper, P. ibid, p187.

50. Gazza, G.E., ibid, p273.

51. Brook, R.J., Bowen, L., Weston, R., Carruthers, T., JMS 13, (1978), p341.

52. Tsai, R.L. and Raj, R., JACS 62, (1982), C88.

53. Hampshire , S. and Jack, K.H., Progress in Nitrogen Ceramics, Ed. F.L. Riley, Martinus Nijohff, (1983), p225.

54. Singhal, S.C., JMS 11, 91976), p500.

55. McDonough, L. and Morgan, P.E.D., JACS 64, (1981), L45.

56. Mitomoto, M., JMS 11, (1976), p1103.

57. Greskovich, C., Progress in Nitrogen Ceramics, Ed. F.L. Riley, Martinus Nijhoff, (1983), p283.

58. Kuwabara, M., Benn, M. and Riley, F.L., JMS, 15, (1980), p1407.

59. Raj, R. and Baik, S., JACS 68, (1985), C124.

60. Lange, F.F., ibid, 65, (1982), C120.

61. Tsai, R. and Raj, R., ibid., p270.

62. Babini, G.N., Belloni, A. and Vincenzeni, P., ibid, 64, (1981), p578.

63. Babini, G.N., Belloni, A. and Vincenzeni, P., JMS 19, (1984), p3487.

64. Lewis, M.H. and Barnard, P., ibid, 15, (1980), p443.

65. Clarke, D.R. and Lange, F.F., JACS 66, (1980), p586.

66. Desmaison, J. and Riley, F.L., JMS 16, (1981), p2625.

67. Babini, G.N., Belloni, A. and Vincenzeni, P., ibid, 19, (1984), p1029.

68. Cubicciotti, D. and Lau, K.M., JACS 61, (1978), p572.

69. Shaeffer, M., Progress in Nitrogen Ceramics, Ed. F.L. Riley, Martinus Nijhoff, (1983), p303.

70. Desmaison, J., Brossard, M., Desmaison, Brut, M. and Goursat, P., ibid, p439.

71. Babini, G.N. and Vincenzeni, P., ibid. p427.

72. Inglis, C.E., Trans. Inst. Naral. Archit., 55, (1913), p219.

73. Griffiths, A.A., Phil. Trans. Roy. Soc. Lond., (1920), A221, p163.

74. Irwin, G.R., Handbuk der Physik, Vol. 6, Springer Verlag, Berlin, (1955), p551.

75. Brown, W.F., Srawley, J.E., ASTM Spec. Tech. Pub., (1966), p410.

76. Smith, H.R., Piper, D.E., Stress Corrosion Cracking in High Strength Steels and in Ti and Al Alloys, Ed. B.F. Brown, Naval Research labs. Wash. (1972), p17.

77. Henshall, J.L., Rowcliffe, D.J. and Edington, J.W., JMS, 9, (1974), Letters. 1559.

78. Brown, H.R., ibid, 18, (1983), p941.

79. Davidge, R.W. and Tappin, G., ibid, 3, (1968), p165.

80. Chantikul, P., Anstis, G.R., Lawn, B.R. and Marshall, D.B., JACS, 64, (1981), p539.

81. Lawn, B.R. and Marshall, D.B., ibid, 62, (1979), p342.

82. Chantikul, P., Anglis, G.R., Lawn, B.R. and Marshall, D.B., ibid, 64, (1981), p539.

83. Hollenberg, G.W., Terwilliger, G.R., Gordon, R.S., ibid, 54, (1971), p196.

84. Marshall, D.B. and Lawn, B.R., JMS, 14, (1978), p2001.

85. Cook, R.F., Lawn, B.R., Dabbs, T.P. and Chantibul, P., JACS, 64, (1981), C121.

86. Lewis, M.H., Fung, R. and Taplin, D.M.R., JMS, 16, (1981), p3427.

87. Wyatt, O. and Dew-Hughes, D., 'Metals Ceramics and Polymers, p401, CUP, 1974.

88. Lewis, M.H., Heath, G.R., Winder, S.M., Lumby, R.J., 'Deformation of Ceramics', 11P Materials Sci. Res. Vol. 18, Ed. R.E. Tressler and R.C. Bradt, (1983), p867.

89. Jasper, K., Unpublished Work, University of Warwick, (1983).

90. Evans, A.G., Wiederhorn, S.M., JMS, 9, (1974), p270.

91. Evans, A.G. and Wiederhorn, S.M., JACS, 59, (1976), p371.

92. Stewart, R.T., Isawa, M., Bradt, R.C., ibid., 64, (1981), C22.

93. Weiderhorn, S.M., ibid., 52, (1969), p99.

94. Simpson, L.A., ibid., 56, (1973), p610.

95. Mussler, B., Swain, M. and Clausse, N., ibid, 64, (1981), p566.

96. Hoagland, R.G., Marshall, C. and Duckworth, D.M., ibid., 59, (1976), p189.

97. Paremore, E.M., Spriggs, R.M., Vasilos, T., ibid., 48, (1965), pl.

98. Lange, F.F., ibid., 57, (1974), p84.

99. Bowen, L.J. and Carruthers, T.G., JMS, 13, (1978), p684.

100. Kirchner, H.P., Gruver, R.M., and Richard, D.M., ibid., 14, (1979), p2713.

101. Lange, F.F., JACS, 56, (1973), p518.

102. Caval, J.Y., Delamarre, E.G., Anamra, M.C. and Bronssard, D., JMS 20, (1985), p381.

103. Palm, J.A. and Greskovich, C.D., Bull. Am. Ceram. Soc., 55, (1980), p447.

104. Cannon, W.R., and Langdon, T.G., JMS, 18, (1983), p1.

105. James, K. and Ashbee, K.H.G., Progress in Materials Science 21 Part 1, Ed. B. Chalmers, J.W. Christian, and T.B. Massalski, Pergamon Press, (1975), p29.

106. Lifshitz, I.M., Sov. Phys. JETP, 17, (1963), p909.

107. Kossowsky, R., Miller, D.G., and Diaz, E.S., JMS, 10, (1975), p983.

108. Herring, C., J. App. Phys., 21, (1950), p437.

109. Coble, R.L., ibid., 34, (1963), p1679.

110. Langdon, T.G., Phil. Mag., 22, (1970), p689.

111. Tsai, R.L. and Raj, R., JACS, 65, (1982), C88.

112. Karunaratne, B.S.B. and Lewis, M.H., JMS, 15, (1980), p1781.

113. Baker, T.W., 'Modern Physical Techniques in Materials Technology', Ed. by T. Mulrey and R.K. Webster, OUP, (1974), p18.

114. Mashai, H. and Kamugaito, O., Yogyo Kyokai Shi, 84, (1976), p508.

115. Lewis, M.H., Powell, B.D., Drew, P., Lumby, R.J., North, B. and Taylor A.J., JMS 12, (1977), p61.

116. Bowen, D.K. and Hall, C.R., Electron Microscopy, MacMillan press, (1975).

117. Pickering, C., PhD Thesis, University of Warwick, (1985).

118. Hendry, A., Perera, D.S., Thompson, D.P. and Jack, K.H., Special Ceramics 6, Brit. Ceram. RA, Stoke on Trent, (1975), p321.

119. Birch, J.M., Wilshire, B., Owen, D.J.R. and Shantaram, D., JMS 11, (1976), p1817.

120. Petrovic, J.J., Dirks, R.A., Jaconsbon, L.A., Mendiratta, M.G., JACS, 59, (1976), p177.

121. Lumby, R.J., JMS Letters, 2, (1983), p345.

122. Frischat, G.H., Ionic diffusion in oxide glasses. Diffusion and Defect Monograph No 314, Trans. Tech. Publications, Aedermannsdorf Switzerland, (1975), p182.

123. Karunaratne, B.S.B., PhD Thesis, University of Warwick, (1980).

124. Butler, E., Schweda, A., Unpublished work, Lucas Cookson Sylon.

125. Mason, S., Unpublished work, University of Warwick, (1984).

126. Winder, S.M., PhD Thesis, University of Warwick, (1985).